Electromagnetic Transient and Dynamic Modeling and Simulation of a StatCom-SMES Compensator in Power Systems

Aysen (Basa) Arsoy

Dissertation submitted to the
Faculty of Virginia Polytechnic Institute and State University
in partial fulfillment of the requirements for the degree of

Doctor of Philosophy

In

Electrical and Computer Engineering

Yilu Liu (Chair)
Paulo F. Ribeiro
Arun G. Phadke
Lamine Mili
Osman Balci

April 2000

Blacksburg, Virginia

Keywords: Superconducting Magnetic Energy Storage (SMES), Static Synchronous Compensator (Statcom), dc-dc Chopper, Transient Analysis, Oscillation Damping

Electromagnetic Transient and Dynamic Modeling and Simulation of a StatCom-SMES Compensator in Power Systems

By

Aysen Arsoy

Yilu Liu (Chair)

Electrical and Computer Engineering

(ABSTRACT)

Electromagnetic transient and dynamic modeling and simulation studies are presented for a StatCom-SMES compensator in power systems. The transient study aims to better understand the transient process and interaction between a high power/high voltage SMES coil and its power electronics interface, dc-dc chopper. The chopper is used to attach the SMES coil to a StatCom. Following the transient study, the integration of a StatCom with SMES was explored to demonstrate the effectiveness of the combined compensator in damping power oscillations. The transient simulation package PSCAD/EMTDC has been used to perform the integrated modeling and simulation studies.

A state of the art review of SMES technology was conducted. Its applications in power systems were discussed chronologically. The cost effective and feasible applications of this technology were identified. Incorporation of a SMES coil into an existing StatCom controller is one of the feasible applications, which can provide improved StatCom operation, and therefore much more flexible and controllable power system operation.

The SMES coil with the following unique design characteristics of 50MW (96 MW peak), 100 MJ, 24 kV interface has been used in this study. As a consequence of the high power/ high voltage interface, special care needs to be taken with overvoltages that can stress the insulation of the coil. This requires an investigation of transient overvoltages through a detailed modeling of SMES and its power electronics interface. The electrical model for the SMES coil was developed based on geometrical dimensions of the coil. The interaction between the SMES coil and its power electronics interface (dc-dc chopper for the integration to StatCom) was modeled and simulated to identify transient overvoltages. Transient

suppression schemes were developed to reduce these overvoltages. Among these are MOV implementation, surge capacitors, different configurations of the dc-dc chopper.

The integration of the SMES coil to a StatCom controller was developed, and its dynamic behavior in damping oscillations following a three-phase fault was investigated through a number of simulation case studies. The results showed that the addition of energy storage to a StatCom controller can improve the StatCom-alone operation and can possibly reduce the MVA rating requirement for the StatCom operating alone. The effective location selection of a StatCom-SMES controller in a generic power system is also discussed.

ACKNOWLEDGMENT

The author would like to express her deepest gratitude to her advisor, Dr. Yilu Liu for her guidance, understanding, encouragement, and her friendship throughout this study. The author also would like to express her acknowledgment to her co-advisor, Dr. Paulo F. Ribeiro, for providing extensive number of resources and data for this work, sharing his industrial experience related to this work, and his guidance and encouragement. Without their guidance and assistance, this work would not have been completed.

The author also would like to thank her Ph.D. committee members Dr. Arun G. Phadke, Dr. Lamine Mili, and Dr. Osman Balci for their valuable comments on this work and serving on her dissertation committee.

A special note of recognition and appreciation goes to Dr. Z. Wang for his assistance in the first phase of this work, Dr. X. Dong for his help in setting up the network analyzer for capacitance measurement, Dr. V. Centeno for providing a good lab environment, Mr. B. Nelson for providing me documents on SMES products developed by American Superconductor, and finally the technical support personal of PSCAD: especially Mr. R. Jayasinghe and Mr. M. Reformat for their help to answer the author's questions related to the PSCAD/EMTDC program.

The author would like to thank his colleagues, especially R. Nuqui, L. Huang, A. Khatib, D. Elizando, A. Bretas, L. Chen, B. Qiu, and S. Rosado for their friendship and enjoyable, stimulating discussions.

The author wishes to thank her parents Sen and Gungor Basa, her brothers Derya and Oguz Basa, her aunt Guner Basa and her in-laws Mecbure and Salim Arsoy for their understanding and support.

Finally, the most sincere appreciation goes to the author's husband Sami Arsoy for his companionship, great understanding and continuous encouragement in this challenging endeavor. Their 20-month-old daughter, Edanur, gave her mother enjoyable and precious moments that her mother is always greatful for.

TABLE OF CONTENTS

LIST OF FIGURES

LIST OF TABLES

CHAPTER I

INTRODUCTION

Power systems have been experiencing dramatic changes in electric power generation, transmission, distribution, and end-user facilities. Continuing electric load growth and higher power transfer in a largely interconnected network lead to complex and less secure power system operation. In addition, certain factors such as technical, economical, environmental, and governmental regulation constraints put a limitation on power system planning and operation. Power system engineers facing these challenges seek solutions to operate the system in more a flexible and controllable manner. Recent development and advances on both superconducting and power electronics technology have made the application of SMES (superconducting magnetic energy storage) systems a viable choice to bring solutions to some of the problems experienced in power systems. Although SMES was initially envisioned as a large-scale load-leveling device, it is now seen as mainly a tool to enhance system stability, power transfer, and power quality in power systems in the process of deregulation. The power industry demand for more flexible, reliable and fast real power compensation devices provides the ideal opportunity for SMES applications [Karas99]

I.1. The Superconducting Magnetic Energy Storage (SMES) Systems and its Role in Power Systems

Superconductivity, the total lack of resistance of conducting materials below critical temperatures, is one of the most fascinating phenomena in nature. Although superconductivity was discovered in 1911 by Onnes [Hasses83], it was not until 1970s superconducting magnetic energy storage (SMES) was first proposed as a technology in power systems. Energy is stored in the magnetic field generated by circulating the DC current through a superconducting coil. SMES is a technology that has the potential to bring essential functional characteristics to the utility transmission and distribution systems. A SMES system consists of a superconducting coil, the cryogenic system, and the power conversion or conditioning system (PCS) with control and protection functions [Hasse89]. Its

total efficiency can be very high since it does not require energy conversion from one form to the other. Depending on its power conversion unit's control loop and switching characteristics, the SMES system can respond very rapidly (MWs/ mili-seconds). Because of its fast response and its efficiency, SMES systems have received considerable attention from electric utilities and the government. SMES systems are reliable (no moving parts) and environmentally benign. Compared to other storage technologies, the SMES technology has a unique advantage in two types of application, power system transmission control and stabilization and power quality. Although SMES systems may not be cost effective, at the present time, they have a positive cost and environmental impact by reducing fuel consumption and emissions [Karas99].

SMES' efficiency and fast response capability has been and can be further exploited in different applications in all level of electric power systems. SMES systems have the capability of providing a) load leveling b) frequency support (spinning reserve) during loss of generation, c) enhancing transient and dynamic stability, d) dynamic voltage support (VAR compensation), e) improving power quality f) increasing transmission line capacity, thus overall enhancing security and reliability of power systems. The characteristics of potential SMES applications for generation, transmission, and distribution are given in Table I.1.

Table I.1: Characteristics of Potential SMES Applications in Power Systems [Giese98]

	Application	***Typical Stored Energy Capacity***	***Typical Discharge Period***
Generation	Load Leveling	100 – 5000 MWh	Hours
	Dynamic Response	80 – 2000 MWh	Hours
	Spinning Reserve	2 – 300 MWh	Minutes
	Frequency Control	500 MJ – 15MWh	Seconds
Transmission	Load Leveling	10 – 1000 MWh	Minutes – Hours
	Stabilization	8 MJ – 10 MWh	Seconds
	Voltage/VAR Control	1 – 100 MJ	Cycles
Distribution	Load Leveling	50 MJ – 10 MWh	Minutes –Hours
	Power Quality	0.1 – 10 MJ	Seconds
	Custom Power	0.1 – 10MJ	Cycles

Among these applications, the ones with the power ranges of 20 – 200MW and the energy ranges of 50 – 500 MJ are cost beneficial applications. As can be seen from Table I.1, the applications of transmission stability, frequency control, and custom power and power quality are economically feasible applications [Ribei99].

SMES applications are becoming attractive as a tool to enhance transmission utilization in the process of deregulation of power utilities. The deregulated environment is forcing new technologies and advancements adopted to enhance the existing system conditions for more reliable secure and flexible systems. SMES can be configured to provide energy storage for flexible ac transmission system (FACTS) controllers at the transmission level, or custom power devices at the distribution level. The SMES ability of injecting/absorbing real or reactive power can increase the effectiveness of the control and enhance system reliability and availability. In addition to the SMES characteristics and benefits, advancements in the superconducting and power electronics technologies will make the utilization of SMES more desirable for power utility applications.

I.2. Improved FACTS Controller: FACTS and SMES

Second generation FACTS controllers are power electronics based devices that can handle both real and reactive power to enhance transmission system performance. With the appropriate configuration and control, they can influence the transmission system parameters such as impedance, voltage, and phase angle. The multi MW proven FACTS technology are now being introduced to the utility industry to enhance the existing transmission assets as opposed to constructing new transmission assets. Several utilities have installed such controllers in their system [Schau95, Schau98]. FACTS controllers can be connected to the system in series, parallel or combined form and they can utilize or redirect the available power and energy from the ac system. Without energy storage, they are limited in the degree of freedom and sustained action in which they can help the power grid [Karas99]. One of the viable energy storage technologies, SMES, can be added to a FACTS controller to significantly improve the control actions of FACTS.

A SMES system requires a PCS that can be either a voltage or current source inverter. Since the inverter utilized for a FACTS controller is voltage source based, it is a logical approach to attach SMES to a FACTS controller. The integration of a FACTS device with SMES can provide independent real and reactive power absorption/injection into/from the grid. If a transmission line experiences significant power transfer variations in a short time notice, a FACTS+SMES combination can be installed to relieve the loaded transmission line. Figure I.1 shows FACTS+SMES (connected to the line in series and parallel) and their power controllability. The combined system would not only provide better performance than separate stand alone devices, but it could also have a lower cost since the combined system can generate the same performance with lower rating. Currently, several SMES magnets are being built for transmission level applications. They could be good candidates to be attached to existing FACTS controllers. This study is based on a 50 MW, 100 MJ SMES coil being built by BWX Technologies, Inc. for a FACTS/ energy storage application.

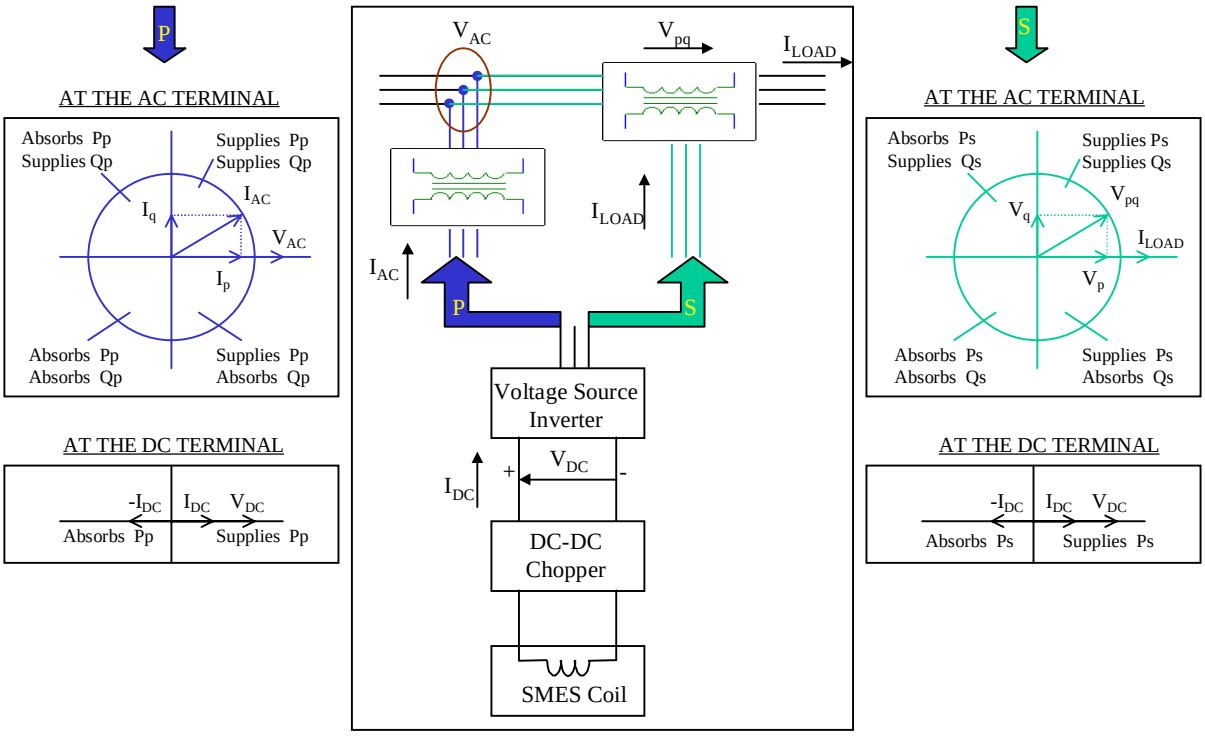

Figure I. 1: SMES with a Parallel or Series connected FACTS Controller, and P-Q Plane for Each Operating Mode

Custom power devices are similar to FACTS devices in topology but at smaller ratings. Most of the current SMES projects use small-scale or micro SMES devices. They can also be attached to custom power devices to increase the effectiveness of the overall system.

I.3. Transient Concerns in SMES Operation

The power electronics applications in power systems continue to increase. Normal and abnormal switching of power electronics devices may generate transient overvoltages. These overvoltages take place in very short time compared to steady state but, they may have potential to damage any equipment that is subject to these transients. Therefore, the control and modeling of power electronics devices is an important task in power system transient studies, where digital simulation tools are widely used [Ieeew99].

A SMES system is comprised of power electronics devices. Switching actions of these devices during charge and discharge may cause serious transient overvoltages. These transients may have potential to damage the coil insulation. The SMES unit may fail simply because the insulation level was not designed to withstand transients. Most of the SMES failures have been experienced due to insulation and protection problems. This is especially more important for large coils [Hayas99]. It is essential to characterize the transients that may be experienced by the SMES coil for insulation and protection purpose. A good analysis of transient interaction between a superconducting coil and its power electronics interface is crucial to avoid any insulation problem that may be experienced.

A detailed modeling of the coil is necessary to identify the transients better. Breaking down the coil into small pieces, representing the entire coil and analyzing the internal node voltages will give a better understanding of the transients that may affect the coil. A detailed modeling of superconducting coil along with the power electronics interface modeling and control are essential in the electromagnetic transient interaction analysis.

I.4. Objectives and Outline of Dissertation

The objectives of this study can be classified into three groups:

1. A comprehensive overview on SMES technology: Reviewing its definition, components, design and cost issues, its power electronics interface requirements, its potential applications in power systems as an independent device or enhancing existing FACTS controllers.

2. An electromagnetic transient interaction analysis: developing a detailed modeling of a SMES coil and its power electronics interface to fully assess the transient overvoltages due to switching operations, simulating the comprehensive model under normal operating conditions, transients, and surge establishing a control mechanism and recommending transient suppression and protection schemes for the SMES coil

3. Integration of a static synchronous compensator (a parallel connected FACTS controller) with SMES: Investigating the impact of SMES in damping power system oscillations.

With these objectives, the outline of the dissertation can be drawn as follows: Chapter II presents an overview of SMES technology. The power conversion system for SMES is discussed in Chapter III. Following this chapter, transient concerns in SMES systems and transient modeling of a SMES coil are presented. In this chapter, the formulas to calculate electrical coil parameters based on geometric dimensions are given, then the calculated parameters in turn to turn level were lumped to obtain parameters representing sections for a reasonable computational effort. Chapter V gives the simulation results of the transient interaction between a SMES coil and its power electronics interface, a dc-dc chopper. The possible transient overvoltages are quantified, and transient suppression schemes are recommended. Additionally, an alternative chopper design is proposed. The integration of a SMES with a synchronous compensator is presented in Chapter VI. It is shown that the SMES coil has a beneficial effect on damping power system oscillations. Finally, Chapter VII summarizes the modeling and simulation study, outlines the contributions and main conclusions. Future work is also recommended in the last chapter.

CHAPTER II

AN OVERVIEW OF SUPERCONDUCTING MAGNETIC ENERGY STORAGE SYSTEMS

This chapter presents a general overview of superconducting magnetic energy storage (SMES) systems including its components, design and cost considerations, potential SMES applications, discussion on development of SMES, comparison between SMES and other energy storage technologies, and present status of SMES technology. A literature review on SMES is prepared from selected SMES related journal/transaction/conference papers including their contents and important remarks, and it is presented in Appendix A.

II.1. Introduction on SMES

A SMES device is a dc current device that stores energy in the magnetic field. The dc current flowing through a superconducting wire in a large magnet creates the magnetic field. The inductively stored energy (E in Joule) and the rated power (P in Watt) are commonly given specifications for SMES devices and they can be expressed as follows:

$$E = \frac{1}{2} LI^2 \qquad \mathrm{P} = \frac{\mathrm{dE}}{\mathrm{dt}} = LI\frac{\mathrm{dI}}{\mathrm{dt}} = VI$$

where L is the inductance of the coil, I is the dc current flowing through the coil, and V is the voltage across the coil.

Any large magnet can store energy, and the relationship between the volumetric energy density (E_v in J/m^3) and magnetic field intensity (B in T) is given by

$$E_v = \int \vec{B} \bullet d\vec{H} = \frac{B^2}{2\mu\mu_0}$$

where $B = \mu\mu_0 H$, μ is the average relative magnetic permeability and μ_0 is μ of free space.

A large volumetric energy density is achieved with a small μ and a large *B*. Certain conducting materials become superconducting below a cryogenic temperature, which means that no resistive losses occur in the winding. The superconductivity allows the coil to be wound very compactly so that a high flux density, therefore, a high specific energy density is achievable. Consequently, the use of superconducting wire can increase E_v.

A SMES system consists of a superconducting coil, the cryogenic system, and the power conversion or conditioning system (PCS) with control and protection functions [Hassen89]. IEEE defines SMES as "A superconducting magnetic energy storage device containing electronic converters that rapidly injects and/or absorbs real and/or reactive power or dynamically controls power flow in an ac system" [Ribei99]. Such a device has a number of advantageous and unique characteristics: No conversion of energy from one form to another is required, consequently SMES has inherently high storage efficiency, a 90% or greater round trip efficiency. Depending on the power conversion unit's control loop and switching characteristics, the SMES device can respond very rapidly (MWs/ mili-seconds) to power demands from maximum charge to maximum discharge. SMES systems can offer very reliable and long lifetime service. Except for certain designs, they are considered to be environmentally benign systems.

Because of its benefits and unique characteristics, the SMES device is quite competitive with other energy storage technologies, therefore the SMES technology has received considerable attention from electric utilities and the government. Throughout the development of SMES, potential applications were identified, cost/benefit analyses were carried out. Although SMES was initially considered as a diurnal energy storage device, other potential applications can be listed as follows:

- Dynamic and Transient Stability
- Spinning Reserve/ Frequency Support
- Voltage/VAR support
- Transmission Capacity Improvement
- Power Quality Enhancement

II.2. The Components of SMES

As can be seen from Figure II.1, a SMES system connected to a power system consists of several subsystems. A large superconducting coil is the heart of the SMES systems. It is contained in a cryostat or dewar that consists of a vacuum vessel and contains liquid vessel that cools the coil. A cryogenic system is to keep the temperature well below the critical temperature for the superconductor. An ac/dc power conversion or conditioning system (PCS) is used for two purposes: One is to convert from dc to ac, and the other one is to charge and discharge the coil. A transformer provides the connection to the power system and reduces the operating voltage to acceptable levels for the PCS.

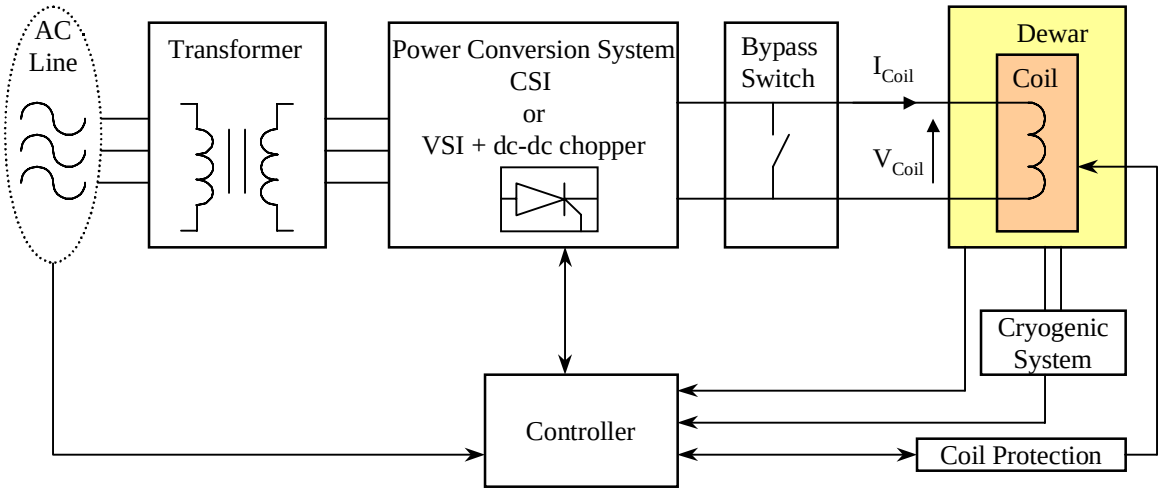

Figure II.1: Components of a Typical SMES System

CSI: Current Source Inverter
VSI: Voltage Source Inverter

There are two types of superconductors used to form a SMES coil; low temperature superconductors (LTS) and high temperature superconductors (HTS). A composite of alloys of Niobium and Titanium (Nb-Ti) copper is used most commonly for low temperature superconductors (LTS). The use of copper serves several purposes: It mechanically supports and separates the individual Nb-Ti filaments, electrically isolates the filaments by providing a resistive barrier that reduces losses during charge and discharge, and stabilizes the super conductor by conducting current during short periods when the conductor undergoes a

transition to the normal state. The HTS material is, at present, bismuth-strontium-calcium-copper-oxide (BSCCO). The operational requirements of these two types of superconductors will be discussed in a later section

During SMES operation, the magnet coils has to remain superconducting. A refrigerator in the cryogenic system maintains the required temperature for the proper superconducting operation. The refrigeration load can affect the overall efficiency and cost of a SMES system. Therefore, the refrigeration load that has loss components, such as cold to warm current leads, ac current, conduction and radiation, should be minimized to achieve a higher efficient and less costly SMES system.

Any abnormal condition that may cause a safety hazard to personnel or damage to the magnet should be detected and protected through the magnet protection system. Monitoring/Protection system may include 1) instrumentation to monitor thermal, structural, and electrical operating conditions of the coil 2) a quench detection system that prevents any temperature to rise above certain level, and 3) an emergency discharge resistor.

A PCS provides a power electronic interface between ac power system and the superconducting coil. It allows the SMES system to respond within tens of mili-seconds to power demands that could include a change from maximum charge rate to maximum discharge power. This rapid response allows a diurnal storage unit to provide spinning reserve and improve system stability. The converter/SMES system is highly efficient, as there is no energy conversion from one form to another. Converters may produce harmonics on the ac bus and in the terminal voltage of the coil. Using higher pulse converters can reduce these harmonics.

The superconducting coil is charged or discharged by making the voltage across the coil positive or negative. The coil absorbs power from the ac system and acts as a load during one half cycle when the converter voltage is positive. During the next half cycle, the coil operates as a generator sending power back into the ac systems when the converter voltage is made negative. When the unit is on standby, independent of storage level, the current is constant, and the average voltage across the superconducting winding is zero.

A PCS could be either a current source inverter or a voltage source inverter with a dc-dc chopper interface. These inverter types will be discussed in great detail in the next chapter.

A bypass switch is used to reduce energy losses when the coil is on standby. The utilization of the switch also serves for other purposes such as bypassing dc coil current if utility tie is lost, removing converter from service, and protecting the coil if cooling is lost.

II.3. Design Considerations

In the design stage of a coil, several factors are taken into account to achieve the possible best performance of a SMES system at less cost. These factors may include coil configuration, energy capability, structure, operating temperature. A compromise is made between each factor considering the parameters of energy/mass ratio, Lorentz forces, stray magnetic field, and minimizing the losses for a reliable, stable and economic SMES system.

Conceptual and prototype designs of SMES systems were carried out since early 1970s. Examples of LTS electrical parameters of designs are given in Table II.1.

Table II.1: Design Parameter Examples for Low Temperature Solenoid SMES Coils

Parameters	***(1)***	***(2)***	***(3)***	***(4)***	***(5)***	***(6)***
Stored Energy	5500 MWh	22 MWh	5000 MWh	30 MJ	1800 MJ	25kJ
Power Cap.	500 MW	400 MW	1000 MW	10 MW	31.5 MW	50 kW
Op. Current (kA)	765	50 max	200 max	5 max	10.8 max	0.115
Peak Voltage (kV)	1.8	13.33	10	2.1	3.375	0.5
Peak Field (T)	7	4.8	6.69	2.85	6.1	NA
Op. Temp. (K)	NA	1.8	NA	4.5	4.45	4.2
Inductance (H)	68	61.2	990	2.4	NA	3.8
Coil Height (m)	15	4.087	19	1.26	2.44	0.123
Mean Diameter (m)	1568	134	2000	2.58	7.57	0.128
Total Turns	112	416	556	920	1900	4500
No. of Layers	1	4	4	24	NA	30
SC material				NbTi/ Cu		NbTi

(1) Low Aspect Ratio Design [Hasse83]
(2) Engineering Test Model Design [Hassa93]
(3) 5000 MWh EPRI Design [Hasse89]
(4) 30 MJ SMES installed in Tacoma Substation [Roger83]
(5) BWX SMES planned to install at Anchorage Municipal Light and Power [Kral97]
(6) 25kJ ASINEL-Spain Project [Bauti97]

II.3.1. Coil Configuration: Solenoid vs. Toroid

The solenoid and toroid shaped SMES coils have been extensively studied. Solenoid type is simple and easy to construct, and it minimizes the amount of conductor for a given storage capacity. However, this type of design results in rather large stray magnetic field, which affects the siting of SMES systems due to the concerns related to environmental and health effects [Giese98]. To reduce the stray magnetic field, an alternative was sought, and a toroid coil design was utilized. This design is more complicated to fabricate, and significantly more expensive since it requires the use of more conductors [Lieur95, Hasse89]. According to the evaluation of these designs in [Boom72], the solenoid stores almost twice the energy stored in a toroid, will be most economical if they are built as solenoids with a height to diameter ratio of about one third and with a maximum field. Solenoid and toroid coils have been used in different variations: single tunnel, multi tunnel, low aspect ratio, single layer and multi layer structures for solenoid, forced balanced scheme and quasi force free structures for toroids. Due to its simplicity and cost effectiveness, the solenoid type (as shown in Figure II.2) has been used widely, though the toroid-coil designs were also incorporated by a number of small-scale SMES projects.

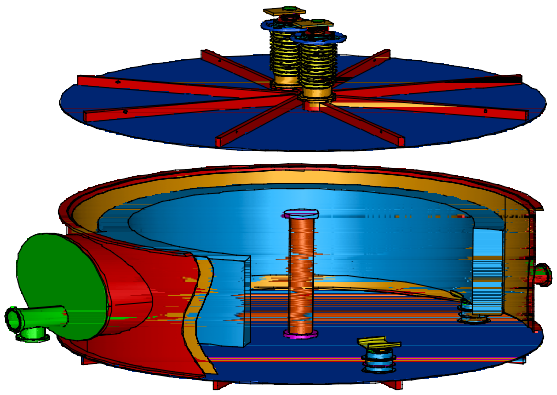

Figure II.2: Solenoid Configuration [Karas99]

II.3.2. Structure: Cold Supported vs. Warm Supported

The theoretical minimum amount of material required to support the electromagnetic forces of a solenoid is given with the Virial Theorem as follows:

$$M \geq \frac{E\rho}{\sigma}$$

where M is the structural mass, E is the stored energy, ρ is the material density and σ is the allowable stress [Luong96]. The magnet structure must be designed to withstand the radial and axial loads. Since early SMES efforts were focused on large-scale devices, the structure required containing Lorentz forces would be expensive with the conductor type they used. Therefore, earth-supported (or warm) structure was proposed [Luong96, Giese98]. The use of the cold-supported (or self-supported) structure was well accepted with the use of a cable-in-conduit NbTi conductor (CICC) and alloy aluminum as a structural material. Although the latter one requires more material, therefore more costly, the overall system cost can be reduced by eliminating the components needed for earth structure and by providing simplifications in construction. CICC has the ability to withstand large magnetic forces and to remain stable in the presence of thermal disturbances. CICC also minimizes the conductor mass subjected to eddy currents, therefore reduce the high ac losses generated during the rapid-cyclic charge discharge period of the coil [Karas99].

II.3.3. Energy Capability

Coil inductance (L) or PCS maximum voltage (V_{max}) and current (I_{max}) ratings determine the maximum energy/power that can be drawn or injected by a SMES coil. Increasing any of these parameters improves the energy/power capability of SMES [Giese98]. But, there are other factors that need to be taken into consideration:

Increasing Imax	$\Rightarrow$	Larger conductor cross section Larger current leads and associated lead losses Larger and more expensive PCS
Increasing Vmax	$\Rightarrow$	Larger more expensive PCS Insulation problem
Increasing L	$\Rightarrow$	More turns in the magnet

What parameter to increase depends on the relative cost of the SMES magnet versus PCS. Compared to the PCS cost, the magnet cost is less expensive for small-scale SMES applications, while it dominates the overall cost for large-scale SMES applications. Consequently, the magnet size can be increased for applications requiring a small amount of energy, and the PCS size can be increased for applications requiring extensive amount of storage. Furthermore, for small SMES systems, high current/low voltage is desired, but it involves higher ac losses during discharge.

The density of volumetric energy is proportional to the square of the magnetic field intensity (B). An increase in B has a positive impact in energy density, but causes larger radial and axial stresses that need to be supported with more structural material that induces more cost. A compromise among conductor cost, magnet size and the cost of the structure should be made to determine the optimal B.

II.3.4. Operating Temperature: LTS vs. HTS

The operating temperature of a superconducting device is a compromise based on the lowest cost while meeting the operational requirements [Hasse89]. LTS devices are widely accepted, and HTS devices are currently in the development stage. Both HTS and LTS devices have advantageous over each other. There are several technical factors that need to be considered in the use of high temperature superconductors for SMES. Operating temperature determines cryogen and current density, while current density affects quantity and material required. Stress/strain and friction are important factors in the design considerations. Material characteristics and operating conditions determines stability. The reliability /safety of the system is also need to be taken into consideration. Pros and cons of the HTS devices are tabulated in Table II.2.

The material when operated at 4.4K can carry currents up to 2000A/mm^2 at field of 5T which is more than 100 times greater than the typical operating current density in copper [Hasse83]. The current density for the present day BSCCO conductors (HTS) is lower, and decreases rapidly for temperature above 30-40K. Therefore, current HTS designs plan to

operate at or below 30K. The attractive advantageous overcome its limitations for small scale SMES applications [Schoe93], and a few projects utilize HTS conductors [Giese98]. Section II.6.4 on ongoing SMES projects give two tables showing LTS and HTS projects with their device specifications.

Table II.2: Pros and Cons of HTS Devices Compared to LTS Devices

Pros	***Cons***
Use of less expensive cryogenic system	Lower current density
Higher refrigeration efficiency	Greater brittleness
Greater reliability	Increased amount of conductor (higher cost)
Easier acceptance within the utility environment	Less margin against quenching

II.4. Benefits/Cost Considerations

SMES can provide a number of benefits to utilities. Among those are 1) diurnal load leveling, 2) automatic generation control (AGC) , 3) optimum loading of generators, 4) damping slow power oscillations, 5) voltage support, 6) spinning reserve, 7) black start, 8) transient stability enhancement, 9) improving the performance of the existing second generation FACTS devices, and 10) environmental values. The sensitivity of several benefits (stability enhancement, voltage support, and AGC) to changes in SMES capacity and power handling capability was explored in [Stees92]. Although the study presented there is system specific, similar benefit versus capacity or power handling capability curves can be obtained for different systems. The result of this study can be summarized as follows:

- For steady state stability enhancement, maximum benefit can be obtained with SMES ratings in the range of [50-100 MW, 70-120 MVAR] real and reactive power capability and about 0.1 MWh storage capacity. High benefits can be obtained with little energy storage capacity.
- Improved steady state stability will also enhance the transient stability. But, additional benefits can be obtained with higher power capability and storage capacity, typically [200-800MW, and 5-20MWh]

- The voltage support benefits are system dependent, and do not require high storage capacity.
- The AGC benefit increase rapidly with SMES power handling capabilities of [100-500 MW]. Storage capacity up to 5 MWh can provide large benefit increase.

The cost of a SMES system can be separated into two independent components where one is the cost of the energy storage capacity and the other one is the cost of the power handling capability. Storage related cost includes the capital and construction costs of conductor, coil structure components, cryogenic vessel, refrigeration, protection and control equipment. Power related cost has the capital and construction costs of power conditioning system. While the power related cost is lower than energy related cost for large-scale applications, it is more dominant for small-scale applications.

For a given design, the cost of a SMES is roughly proportional to its surface area and the required quantity of superconductor. The cost of per unit of energy (MJ or MWh) decrease as storage capacity increases. Therefore, early cost estimates showed that only a very large SMES unit would be economical [Hasse89].

Reducing stray magnetic field, achieving a higher energy density, conductor selection, and optimum operating temperature are all cost related. A cost estimate for the 5000MWh SMES device shows that the cost of conductor and structure support constitutes of 30% of the total cost for low temperature devices When a HTS with lower current density is utilized, the total cost was reduced up to 15%.

Three scenarios presented in [Stees92] will be used as an example to demonstrate benefit/cost ratios for each case. This is tabulated in Table II.3. As can be seen, the benefit/cost ratio for very large SMES is lower than 1, whereas the ratio is higher than 1 for smaller scale SMES, which encourages the use of mid or small size scaled SMES.

Table II.3: Benefit/Cost Summaries for Three Scenarios at $M (1992) [Stees92]

	1	2	3
Energy Storage Capacity (MWh)	8000	20	20
Power Handling Capability (MW)	1500	400	1200
Construction Time (years)	7	3	3
Cost			
Capital: Energy Storage Cost	1257	39.2	39.2
Capital: Power Handling Cost	88	37.2	79.9
Capital: Total Cost	***1345***	***76.4***	***119.1***
Annual: Levelized Capital Cost	99	5.2	8.1
Annual: Fixed O&M Cost	15	2.5	3.0
Annual: Total cost	***114***	***7.7***	***11.1***
Benefits			
Capital: Displaced Thermal plant Cap. (MW)	1144	-	-
Capital: Thermal Plant Capital Construction Cost	694	-	-
Annual: Levelized thermal Plant Capital	43	-	-
Annual: Thermal Plant fixed O&M	30	-	-
Annual: Net Production Cost Savings	17	-	-
Annual: System Stability Enhancement	10	7.9	23.7
Annual: Automatic Generator Control	1	1.0	1.0
Annual: Voltage Support and Equipment Subs.	1	1.2	1.2
Annual: System R&D Testing	-	0.4	0.4
Annual: Total benefits	***103***	***10.5***	***26.3***

Scenario 1: Unit near major load for the applications of 1) Diurnal Storage and Reserve, 2) Stability Enhancement, 3) Automatic Generator Control, and 4) Control Equipment Substitution.

Scenario 2: ETM Size for the applications of 1) Stability Enhancement, 2) Automatic Generator Control, 3) Control Equipment Substitutions, and 4) System R&D and test

Scenario 3: ETM Size for the applications of 1) Stability Enhancement, 2) Automatic Generator Control, 3) Control Equipment Substitutions, and 4) System R&D and test

II.5. Potential SMES Applications

A new technology finds its applications if it replaces the existing technology at lower cost or has unordinary capabilities to serve the needs. There exist concerns at the generation, transmission and distribution levels of power systems. These concerns were identified by A.D. Little by interviewing utility executives [Giese98], and summarized in Table II.4.

Early SMES efforts were concentrated on designing large-scale SMES devices, as an alternate to pumped energy storage and gas turbines, for load leveling. It was also recognized that SMES has the capability of providing stabilization and meeting spinning reserve requirements [Boom72, Hasse83]. Indeed, a 30MJ SMES unit was designed and commissioned at BPA's Tacoma substation to damp poorly synchronized power oscillations

experienced due to major loads located far away from generating units [Roger89, Mitan88]. Small perturbations that continuously disturb the normal operation in a power system may cause load frequency control problems. A study presented in [Baner90] proposes the use of small sized magnetic energy storage units for this application. As a result of 1800MJ SMES program led by BWX and AML&P, several applications were identified for mid-size SMES devices: a) frequency support during loss of generation capacity, b) damping transmission power line oscillations, c) transmission voltage/VAR support, and d) automatic generation control [Kral95]. Several papers [Kral95, Huang95, Kral97, Feak97] discusses the utility applications of SMES for utilities. All simulation studies presented in these papers verified that the SMES system is indeed very effective and beneficial in particular cases, but it was costly. One of the ongoing projects (Intermagnetics IPQ) presented in [Parizh97] discuses the use of small-scale SMES to solve power quality problems for substation applications. Latest SMES efforts tend to use small-scale SMES devices for distribution applications. Figure II.3 shows a plot presenting potential SMES utility applications with their power/energy requirements. Typical discharge period of SMES for each application is also given on the plot.

Table II.4: Utility Concerns in Power Systems Generation, Transmission and Distribution

Generation	Inadequate peak power capacity (load leveling) Need for improved load following (spinning reserve and frequency control) Need for better control of bulk power transfers (dynamic response) Economy power for peaking needs (load leveling)
Transmission	Insufficient transfer capacity Flow control, loop flows, and bottle necks Voltage regulation, stability and quality Transient and dynamic stability
Distribution	Local generation related problems Long duration power quality and reliability problems Capacity limitation problems

One or more SMES attribute is vital for each application. While high round trip efficiency is very important in load leveling, rapid response is a driving factor in power quality applications. On the other hand, the transmission applications such as voltage/VAR control and stabilization relies on the ability of a SMES system to absorb/inject both real and reactive power on alternate cycles. High power/energy ratio is preferred in small-scale SMES systems. The advantage is that the SMES with lower stored energy is better capable of a higher than specified power for a short time.

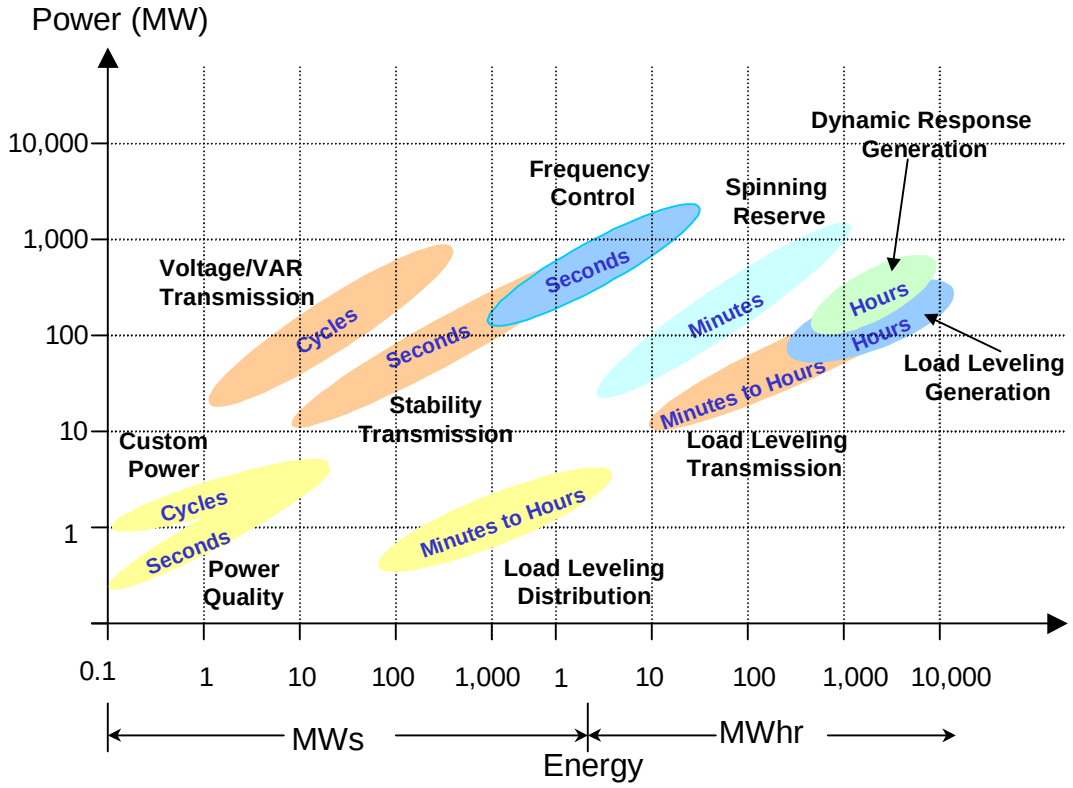

Figure II.3: Power vs. Energy Requirements for SMES Utility Applications

The SMES technology can also be employed for other applications in different scales besides bulk power systems. Extended applications of SMES include transportation systems such as aircraft carrier and naval shipboard power and electric and hybrid-electric vehicles, and electrically sensitive manufacturing and remote energy usage, such as weather research stations, island systems, and ground based defense systems. Enhancing the utilization of

photovoltaic system with SMES and application of SMES in an asynchronous link between power systems has been also explored in [Kumar89].

II.6. Development of SMES Technology

In this section, the development of SMES technology is discussed based on the studies, programs or projects undertaken by different groups and their conclusions starting from early 1970's to this date.

II.6.1. Early Years (1970-1985)

The concept of large SMES units was first proposed by Ferrier in 1970. He presented a single, large, centrally located SMES unit to satisfy all of the cyclic power requirements for the French utility. This idea was not pursued due to high capital and development costs.

Present day SMES programs development started with a study conducted by Peterson and Boom in 1972. They studied the fundamental interaction between an energy storage unit and an electric utility system through a multiphase Graetz Bridge. This study also included an evaluation of the stabilizing effects of the rapid response of the converter on load variations. In 1972, US Atomic Energy Commission asked Los Alamos National Laboratory (LANL) to determine the value of SMES compared to other technologies and to determine potential applications for utility systems. In 1976, a collaboration of the Los Alamos group and Bonneville Power Adm. (BPA) suggested the use of small rapid response energy storage unit to help stabilizing the power flow. They designed and constructed a 30MJ SMES coil to provide stability support to the BPA's pacific tie. To the date, it is the only instance of a SMES coil fully connected to a utility grid. Los Alamos National Laboratory developed a single tunnel designed 1 GWh SMES unit in 1980. A year later, EPRI initiated a study to evaluate the technology. Japanese researchers have also evaluated the status of the SMES technology and discussed future projects starting mid 1970s.

Several results can be drawn from the early efforts to develop SMES devices.

- The main purpose of early SMES efforts was to develop a diurnal large scale SMES for load leveling utility generation facilities to minimize the use of fossil powered peaking units after the realization of nuclear era and oil crisis in early seventies.
- A SMES design incorporating a conventional cold support structure is uneconomical. A warm support structure is more cost effective for large units.
- Larger size units ranging from 1 to 5GWh could be economically competitive (i.e. the cost of a 5000 MWh/1000 MW SMES unit built in rock or earth would cost between 1 and 1.5 billion 1985 U.S. Dollars).
- To provide stability support for the BPA's system, a 30 MJ small-scale unit was commissioned at the BPA's Tacoma substation for one year until another less cost solution replaced the SMES system.

II.6.2. The Last 15 Years (1986-Present)

Since 1986, several SMES projects were carried out throughout the world. This section summarizes the resulted studies/projects at present (tabulated in Table II.5), and two of those are discussed in detail. Ongoing projects are given in the next section.

Engineering Test Model*:* In 1986, EPRI proposed the construction of an Engineering Test Model (ETM) as a solution to the dilemma of how to build large-scale warm structure test device. A year later, the Strategic Defense Initiative (SDI) office and EPRI have jointly initiated a program to design and built the ETM. This project was to serve two functions: 1) to provide a power source for free electron laser project (11.1 MWh/400MW) 2) to serve as a 2 hour load leveling storage device (20MWh/10MW) for a host electric utility. Two teams leaded by Bechtel and Ebasco were formed to develop a detailed design, improve cost estimates and develop hardware components for the ETM. The two proposed designs had shared only a few features, otherwise they were functionally and structurally different. Both teams developed earth supported SMES device operated in Helium and with self-protection scheme. One team developed a cable in conduit NbTi conductor (CICC), while the other one

used a traditional monolithic NbTi conductor. Although this project had to be canceled due to lack of funding and other uncertainties, an important outcome was resulted out of this program. It was the realization that the self-supported SMES device is cheaper than the earth-supported equivalent for stored energies up to 1000MWh. CICC design can satisfy several functional requirements with a single structure in a cold structure design.

Table II.5: Projects (1986-present) [Giese98]

Year (19-)	***Project or Study name***	***Storage/Power***	***Status/Conclusion***
86	Engineering Test Model (ETM)	11.1MWh/ 400 MW 2) 20 MWh /10 MW	Canceled, lack of funding, uncertainties
91	MITI/ISTEC SMES Project, Tokyo	100 kWh/40 MW, later 10MWh	Built and successfully tested
93	BWX Spinning Reserve Project	0.5MWh/31.5MW	On hold, lack of funding
93	Hydro Quebec Simulation Study	278kWh	Decision of not to built the device due to its cost
94	Siemens Spinning Reserve Study	2MWh/125MW	No funding to build the device
93	ABB Train Study	250kWh/ 20MW	Not proceeded, lack of funding
95	Japanese MAGLEV /study	5.6MWh/75MW	Not proceeded
91	Japanese Office Building	64.MWh1.4MW	Not proceeded

BWX Spinning Reserve Project*:* A project funded by Anchorage Municipal Light and Power System (AML&P) and Defense Advanced Projects Research Agency led by BWX Technologies, Inc. to provide short-term spinning reserve for AML&P. A preliminary design study showed that an energy storage device with 0.5MWh/31.5MW specification would satisfy the spinning reserve requirement. In addition to providing spinning reserve, several potential applications such as VAR compensation, system stabilization were identified with more detailed SMES design analysis. As the design was finalized, funding difficulties led the project to be placed on hold.

II.6.3. Ongoing SMES Projects

Tables 6 and 7 give ongoing low temperature and high temperature SMES projects throughout the world. Among these projects, there are only two SMES projects aimed for transmission level applications. Others are all micro level SMES devices characterized by high power and short duration (1 second or less) and a relatively small storage capacity (around 1MJ). There are a few μSMES devices designed with high temperature superconductors.

Table II.6: Ongoing Low Temperature SMES Projects [Giese98]

Organization	*Power (MW)*	*Energy (MJ)*	*Status*
FZK-Germany	0.21	0.250	Demo
FZK/DESY - Germany	15	0.220	First of a kind
TUM - Germany	4.14	1	Prototype
ENEL - Italy	NA	4	Prototype
KAN –-Japan	0.14	1.2	Experimental
KYU - Japan	1	3.6	Prototype
ISTEC - Japan	40	360	Pilot
DU –-Korea	NA	0.5	Prototype
KERI - Korea	0.76	0.7	Prototype
EI - Russia	NA	0.2-1	Experimental
TI - Russia	NA	5	Prototype
ASINEL -Spain	0.5	1	NA
BWX - USA	96	100	Demo
IGC - USA	0.75	6	Commercial
SI - USA	2	3	Commercial

Table II.7: Ongoing High Temperature SMES Projects [Giese98]

Organization	*Power (kW)*	*Energy (kJ)*	*Status*
TAM - Finland	32	5 – 10	Demo
EDF- France	NA	1000 and up	NA
EUS – Germany	20	8	Prototype
BIU - Israel	69	1	Prototype

As can be seen, there is a tendency to use micro-level low-temperature SMES devices. In order to promote the use of SMES devices on the electric utility grid, collaboration between US. Team (Bechtel) and German team (Siemens) has been coordinated.

The use of distributed SMES (D-SMES) was proposed by American Superconductor (Previously known as Superconductivity Incorporation) to provide voltage support and relieve instability problems in a transmission grid of Wisconsin Public Service (WPS) Corporation. The proposal was to adapt the SMES technology by placing multiple micro-SMES units at key substation locations to inject real and reactive power to the grid responding independently and as required. WPS agreed that the use of D-SMES would provide very good performance at a lower cost than the other options under consideration [Borga99].

II.7. Comparison between SMES and Other Energy Storage Devices

As with any technology trying to find its widespread acceptance and commercialization, the new technology either has to represent a breakthrough in its functionality and capabilities irrespective to cost, or has to match the performance of a conventional technology at a lower cost. SMES seems to fall in the first category. In order to distinguish its benefits and capabilities from other energy storage technologies, four selected energy storage devices (Pumped hydro, compressed air, batteries and flywheels) are briefly described below.

Pumped Hydro storage energy is potential energy represented by a body of water at a relatively high elevation. The water is elevated with a motor/pump during periods of low

electric power demand. Dropping the elevation to allow water flow through hydroturbines at a lower elevation produces the electrical energy. The round trip efficiency is greater than %60. Due to its massive mechanical assemblies, it responds slowly, typically minutes. It requires two reservoirs at different elevations, which makes it difficult to find suitable sites.

Compressed Air is stored by a compressor that is supplied by energy generated during periods of low electric power demand. When electric power demand nears peak, the compressed air is released to turn a combustion turbine. Since it also consumes fuel, the efficiency of the device can not be given directly. But compared to gas turbines, its efficiency is approximately 70%. It operates either full ON or full OFF. Its response to demand is typically in seconds. Finding sites and storing air without significant leakage limit the potential use of these devices.

Batteries store energy in electrochemical form. A series of low-voltage/power battery modules connected in parallel and series to achieve desired electrical characteristic forms the battery system. Battery energy storage is one of the most cost effective energy storage [Schoe96]. Batteries require an ac/dc power conversion unit. Modular type small batteries with advanced power electronics technologies can provide four-quadrant operation along with rapid response. The round trip efficiency of batteries is approximately 80%. Due to chemical kinetics involved, they can not handle high power for long periods. Rapid deep discharges may eventually lead to replacement of the battery, since this kind of operation reduces battery lifetime [Giese98, Luong96]. There also exist environmental concerns related to battery storage because it generates toxic gas during charging and utilize hazardous materials presenting potential disposal problems.

Flywheels store kinetic energy within a rotating mass driven by a motor/generator. A PCS is used to drive the motor/generator. Like batteries, flywheel systems are also modular and low cost. Like SMES, they have high efficiency, have the ability to absorb and supply both reactive and active power, and responds rapidly to power demand. However, charging and discharging at very high power require large torque to be generated, which may result in increased complexity and cost. Since they involve parts that rotate at very high speed, low reliability and high maintenance are the concerns of this technology.

At present, both hydro pump and compressed air are commercial technologies, several test sites incorporating batteries have been demonstrated. SMES systems have found its commercial applications in the area of power quality, though most of them are still under construction. Advanced flywheel storage incorporating HTS bearings is in the development stage [Giese98].

Without any doubt, the cost of SMES is currently high, compared to the above described storage technologies. However, SMES systems have a unique advantage in two types of application. The first type is the transmission control and stabilization since SMES can respond to power demand very fast and can handle high power demand for longer periods. The second type is the power quality application where SMES can easily be sited near industrial loads.

II.8. Present Realization and Future View

The conditions that boosted the need for large-scale energy storage and SMES no longer exist. Those conditions envisioned 30 years ago are very different from today's conditions. SMES is not now seen as energy storage but as a new tool to help utilities in the competitive market [Luong96]. The SMES devices with the power ranges of 20 – 200MW and the energy ranges of 50 – 500 MJ are considered cost effective. The applications of this range include transmission stability, frequency control, and custom power/power quality [Ribei99].

As the electric power industry is undergoing restructuring and deregulation, many utilities are facing an uncertain future that may make them reluctant to fund development of new technologies. On the other hand, deregulation puts additional burdens on electric power systems, and makes the system more prone to a stressed and congested operation. As these scenarios are often faced by the utilities, which may bring out new opportunities for advanced technology candidates to be adapted. SMES has the capability of providing desired characteristics, therefore could be useful increasing the flexibility of the power system.

Although many studies showed SMES capabilities and benefits, SMES has not fully emerged from a developmental stage to become commercial due to its cost attributes. These

attributes vary depending on the applications. HTS SMES coils may eventually be adopted, but not until their cost and technical performance are improved. Constructed small scale LTS SMES devices and government funded HTS projects may lead to emergence of additional markets for SMES devices [Giese98, Luong96].

Several cost effective SMES applications can be mentioned here. Distributed SMES concept shows potential future to help transmission grid. Integration of SMES with wind power or photovoltaics can be used to supply electricity to remote conditions. Although its cost effectiveness has not been proved, SMES also has been proposed to incorporate it with HVDC and LVDC systems. Further study is needed in this area. Another application can be integration of SMES with an existing second-generation FACTS device. This application can increase the performance of the FACTS device, and reduce the cost for the power conversion unit needed for the SMES. The study presented in this work shows that an integration of SMES with a static synchronous compensator can be very effective in damping power oscillations. The combined compensator can be used in two ways, either StatCom operating alone to provide reactive power voltage support or StatCom-SMES operating to provide additional benefits due to real power injection/absorption.

CHAPTER III

POWER ELECTRONICS CONVERSION AND CONTROL OF SMES

Power electronics can be defined as the use of solid state devices to control and convert/process electric power. It supplies voltages and currents in a form that is desirable for user loads [Mohan95]. As a consequence of the advances in power electronics technology, power electronics has found its applications in power system, spreading out to all voltage levels [Ieeew99]. Emerging power electronics applications are given in Table III.1.

Table III.1: Emerging Power Electronics Applications [Carro98]

Power System Segment	***Applications (Typical Power Ratings (MW))***
Generation	VARspeed (30), Local Generation (2)
Transmission/Distribution	Static Compensator (100), Unified Power Flow Controller (200), Energy Storage/UPS (1-100), Short dc Link (50)
Industry	StatCom (100), Intertie (2-300), Energy Storage/UPS (1-100)
Traction	StatCom (100), Static Breaker (5-30), Energy Storage/UPS (1-100), Intertie (2-300)
Power Quality	Dynamic Voltage Restorer (2-30), Energy Storage/UPS (1-100), Transfer Switch (5-30), Static Breaker (5-30), Active Filter (1-30)

The importance of energy storage applications of power electronics can be noticed from this table. One of the viable energy storage systems is SMES. The power electronics interfaces between a superconducting coil and the ac power system, and it is called a SMES power conversion/conditioning system (PCS). A PCS is expected to transfer energy into or out of the SMES on command, to control real and reactive power, and to be able to bypass the coil when there is no need for energy into or out of the coil [Kustom91, Lasse91, Han93].

A number of converter/inverter circuit topologies have been developed to operate SMES. Certain factors such as semiconductor device types, switching technologies, system configuration and reactive power requirement have been considered/evaluated for a PCS design. These factors will be addressed in the following sections.

III.1. Semiconductor Device Types

Power semiconductor devices are at the heart of power electronics circuits. The selection of an appropriate device affects the reliability and efficiency of overall. The following device requirements are considered in high power device selection [Carro98].

- Low devices cost
- Rugged operation, modularity ,and high reliability
- High current (turn-off, rms, average, peak), high voltage (peak repetitive, surge, dc-continuos)
- Fast switching, high frequency and low conduction and switching losses

There has been tremendous progress in device technology. Although natural commutated devices were initially used in power conversion of SMES systems, they were replaced by high power forced (self) commutated semiconductor devices. The latter ones offer more controllability and flexibility. Available semiconductor devices are shown in Table III.2.

Table III.2: Available Self-Commutated Semiconductor Devices

Thyristors	***Transistors***
GTO (Gate Turn-Off Thyristor)	BIPOLAR TRANSISTOR
MCT (MOS-Controlled Thyristor)	DARLINGTON TRANSISTOR
FCTh (Field-Controlled Thyristor)	MOSFET
SITh (Static Induction Thyristor)	FCT (Field Controlled Transistor)
MTO (MOS Turn-Off Thyristor)	SIT (Static Induction Transistor)
EST (Emitter-Switched Thyristor)	IEGT (Injection Enhanced Gate Transistor)
IGTT (Insulated Gate Turn-off Thyristor)	**IGBT** (Insulated Gate Bipolar Transistor)
IGT (Insulated Gate Thyristor)	
IGCT (Integrated Gate-Commutated Thyristor)	

Among those shown in Table III.2, the present-viable devices for high power applications are GTO, IGBT, and IGCT. A brief description and capabilities of these devices are given below.

A ***GTO*** is a four-layer thyristor with a turn-off capability. Current is conducted by applying a positive gate signal and positive voltage, and is terminated by applying a negative gate signal. To provide the energy for turn-on and off functions, a snubber circuit is used. For high power applications, excessive voltages are produced during turn-off, therefore the snubber parameters should be selected carefully. GTOs have been developed in during 1980s. Their current and voltage handling capabilities are very high, but they have slower switching speeds, higher losses and higher costs than conventional forced commutated thyristors.

An ***IGCT*** is an improved GTO device. Its substantial improvements include the low inductance gate drive, raggedness of thyristors, the change of turn-off process (hard switching) and the inverse diodes. The IGCT technology offers higher switching rates of transistors, and reduced switching losses. . The higher rate of gate current change vastly improves minimum on and off times. More uniform turn-on characteristics and faster turn-off times make IGCT devices ideal for series connection without significant derating or parametric selection.

An ***IGBT*** is a device that is part way to being a thyristor, part way to latching stays as a transistor. It contains an integrated MOS structure with insulated gate. They are fairly new developments for high power applications. Like transistors, they potentially have the ability to limit current flow by controlling the gate voltage. Their turn-on and turn-off actions are faster, but their power handling capability is lower than GTOs and IGCTs.

Present power rating of GTO, IGCT, and IGBT are 6kV/6kA, 4.5kV/3.3kA, and 3.3kV/1.2kA, respectively [Bernet98]. Although IGBT and IGCTs are considered to be foreseeable future devices, GTOs are well established and employed devices. Therefore, the simulation work presented in this dissertation uses GTO devices for the power electronics interface.

III.2. Power Electronics Inverter Types for SMES

Two basic types of inverters, current-sourced inverters (CSI) or voltage-sourced inverters (VSI) are commonly used for the power conversion unit between SMES and ac power system. Basic concepts of these inverters are schematically drawn in Figure II.1. From this figure, it seems that a CSI is more appropriate for SMES applications since SMES is also a current source. But, there are applications where VSI based FACTS controllers are used in power systems, and attachment of SMES devices can improve the effectiveness and capability of overall system. Both CSI and VSI are described with their circuit topologies, switching schemes and applications. *Since the SMES coil studied in this work is being build for a FACTS application, VSI along with a dc-dc chopper interface are detailed more.*

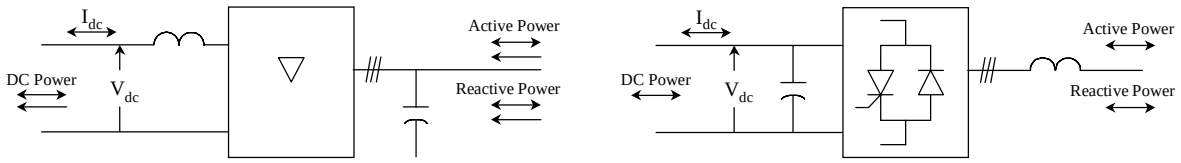

a) Current Source Inverter b) Voltage Source Inverter

Figure III.1: Basic Concepts of Current and Voltage Source Inverters [Hingo00]

III.2.1. Current Source Inverters

As can be seen from Figure II.1.a, a CSI consists of a power electronics block, a large inductance on the dc side, and capacitor or filter on the ac side. While the inductor maintains constant dc current, ac capacitors provide a stiff ac bus for supplying the fast changing current pulses needed for the commutations. The dc current flow is maintained in one direction, and the power flow direction can be changed by reversing the dc voltage. The power electronic block can be either a line commutated diode based, or line commutated thyristor based or self commutated turn-off devices.

The operating principle of a 3-phase 6-pulse CSI consisting of thyristor or turn-off devices controlled by a firing circuit can be explained as follows: Positive gate signal

initiates the current conduction at a prescribed time and 16ms-cycle sequence to maintain the desired average voltage across the coil. By changing the firing angle (α), the variation from the maximum positive value to the maximum negative value of voltage across the coil (V_o) can be obtained. The average voltage and real and reactive powers (P and Q, respectively) are expressed as follows:

$$V = V_0 \cos\alpha$$
$$P = P_0 \cos\alpha$$
$$Q = Q_0 \cos\alpha$$

The development of CSI for SMES conversion units is summarized in Table III.3. As a result of this table, independent control of real and reactive power in a wide range and fast response can be achieved by using turnoff devices. Harmonics can be eliminated using PWM scheme. A fast response and wide range power controllability is essential for the stabilizing mode of SMES.

Table III.3: Summary of CSI Development for SMES

Converter Type	***Comments***
12 pulse thyristor based CSI (Graetz Bridge) [Hasse89]	The first used CSI for SMES, generates large reactive power resulting in higher MVA rating, and limits the range of simultaneous control of real and reactive power (2-quadrant operation).
Hybrid Thyristor/GTO CSI	Can provide a four-quadrant independent controls of power, generates large amount of harmonics and does not improve power factor in a wide range.
6-pulse GTO CSI connected in series [Hassa93]	Studied for the ETM project, allows independent control of real and reactive power resulting in significant reduction in the converter MVA, requires more GTO and higher rated transformer due to harmonic currents (compared to VSI). A hybrid CSI is shown in Figure III. 2
12 pulse GTO converter [Ise86, Shira94]	Faster response and a wider range of power control characteristics, reduce reactive power requirement
GTO-PWM circuited CSI [Shira94]	Reduces the magnitude of the ac current harmonics of SMES, cause switching losses.
12 Pulse GTO and tap changed transformer [Han93]	reduction of system rating and an independent control of real and reactive power by regulating ac voltage through the tap changed transformer
IGBT based CSI [Giese98]	Faster response

III.2.2. Voltage Source Inverters

A VSI is comprised of a turn-off device based converter, a dc link capacitor, and inductance on the ac side. The large capacitance ensures that the voltage is unipolar. It also handles sustained charge/discharge current. An inductive interface is needed to ensure that the dc link capacitor is not short-circuited. It should be noted that the VSI must have bi-directional valves (Combination of a turn-off device and diode) to allow current flow in either direction. Furthermore, there is no need for reverse voltage capability of the turn-off devices, since the dc voltage does not reverse.

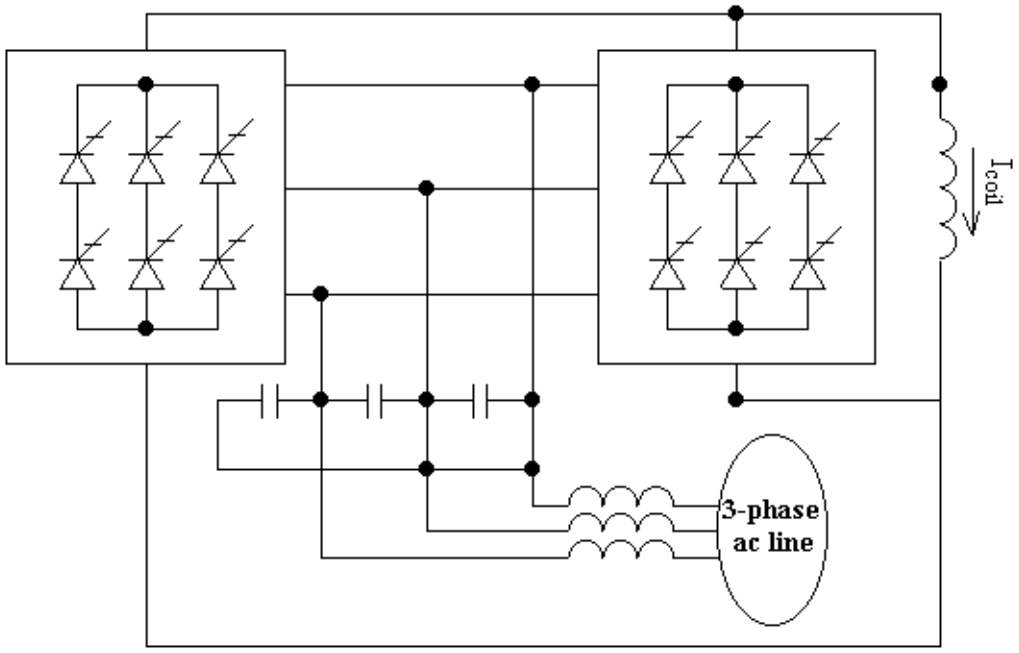

Figure III.2: The Configuration of Hybrid CSI

A three phase two level VSI operates by turning on or off per device per cycle. The ac output voltage can be controlled by varying the width of the voltage pulses, and/or the amplitude of the dc bus voltage. Due to the nature of converters, harmonics are present. To reduce harmonic magnitude, either a multi-pulse VSI with 180-degree conduction or a three-phase PWM schemes are utilized. PWM scheme has not been justified for high power

converters due to the switching losses [Hingo00]. A three-leveled converter may allow changing ac voltage without changing the dc voltage to some extent.

The use of VSI for SMES applications has been proposed for the ETM project [Lasse91, Hassa93]. A 24-pulse VSI and a two-quadrant multi-phase dc-dc chopper for SMES has been introduced. The VSI and the chopper are linked by a dc link capacitor that behaves as a stiff but controllable dc voltage source providing the desired characteristics. A three-phase VSI and single-phase chopper connection is illustrated in Figure III.3. VSIs can provide continuous rated capacity VAR support even at low or no coil current whereas CSIs is dependent of coil in providing VAR support.

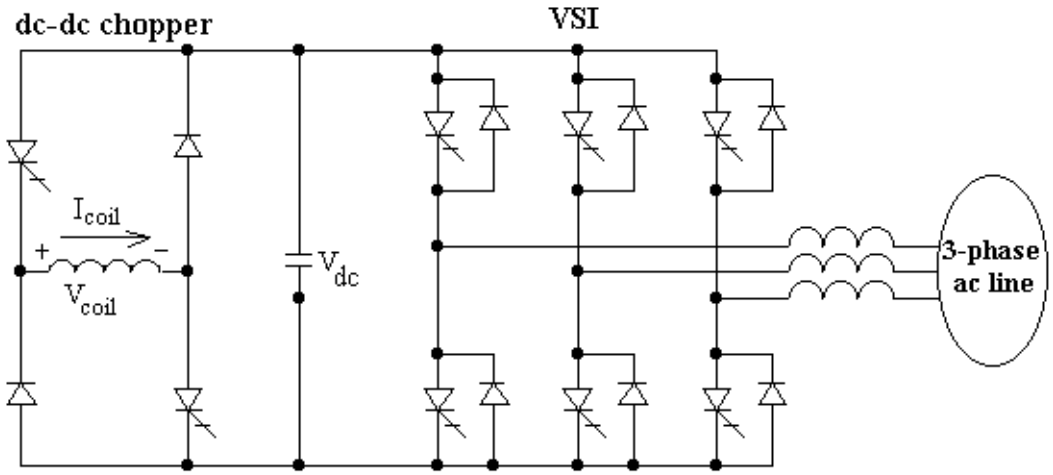

Figure III.3: VSI/dc-dc Chopper Configuration for SMES

III.2.3. FACTS Controllers

FACTS controllers can be CSI or VSI topologies that can rapidly influence transmission system parameters to enhance controllability and increase power transfer capability. From overall cost point of view, VSI based controllers are preferred over CSI controllers. FACTS controllers (Table III.4) can vary transmission system impedance, voltage and angle, and they can provide the following attributes.

- Voltage, current and reactive power control

- VAR Compensation
- Damping oscillations
- Voltage, transient or dynamic stability
- Automatic generation control
- Current or voltage limiting

Table III.4: FACTS Controllers [Hingo00]

Categories	***Varied parameters***	***Controllers***
Series Controllers	impedance, angle	Thyristor Controlled Series Capacitor (TCSC) Thyristor Controlled Series Reactor (TCSR) Thyristor Controlled Voltage Regulator (TCVR) Static Synchronous Series Compensator (SSSC)
Shunt Controllers	impedance, voltage	Static VAR Generators (SVG) Static VAR Compensators (SVC) Static Synchronous Compensator (StatCom)
Combined series-series Controllers	voltage, impedance, angle	Interline Power Flow Controller (IPFC)
Combined series-shunt Controllers	voltage, impedance, angle	Unified Power Flow Controller (UPFC) Thyristor Controlled Phase Shifting Transformer (TCPST)

While a combination of a StatCom or SSSC with energy storage such as batteries, SMES has been proposed in theory and recognized as a FACTS controller with added dimension, the development of this combination has lagged far behind that of traditional FACTS. One of the objectives of this dissertation is to study the integration of a StatCom with SMES.

III.3. Attachment of SMES to a StatCom

SMES, one of the viable energy storage, can be combined with a StatCom to add another dimension to the controllability of the StatCom-alone. A StatCom is a VSI based converter, and it can absorb or inject desired VAR at the point of connection by adjusting the phase angle between inverter and line voltage. The role of a dc link capacitor in a StatCom is not to

generate/absorb reactive power but to establish a way to allow a ripple current flow generated in the ac output (Gyugy94, Schau97). The inverter operates in such a way that three reactive power currents can freely flow between its valves.

III.3.1. StatCom Modeling and Control

A simplified equivalent circuit of a StatCom is shown in Figure III.4. This figure is used to explain the power control and to derive the mathematical model of the VSI based controller.

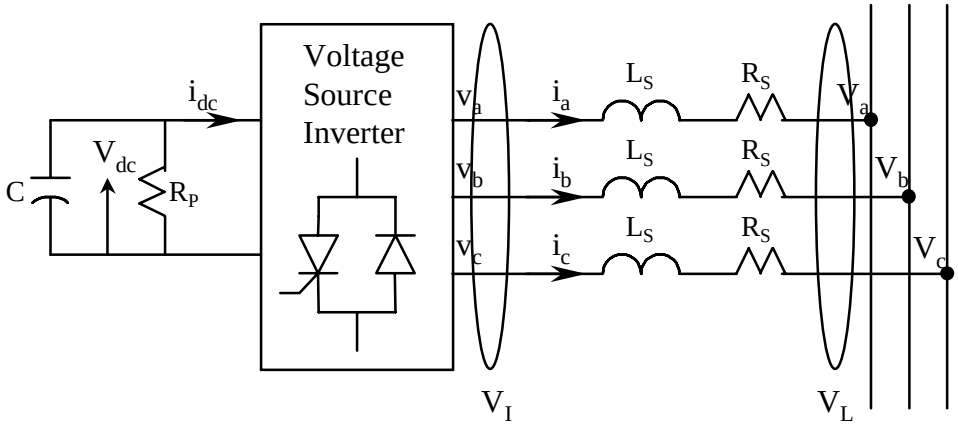

Figure III. 4: Equivalent Circuit of StatCom

The three phase real (P) and reactive power (Q) can be expressed as follows:

$$P = \frac{V_L V_I \sin\delta}{X} \qquad and \qquad Q = \frac{V_L(V_L - V_I\cos\delta)}{X} \qquad (V_I = kV_{dc})$$

where V_L is the ac system line voltage, V_I is the inverter output voltage, V_{dc} is the dc link capacitor voltage, δ is the angle between V_L and V_I or inverter firing angle, X is the transformer leakage reactance , and k is a constant showing the relationship between V_I and $V_{dc,}$ dependent of the pulse number of the inverter.

A StatCom can only generate or absorb reactive power by controlling the relative magnitudes of the dc link capacitor and the ac system voltage, and in the meantime keeping δ

to be zero to maintain no real power flow. With the addition of SMES, four-quadrant real and reactive power control is achieved.

[Schau93] gives the vector analysis and control of StatCom based on Figure III.4. The equivalent circuit equation in terms of instantaneous variables is derived. Three-phase quantities are written in rotating reference frame for its simplicity and easiness in deriving the transfer functions needed for control system synthesis. Vector representations of instantaneous three-phase variables, orthogonal co-ordinates and rotating reference are demonstrated in Figure III.5.

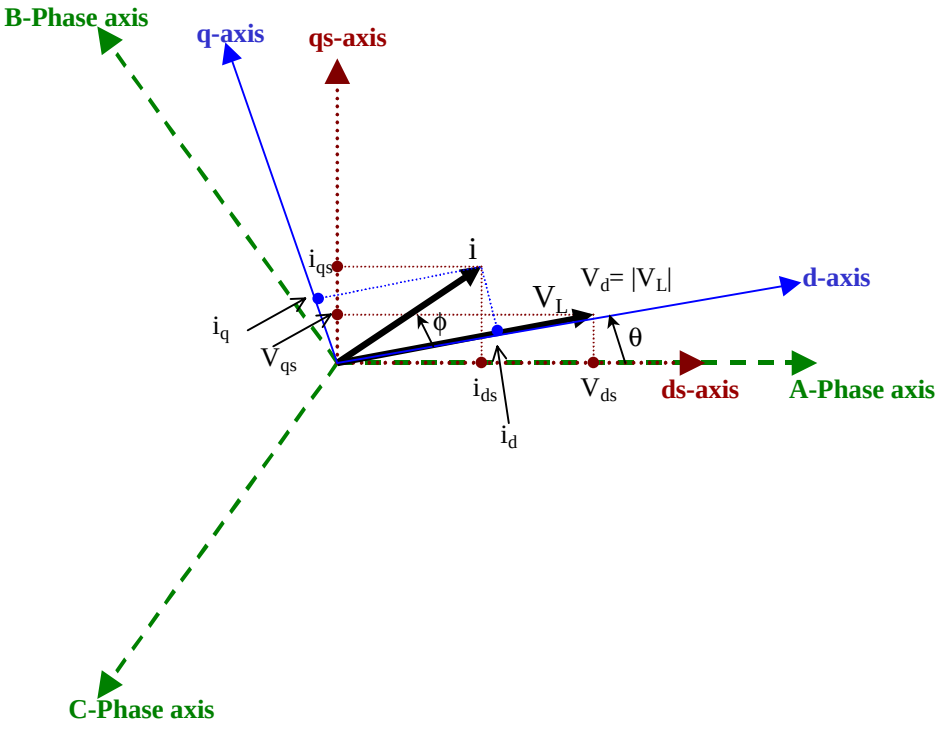

Figure III. 5: V-I Characteristics in Different Reference Co-ordinates

The ac side circuit equations can be written in terms of instantaneous variables as follows:

$$\frac{d}{dt}\begin{bmatrix} i_a^{'} \\ i_b^{'} \\ i_c^{'} \end{bmatrix} = \begin{bmatrix} \frac{-R_s^{'} w_b}{L^{'}} & 0 & 0 \\ 0 & \frac{-R_s^{'} w_b}{L^{'}} & 0 \\ 0 & 0 & \frac{-R_s^{'} w_b}{L^{'}} \end{bmatrix} \begin{bmatrix} i_a^{'} \\ i_b^{'} \\ i_c^{'} \end{bmatrix} + \frac{w_b}{L^{'}} \begin{bmatrix} (v_a^{'} - V_a^{'}) \\ (v_b^{'} - V_b^{'}) \\ (v_c^{'} - V_c^{'}) \end{bmatrix}$$

where all prime variables correspond to per unit variables. This equation can be transformed to the synchronously rotating reference frame and combining this with the dc-side equations, the following equation is obtained.

$$\frac{d}{dt}\begin{bmatrix} i_d^{'} \\ i_q^{'} \\ V_{dc}^{'} \end{bmatrix} = \begin{bmatrix} \frac{-R_s^{'} w_b}{L^{'}} & w & \frac{k w_b}{L^{'}}\cos(\alpha) \\ -w & \frac{-R_s^{'} w_b}{L^{'}} & \frac{k w_b}{L^{'}}\cos(\alpha) \\ -\frac{3}{2}kC^{'} w_b \cos(\alpha) & -\frac{3}{2}kC^{'} w_b \sin(\alpha) & \frac{-w_b C^{'}}{R_p^{'}} \end{bmatrix} \begin{bmatrix} i_d^{'} \\ i_q^{'} \\ v_{dc} \end{bmatrix} - \frac{w_b}{L^{'}} \begin{bmatrix} |V_L| \\ 0 \\ 0 \end{bmatrix}$$

where $v_d^{'} = kV_{dc}^{'}\cos(\alpha)$, $v_q^{'} = kV_{dc}^{'}\sin(\alpha)$, $w = \dfrac{d(\tan^{-1}(\frac{V_{ds}}{V_{qs}})}{dt}$, $V_d = |V_L|, V_q = 0$; and k is a factor which relates the dc side voltage, $V_{dc,}$ to the peak of the phase to neutral voltage at inverter ac terminals, $\sqrt{2}V_I$.

In a StatCom control, there are two control blocks: Internal control is the one generating gating commands to the inverter switches in response to the demand for reactive/real power reference signal. External control is the second one providing these reference signals from the system variables and desired system operation, which determines the functional operation of the StatCom. Utilizing direct or indirect approaches can provide internal control. The first one regulates the desired reactive power by controlling the dc capacitor voltage, V_{dc} (or the angle of output voltage, V_I), whereas the latter one utilizes PWM technique to vary the magnitude and angle of the output voltage, in the meantime keeping the dc voltage constant. The dynamic study presented in Chapter VI uses the indirect approach.

III.3.2. Chopper-SMES Modeling and Control

Since the SMES coil is a current source device, another electronics interface is needed to control the voltage across the coil (to attach the coil to a voltage source inverter). This interface is called a dc-dc chopper. [Lasse91a] states that the dc-dc chopper reduces the ratings of the overall PCS by regulating the current to the converter and allows a harmonic free and a smooth transition operation from charge to discharge mode. In a single-phase dc-dc chopper shown in Figure III.3, while the two turn-off devices (hereafter referred to as GTOs) are fired simultaneously and the diodes are reverse biased to charge the coil, the GTOs are turned off and the diodes become forward biased to discharge the coil. Adjusting the duty cycle of GTOs can regulate the coil voltage, and control the rate of charge/discharge. The following voltage and current relationships exist within the chopper.

$$V_{coil} = [1-2d]V_{dc}$$
$$I_{dc} = [1-2d]I_{coil}$$

where V_{coil} is the average voltage across the SMES coil, I_{coil} is the coil current, V_{dc} is the dc link capacitor voltage, V_{coil} is the average VSI dc current, and d is the GTO conduction time over the period of switching cycle or duty cycle.

These relationships can be interpreted as follows [Hassa93, Skile96]:

Condition	***Status***
d>0.5	Coil is charging
d<0.5	Coil is discharging
d=0.5	Coil is on standby

In multiphase dc-dc choppers, small inductors are placed at the output of each chopper phase to allow current sharing. The low order ripple frequencies may exist in the chopper output voltage and input current. Since the lowest ripple frequency is the chopper switching frequency times the number of chopper phases, either the use of fast switching device such as IGBT or the use of multiphase chopper can eliminate the low-order ripples. A bypass switch connected across the coil may serve several purposes:

- to reduce energy losses when the coil is on standby,

- to bypass dc coil current if utility tie is lost, and
- to remove inverter from service, and protecting the coil if cooling is lost.

The overall objective of the StatCom-SMES control strategy is to meet real and reactive power demand at all levels. Real and reactive power flow can be regulated either by firing angle control of the converters or pulse width modulation (PWM) control of GTO converters; the latter one is considered to be effective in reducing the magnitude of the ac current harmonics in SMES. The control strategy used on the ETM project can be given as an example; it is based on constantly adjusting the dc-dc chopper duty cycle and the voltage source converter firing angles to maintain the dc link capacitor voltage and meet real and reactive power demand at all levels [Hassa93].

CHAPTER IV

TRANSIENT MODELING OF A DISK TYPE SMES COIL

IV.1. Electromagnetic Transients in SMES Systems

IV.1.1. A Brief Overview of Electrical Transients

Electrical transients in power systems can be generated either during normal operating conditions such as opening or closing operation of switches/breakers or abnormal operating conditions such as electrical faults, and physical phenomena such as lightning strikes. Most power system transients are considered to be oscillatory in nature, thus they are characterized with the frequency of oscillation. A classification of power system transients based on frequency of oscillation is given in Table IV.1.

Table IV.1: Classification of Power System Transients [Melio93]

MODE	*FREQUENCY(Hz)*	*EVENT*
Electromechanical Phenomena	.001	Load Frequency Control
	.01	
	.1	
	1	Transient Stability
	10	Stabilizer
	10^2	Short Circuits, Sub-synchronous resonance
Electromagnetic Phenomena	10^3	Harmonics, Power Conversion Phenomena
	10^4	Switching Transients
	10^5	
	10^6	Traveling Wave Phenomena
	10^7	Transient Recovery Voltage

Transients take place in a very short period of time, but they are capable of causing flashovers, insulation breakdowns as a result of high transient voltage and current. Overvoltages and overcurrents may affect the reliable operation of the overall power system. A good modeling and analysis of transient behavior of a device is essential to predict overvoltages that may damage the system. Any physical power system element can be

represented either with a lumped or distributed parameter model. Analyses of these models employ three methods [Green91]: graphical method, analytical method, and digital computer program method. The computer programs use ordinary analytical methods such as time and frequency domain solutions, and can process enormous amounts of data in a systematic way and short period of time. The fast comprehensive computer program called Electromagnetic Transient Program (EMTP) has been developed by H.W. Dommell at the Bonnevile Power Administration in the late 1960s. This program performs transient analysis in a methodical and efficient manner [Green91]. The capacity and the functionality of the program have been improved since then. Several electromagnetic transient simulation tools were developed. [Domme97] One of these tools is the PSCAD^{TM}/EMTDC^{TM} (Power Systems Computer Aided Design/ Electromagnetic Transients for dc) program developed by Manitoba HVDC Research Center. The feature of a very sophisticated graphical interface allows the user to assemble the circuit and observe its behavior while the simulation is proceeding [Manit88, Dugan96, Nayak95]. This advanced program has been used to simulate the electromagnetic transients interaction between SMES and it power electronics interface, dc-dc chopper.

As can be seen from Table IV.1, most power system transients in the frequency range is between 1 Hz – 1 MHz [Melio93]. For low frequency range simulation (from DC up to several kHz), general built-in models in electromagnetic transient simulation programs such as EMTP^{TM}, EMTDC^{TM} can be used [Manit88]. For high frequency transient studies such as the study of impulse propagation in a component, a more detailed modeling of the component is necessary [Melio93, Green91].

Several types of switchings such as load switching, electric faults, capacitor switching and transformer energization may cause to generate severe transients. These transients should be well-evaluated in order to predict and determine protection to overvoltages or overcurrents. The basic principles of overvoltage protection can be classified as follows [Dugan96]:

a) Limiting the voltage across sensitive insulation

b) Diverting the surge current and thus preventing the surge entering the load

c) Bonding ground references together at the equipment

d) Creating a low pass filter across the sensitive load to limit high frequency transients.

To limit switching based transients, transient voltage surge suppressers (or surge arresters) have been developed. These devices should be located as closely as possible to the critically insulated equipment. Surge arresters are characterized by a voltage-current (*V-I*) curve, which indicates that the device will never allow the voltage to exceed the value of permissible voltage level. Due to the closeness of its characteristic to ideal protective device's characteristic, metal oxide varistors (MOVs) are the most favored surge arresters. MOVs use zinc oxide as a metal oxide material. Maximum continuous operating voltage (MCOV, 15-30% higher than its rated voltage) and energy handling capability measured in kJ are the two parameters used mostly. Its *V-I* characteristics are practical for manufacturers and utilities. A typical *V-I* characteristic of an MOV shown in Figure IV.1 can be explained as follows [Ekstro89]:

- In the region below 10^{-2}A current, the material changes with the temperature, therefore it may experience thermal runaway due to heating.
- The voltage variation is very small in the range of currents from 10^{-3}-10^{4}A
- The curve turns upwards in the high current region, where the material shows its resistivity.

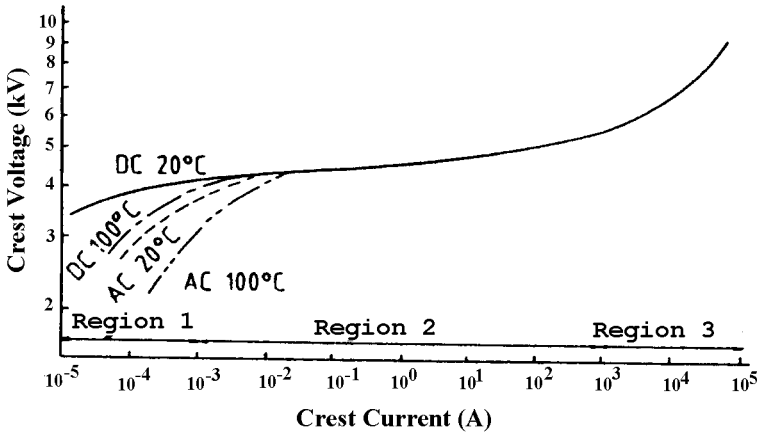

Figure IV.1: Typical MOV V-I Characteristics

IV.1.2. Transient Concerns in SMES

A SMES coil is subjected to transients originated from normal or abnormal PCS switching operations, or lightning and switching surges coming from the ac system. Transient overvoltages can endanger the insulation of a superconducting coil, especially in its cryogenic operating environment where the insulation characteristics are different from that at normal conditions. The transients may usually take place for a very short time as compared to the steady state, but have the potential to stress the coil insulation. The understanding of the transient behavior of a SMES coil is essential in the design of its insulation and transient suppression schemes. A SMES coil may experience unexpected failures if the behaviors of the transient overvoltages associated with the coil are not well understood. The design of SMES coil insulation and protection systems plays an important role in avoiding SMES coil failures.

Several studies conducted by German researchers (Miri95, Miri98] investigate the transient behavior of a large and micro-level superconducting coil. Large superconducting energy storage subjected to high power pulses was used for magnetic confinement in fusion, ITER (International Thermonuclear Experimental Reactor). A distributed coil model was constructed to predict overvoltages that can endanger the coil insulation. The coil comprises of dc self and mutual inductance and plate-to-plate and plate-to-ground capacitances along with the effective resistances. To calculate these parameters, the following formulas are used. The inductance matrix calculation is based on the formula of

$$A(r) = \frac{\mu}{4\pi} \iiint \frac{J(r')}{|r - r'|} dv'$$

where A is the magnetic vector potential, J is the current density vector, μ is the permeability in free space, r' is the position vector of the source point, r is the position vector of the field point, and dv' is the differential volume element in the inductor. Mutual inductances calculation uses the formula

$$M_{ab} = (J_b S_a S_b) \oint_{l_a} \int_{S_a} A_b dl_a dS_a$$

where M_{ab} is the mutual inductance between winding *a* and winding *b*, J_b is the current density in winding *b*, S_a and S_b are the respective cross-sectional areas, l_a is the vector differential element in direction of the current flow in winding *a* and A_b is the vector potential due to winding *b*. Distributed capacitance parameter calculation is based on the parallel plate formula. With these formulas, a detailed coil model was developed and internal voltage distribution of the coil was analyzed. Some of the main conclusions of these studies are as follows:

- Internal coil voltage can be higher than the terminal voltage if the coil is excited at resonant frequency
- The resonant frequencies could be much less for large superconducting coils depending on the winding structure.
- The damping of the transient oscillations at cryogenic temperature is weaker than in the normal conducting coil.

An analytic analysis of an insulation of breakdown for the KYU-Japan SMES has been carried out in [Hayas99]. The insulation damage was due to an abnormal high voltage generated by an accidental short circuit. The SMES coil used in this study was 1H, and it was modeled with its distributed electrical parameters. This study emphasizes the importance of the protection of large-scale SMES magnets against insulation damages.

IV.1.3. Coil Modeling Considerations

The integrity of the coil insulation structure is a major concern in the superconducting coil design, which can effect the reliable and economic operation of the entire SMES system. Having a geometrically large coil even makes the design more complex. In order to design the insulation structure of a winding, the transient voltage stresses to which all sub-components of the structure will be exposed must be known. The knowledge of frequency response of the winding is likewise essential in the coil insulation design.

A number of methods are available to determine these characteristics: direct measurement on the actual winding, direct measurement on an electromagnetic model of the coil, or building a mathematical model and determining the voltage distribution and frequency response by means a suitable computer analysis program. As explained in [Mcnut74] and [Degen77], the first two methods, with no doubt, give more reliable and accurate results than the mathematical analysis, but setting up a mathematical model is the most convenient and lowest cost method. Consequently, a greater variety of design alternatives and more detailed analysis can be achieved with the mathematical model of a winding.

The most detailed model is one in which every turn of the winding is represented with their self and mutual inductance (*L* and *M*), and the capacitance between adjacent turns (*Cadj*), axially separated turns (C*ax*) and turn to ground (C*g*). Due to high memory and computing cost, various degrees of simplification are necessary. The simplification methods are given in [Mcnut74]. According to [Abet53], relatively small number of frequencies is sufficient, therefore a distributed winding can be represented by an equivalent circuit of a finite but sufficient number of lumped elements. In this paper, it has been emphasized that mutual inductance must be included in transient analysis purpose modeling for more accurate solutions.

When a circuit is excited by an applied voltage, the steady state or transient behavior of the circuit is established by the location of the zeros and poles of the impedance function of the circuit in the complex frequency plane. By definition, the zeros coincide with the natural frequencies of the circuit. Series resonance occurs where the terminal impedance is at its minimum, and parallel resonance occurs where the terminal impedance is at its maximum [Abet53].

When a superconducting coil is simulated for a purpose of dynamic operation, it is a common practice to represent the coil with a big inductor. On the other hand, for transient analyses, the more detailed coil model representing disks, even turns, with associated mutual inductance and capacitance yields to more accurate results.

IV.2. Calculation of Electrical Parameters for a Disk Type Winding

An electrical lumped parameter model is constructed for a superconducting coil to determine voltage distribution and frequency response of the coil. A generic lumped parameter model is given in Figure IV.2. It is assumed that the coil consists of a number of disks (pancakes) comprising of a number of turns. Given the geometrical dimension of a coil, the following parameters need to be calculated for turns of the coil.

- Self inductance of a turn
- Mutual inductance between turns
- Capacitance between adjacent turns
- Capacitance between axially separated turns
- Capacitance between turn to ground

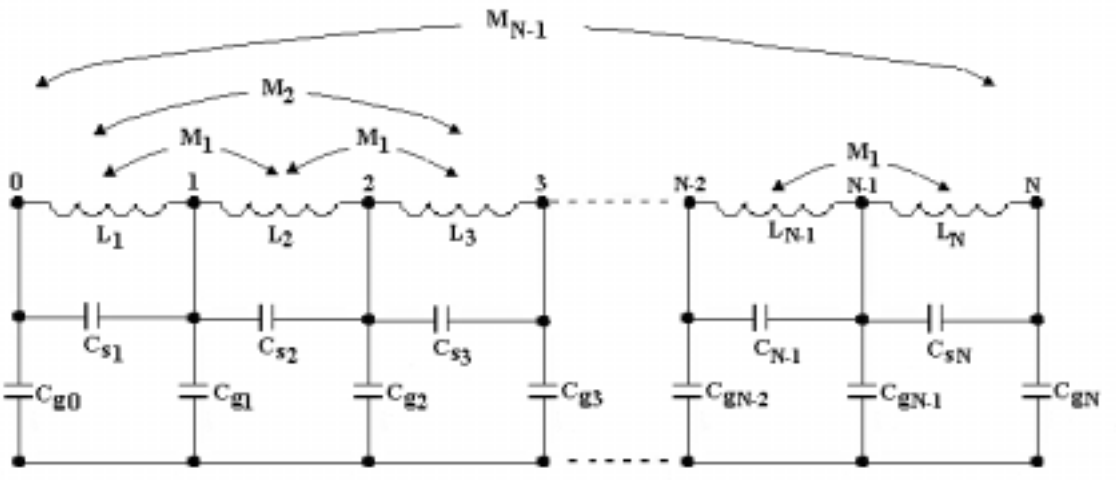

Figure IV.2: Schematic Representation of a Winding as a Lumped Circuit [Chowd94]

Cgi = Shunt Capacitance, Csi = Series Capacitance, Li = Self Inductance, Mi = Mutual Inductance

In order to avoid computing cost, a lumped double pancake parameter model will be developed using the parameters computed for turns. In transient analysis simulations, representing the first and last few double pancakes with turn to turn representation may satisfy the requirement for detailed modeling.

Physical dimensions of the coil as illustrated in Figure IV.3 should be given in order to calculate the inductance and capacitance parameters for a particular turn in the coil. Figure IV.3.(a) shows the cross section of the entire coil having a number of disks, IV.3.(b) illustrates two disks at top each other, and IV.3.(c) displays the required dimensions in parameters computation for a turn/disk coil. In the following subsections, approximated formulas in parameter calculations will be given. It should be noted that, the MKS unit system is observed in all the parameter formulas.

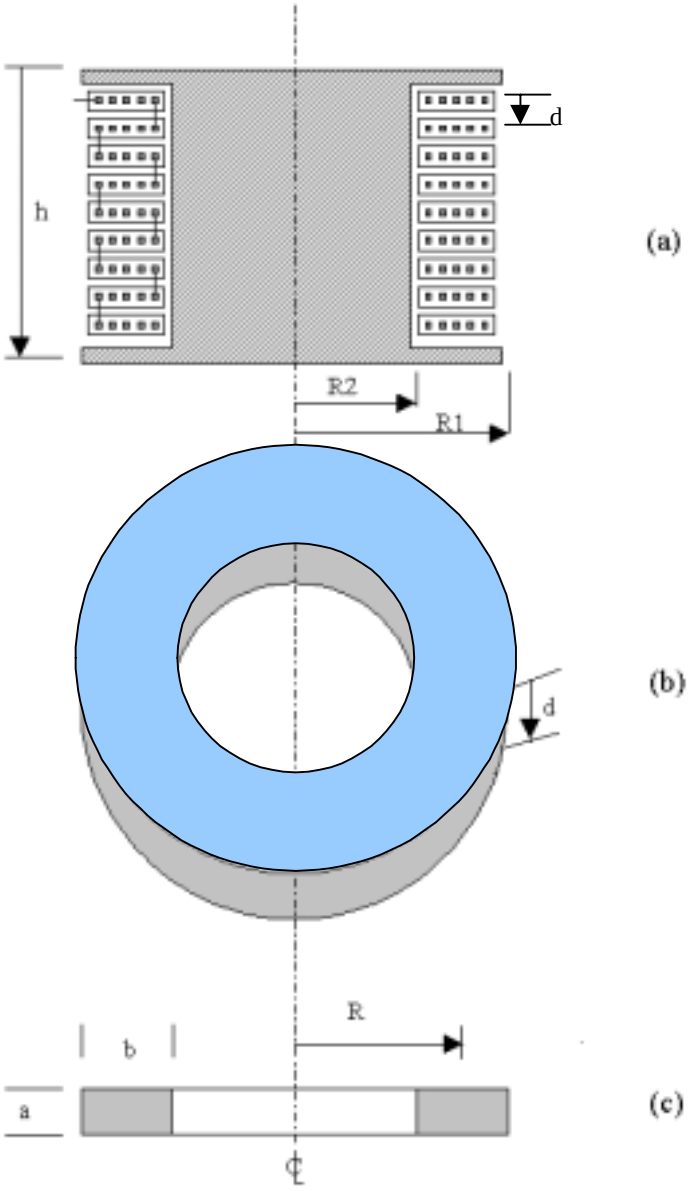

Figure IV.3:Illustration of the Physical Dimensions for a Disc Coil

(a) Disc Winding, (b) Two Disk Coils (c) Disk Coil with Rectangular Cross Section

IV.2.1. Self and Mutual Inductance Calculation

Inductance calculations are based on geometric entities. The formula developed in [Miki74] to compute the self-inductance (in Henry) is as follows:

$$L = \mu_0 R N^2 (\ln(\frac{8R}{R1} - 2),$$

$$\ln R1 = \frac{1}{2}\ln(a^2+b^2) - \frac{b^2}{12a^2}\ln(1+\frac{a^2}{b^2}) - \frac{a^2}{12b^2}\ln(1+\frac{b^2}{a^2}) + \frac{2b}{3a}\tan^{-1}\frac{a}{b} + \frac{2a}{3b}\tan^{-1}\frac{b}{a} - \frac{25}{12} \quad \textbf{(1)}$$

N is the number of turns in a pair of disk coils (double pancake), other dimensions are shown in Figure IV.2.(c). If the inductance of a turn is to be calculated, then N is equal to 1.

Another formula was developed [Grove74] by using tables.

$$L = 10^{-7} R N^2 P_0 \quad \textbf{(2)}$$

P0 is determined by the ratio of b/2R which determines the thickness of the coil.

$$\text{If } b/2R < 0.2 \quad \text{then } P_0 = 4\pi(0.5(1+\frac{b/2R}{6})\log(\frac{8}{b/2R}) - 0.84834 + 0.2041\, b/2$$

$$\text{If } b/2R \geq 0.2 \quad \text{then } P_0 \text{ is found from the tables given in [6]}$$

Mutual inductance between two circular filaments is calculated using the formula developed by Maxwell [Miki74], [Green91].

$$M_{1-2} = \mu_0\sqrt{(R_1R_2)}[(\frac{2}{k} - k)K(k) - \frac{2}{k}E(k)]$$

$$k = \sqrt{\frac{4R_1R_2}{(R_1+R_2)^2 + d^2}} \quad \textbf{(3)}$$

where R_1 and R_2 are the radius of the circular filaments 1 and 2, d is the distance between circular filaments, μ_0 is the permeability of free space and K(k) and E(k) are the complete elliptic integrals of the first and second kind.

Equation (3) is valid for circular filaments of negligible cross section. If the cross sectional dimensions are not small enough compared to the distance between the coils, then Lyle's method is applied to calculate the mutual inductance between turns or coils. Lyle's method states that each coil (Coils 1 and 2) can be represented by two equivalent filaments as shown in Figure IV.4.

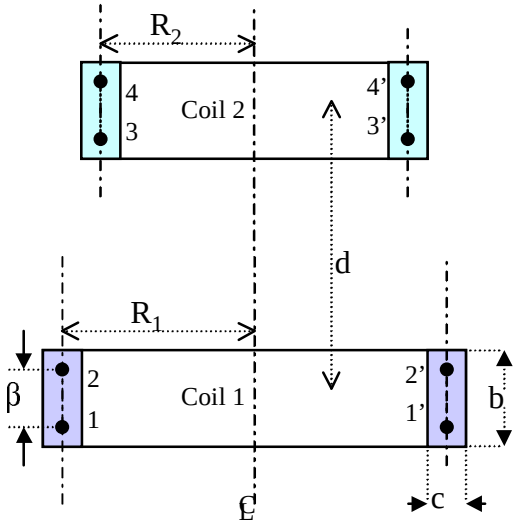

Figure IV.4: Coil representation by Lyle for b>c

Mutual inductance between each equivalent filament (11'-33', 11'-44', 22'-33' and 22'-44') is calculated using Equation (3), where R_1 and R_2 are replaced with an equivalent radii of r and spacing between coils vary between $d+2\beta$ and $d-2\beta$.

$$r_i = R_i\left(1+\frac{c^2}{24R_i^2}\right), \beta = \sqrt{\frac{b^2-c^2}{12}} \quad \textbf{(4)}$$

The average of each calculated mutual inductance gives the mutual inductance between the two coils.

IV.2.2. Capacitance Calculation

Capacitance calculation is also based on the geometric entities. In a double pancake, the series capacitance between turns, shunt capacitances between axially separated turns and turn

to ground can be easily and accurately calculated using the parallel plate formula given in Equation 5.

$$C = \frac{\varepsilon_0 \varepsilon_r A}{d} \quad \textbf{(5)}$$

Where $\varepsilon_0 = 8.854e\text{-}7$, ε_r is the constant of the dielectric between two plates, A is the area between two plates, and d is the distance between plates.

In order to avoid the computing cost, the capacitances of turns in a double pancake are combined to represent capacitances between double pancakes and to ground. Equations for series capacitance of the total winding developed by several authors have been summarized in [Chowd94].

IV.3. Developing a Distributed SMES Coil Model

IV.3.1. Modeling Assumptions

It is assumed that the SMES coil can be accurately represented with a combination of self and mutual inductors and capacitors. The following additional assumptions are made throughout the modeling [Degen95]:

- The dielectric constant of the insulating material does not vary with frequency
- The thermal enclosure and the tank does not carry current, and they were represented as ground plane
- A small value of resistor represents skin effect and eddy current losses.
- Parallel plate model is employed to calculate ground and series capacitances of each turn.

- To reduce the computing cost, each double pancake (two single pancakes) is represented by its series inductance, capacitance, mutual inductance and ground capacitances.

The SMES coil is essentially a complex air core inductor, therefore the transient voltage response can be computed using EMTP or EMTDC programs which employ linear solution methodology. A linear voltage drop is also assumed to calculate the capacitance of a winding that consists of a number of turns. Schematic representation of capacitive parameters of the entire coil is shown in Figure IV.5. Note that the mutual capacitances between turns are not seen in this figure.

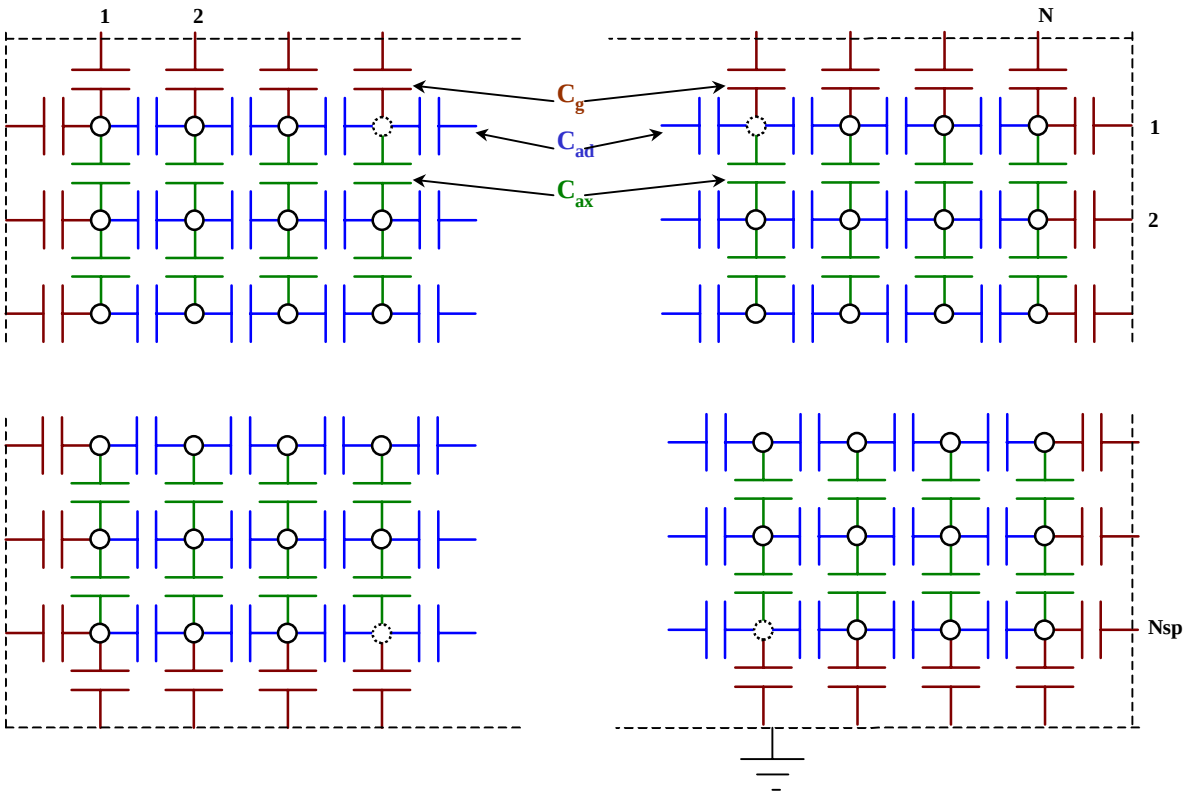

Figure IV.5: Schematic Illustration of Capacitive Parameters in the Entire Coil

Cad = Capacitance between adjacent turns within a disk coil
Cax = Capacitance between axially separated turns
Cg = Capacitance between a turn and ground
N = number of turns in a single pancake
Nsp = Number of single pancakes in a coil

IV.3.2. Modeling Steps

As stated before, the most detailed mathematical model for a coil can be obtained if each turn in the coil is represented by its associated *L*, *M*, *Cadj*, *Cax*, and *Cg*. However, this detailed model requires more memory and computing time if the coil consists of excessive numbers of turns. *N* number of turns in a *Ndp* number of double pancakes in a coil can be lumped to model the coil in the level of double pancakes. This will be given below step by step. To give a better understanding , an example coil is considered with *Nsp*=12 single pancake (*Ndp*=6 double pancake) where each single pancake (SP) consists of *N*=10 turns.

Forming Inductance Matrix

1. Calculate self inductances for each turn in a SP by applying the Miki's formula, and mutual inductances between each turn in a SP by applying the Lyle's method.

2. Construct a *NxN* (10x10) matrix block (*A* in Equation 6) where *N* is the number of turns in a SP. Diagonal elements correspond to the self inductances and off-diagonal elements correspond to mutual inductances between each turns in a SP

$$Lturn = \begin{bmatrix} [A]_{NxN} & [B]_{NxN} & [C]_{NxN} & .. & .. & .. & .. & .. & .. & [L]_{NxN} \\ [B]_{NxN} & [A]_{NxN} & [B]_{NxN} & .. & .. & .. & .. & .. & .. & [K]_{NxN} \\ [C]_{NxN} & [B]_{NxN} & [A]_{NxN} & .. & .. & .. & .. & .. & .. & [J]_{NxN} \\ [D]_{NxN} & [C]_{NxN} & [B]_{NxN} & .. & .. & .. & .. & .. & .. & [I]_{NxN} \\ [E]_{NxN} & [D]_{NxN} & [C]_{NxN} & .. & .. & .. & .. & .. & .. & [H]_{NxN} \\ .... & ..... & ..... & ..... & ..... & ..... & ..... & ..... & ..... & ..... \\ .... & ..... & ..... & ..... & ..... & ..... & ..... & ..... & ..... & ..... \\ [L]_{NxN} & [K]_{NxN} & [J]_{NxN} & .. & .. & .. & .. & .. & .. & [A]_{NxN} \end{bmatrix}_{NNsxNNs} \quad \textbf{(6)}$$

3. Apply Lyle's method to calculate mutual inductances between turns in the first SP and turns in the other SPs. A series of NxN (10x10) matrix blocks (*B* to *L* in Equation 6) are constructed where each *NxN* (10x10) represents mutual inductances between the first SP and other SPs. These matrix blocks and the one constructed in step (2) builds a column with a size of *N*NspxN* (120x10).

4. Once the first column of *Lturn* is formed, a lumped inductance matrix representing the double pancakes of the coil is computed as given in Equation (7).

$$Ldb = \begin{bmatrix} sum(ABAB) & sum(CBCD) & \ldots\ldots\ldots & sum(KJKL) \\ sum(CBCD) & sum(ABAB) & \ldots\ldots\ldots & \ldots\ldots\ldots \\ sum(EDEF) & sum(CBCD) & \ldots\ldots\ldots & \ldots\ldots\ldots \\ \ldots\ldots\ldots & \ldots\ldots\ldots & \ldots\ldots\ldots & \ldots\ldots\ldots \\ sum(KJKL) & \ldots\ldots\ldots & \ldots\ldots\ldots & sum(ABAB) \end{bmatrix}_{2Nsx2Ns} \quad \textbf{(7)}$$

Where $sum(ABAB) = \sum_{i=1}^{N}\sum_{j=1}^{N} A(i,j) + \sum_{i=1}^{N}\sum_{j=1}^{N} B(i,j) + \sum_{i=1}^{N}\sum_{j=1}^{N} A(i,j) + \sum_{i=1}^{N}\sum_{j=1}^{N} B(i,j)$, so on so for.

Calculating Capacitances for a double pancake

1. Calculate capacitances between adjacent turns (*Cad*), axially separated turns (*Cax*) and turns to ground (*Cg*) shown in Figure IV.4 using Equation 5.
2. Capacitances between adjacent turns and axially separated turns are combined in such way shown in Figure IV.6 to compute the equivalent series capacitance for a double pancake.
3. Ground capacitances calculated for each turn within a double pancake are summed to obtain an equivalent ground capacitance for a double pancake.

IV.3.3. Credibility of Modeling

Modeling and simulation studies produce a sufficiently credible solution if they can be verified, validated and experimentally tested (VV&T). The following questions can be posed in a modeling and simulation study:

1. Is the model transformed from one form into another form with sufficient accuracy?
2. Has the right model been established?
3. Does the model function properly for different cases?

These are the definitions of model verification, validation and testing given in [Balci98] where the taxonomy of VV&T techniques is presented. This section will employ a few of these techniques to validate the modeling developed.

Given the coil dimensions, the coil parameters were calculated based on well-developed formulas. These formulas are used in transformer coil modeling. The voltage response of the model is well compared with the measured response [Mcnut74]. The inductance calculation method developed here was applied for the example coils given in the literature [Wirga76]. The results are well matched.

A capacitance measurement experiment was conducted on a sample coil to compare calculated and measured values. This is given in Appendix B. As can be seen, the calculated and measured values are in the same order of magnitude. Since the actual coil has not been built yet, an experimental test on the coil to validate the calculated coil parameters can not be conducted. However, the sample coil has been built so that its turn dimensions are replicas of the actual coil that is to be built. This test encouraged the validity of the modeling.

IV.3.4. Description of the Studied SMES Coil

This study is based on a 50 MW, 100 MJ SMES coil being built by BWX Technologies, Inc. for a FACTS/ energy storage application. The coil design has not been finalized yet, but according to the current design provided, the entire SMES coil has a width/ height ratio of 3.66 m (144 in) / 1.53 m (60 in) made of 48 double pancakes. Each double pancake has 40 turns. A distributed model of the coil is obtained as shown in Figure IV.2 where each double pancake is represented by its self and mutual inductance, series and ground capacitances. A MATLAB code given in Appendix C was developed to calculate electrical parameters for each double pancake. Appendix D gives the calculated electrical parameters for individual turns. The calculated series and shunt capacitances for each turn has been lumped according to the procedure given in Section IV.5.2 to represent capacitances for a double pancake, and lumped further to obtain the equivalent capacitances for the entire coil. These capacitance values are tabulated in Table IV.2.

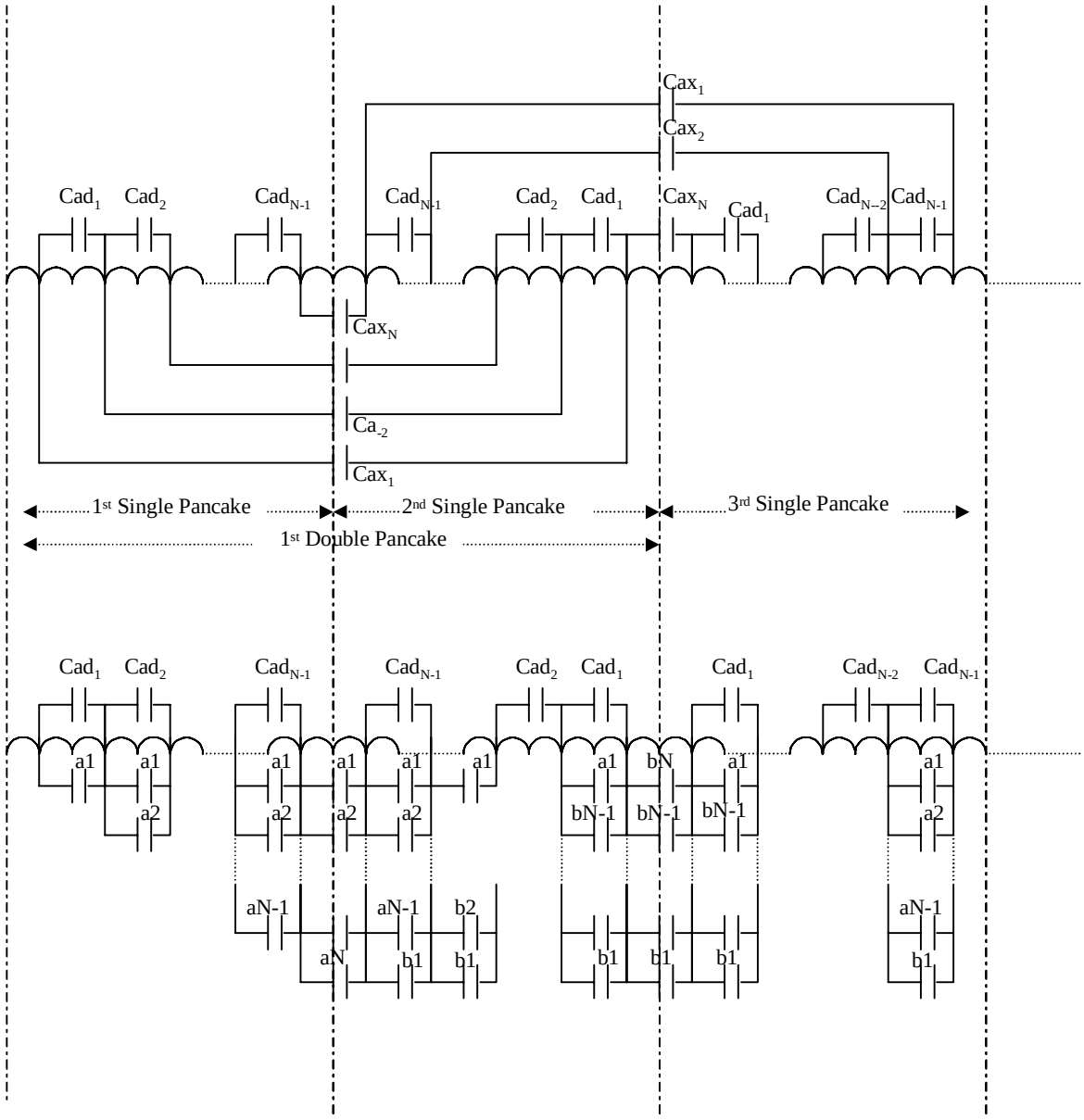

Figure IV.6: Derivation of Equivalent Series Capacitance for a Double Pancake

$a1 = (2N-1)Cax_1$, $b1 = (2N-1)Cax_N$
$a2 = (2N-3)Cax_2$, $b2 = (2N-3)Cax_{N-1}$
$a3 = (2N-5)Cax_3$, $b3 = (2N-5)Cax_{N-3}$

$aN-1 = 3Cax_{N-1}$, $bN-1 = 3Cax_2$
$aN = 1Cax_N$, $bN = 1Cax_1$

The self and mutual inductances for each turn also have been lumped to obtain the equivalent self and mutual inductances for each double pancake. The total inductance is 12.5 H. and the mutual inductance distribution of the first double pancake to others are shown in Figure IV.7, where each double pancake follows this distribution.

Table IV.2: Parameters of the Studied Coil

	Series Capacitance	***Shunt Capacitance***
Double Pancake	42nF	2.05nF
First and last DP	22nF	9.65nF
Entire Coil	0.840nF	114nF

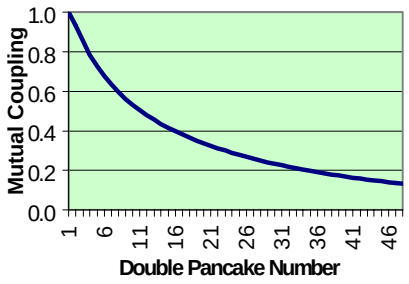

Figure IV.7: Mutual Inductance Distribution of a Double Pancake

IV.4. Analysis of Transient Behaviour of the Coil

Once an electrical lumped parameter model is obtained, the next task is to determine the frequency response of the coil in order to assess the coil's resonance frequencies. This is simulated using the technique described in EMTDC. The coil has been represented with 48 double pancakes, where each double pancake modeled with series inductor, series capacitor and shunt capacitor. Since currently available version of EMTDC can not model 48 mutual representation, lumped inductors are used representing both self and mutual inductances. In order to obtain the frequency response of the coil, a harmonic injector inserting 1 A current at different frequencies is connected to the coil. The terminal voltage is plotted first, then the Fourier analysis applied to the voltage waveform and the frequency response (magnitude and phase angle) of the coil is obtained as shown in the second and third row of Figure IV.8.

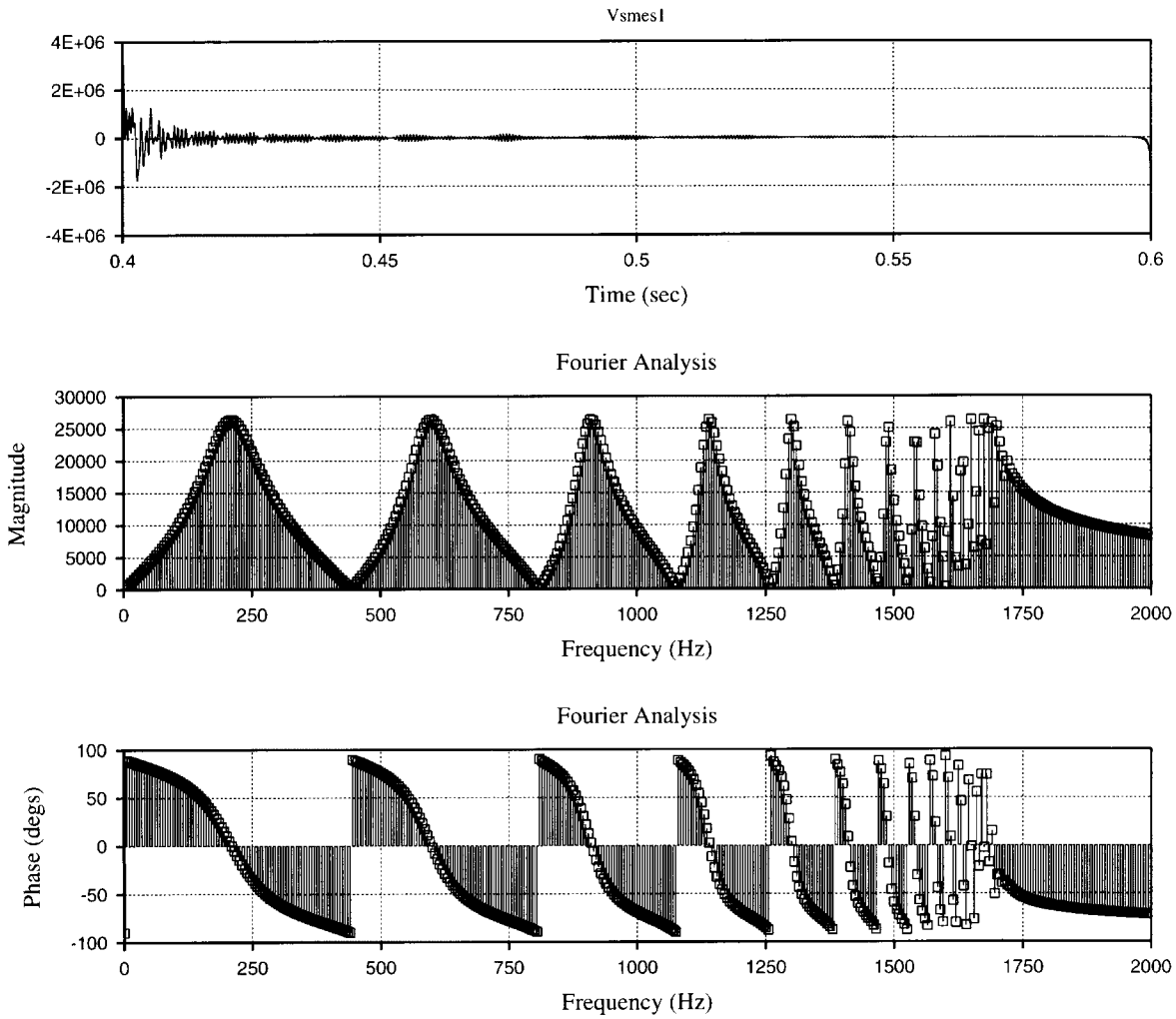

Figure IV.8: Frequency Scan of the SMES Coil

As can be seen from the figure, the coil resonances occur between the frequency range of [200-1800] Hz. If a coil is excited at one of these resonant frequencies, we expect overvoltages. This has been examined through a simulation study. The coil is connected to a one-phase chopper. The switching frequency of the chopper was selected to be one non-resonant frequency and one resonant frequency. Several internal voltages (in volts) are plotted and compared in Figure IV.9, where the first column corresponds to the case that the coil is excited at non-resonant frequency, and the second one corresponds to the case that the coil is excited at resonant frequency. This figure clearly shows that accidental operation of the coil at its natural mode frequencies, an internal overvoltage is observed in the coil which, in no doubt, breaks down the coil insulation. Low natural frequencies can be avoided by connecting capacitors tuned at several times of the natural frequency to avoid this operation.

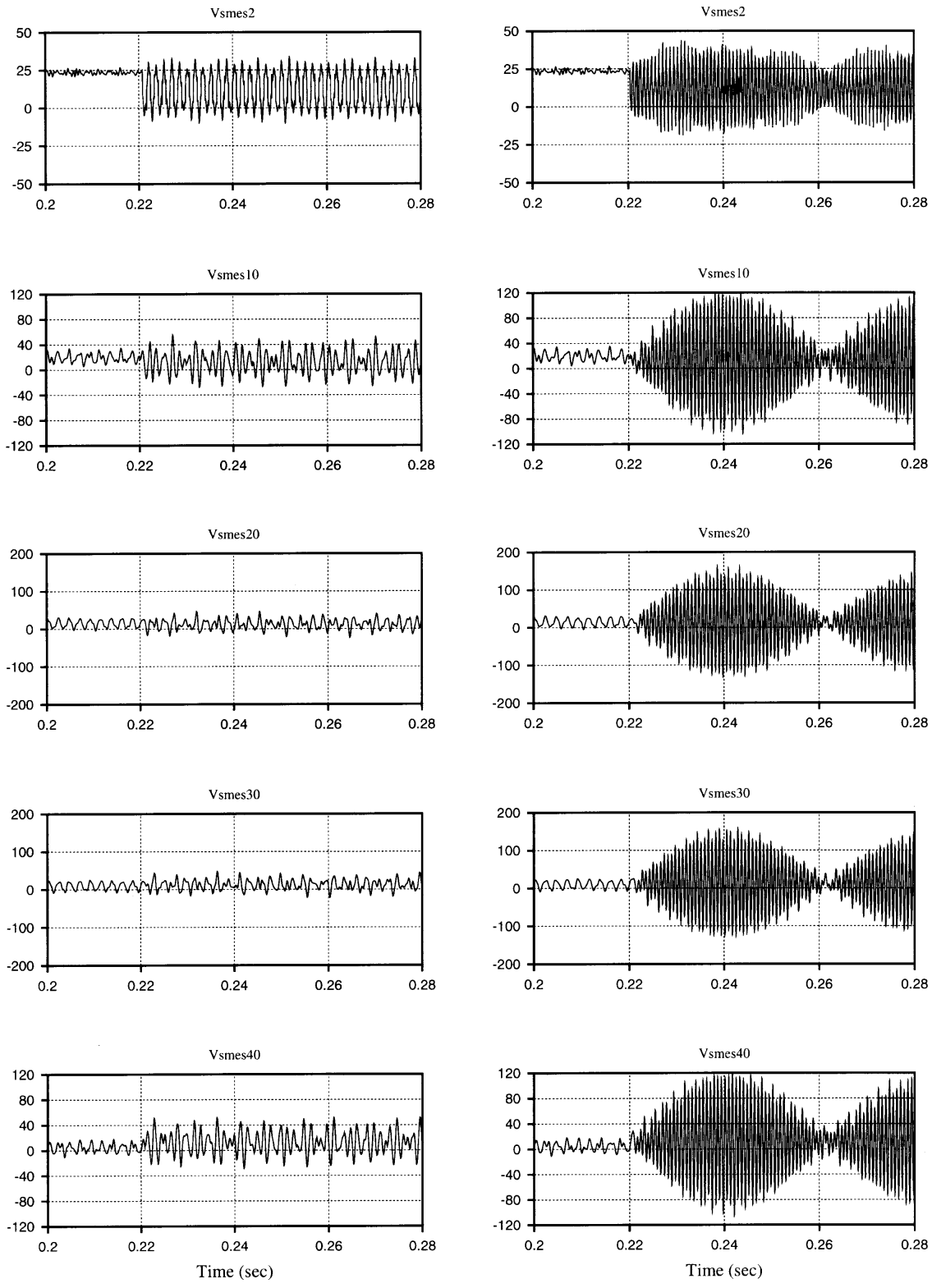

Figure IV.9: Comparison of Internal Node Voltages when the Coil is Excited at f=100 and 900Hz.

Determining voltage distribution along the coil is essential in the coil insulation system design. The voltage distribution is obtained by recording the internal voltages at a snapshot time after a surge impulse is applied to the coil. EMTDC/PSCAD is used as a platform to compute the voltage distribution of the SMES coil.

An amplification ratio is defined as the square root of the ratio of ground capacitance to series capacitance of the coil. This factor plays an important role in the voltage distribution of the coil. The amplification ratio of each double pancake in the SMES coil is found to be approximately 0.22. The per-unitized initial voltage distribution of the coil at this amplification ratio can be obtained, when an impulse surge voltage is applied to the SMES coil. This is depicted in Figure IV.10. The same scenario is considered for the 6-segment coil model that is derived by lumping the double pancake parameters further. It is observed that similar voltage distribution curves were obtained.

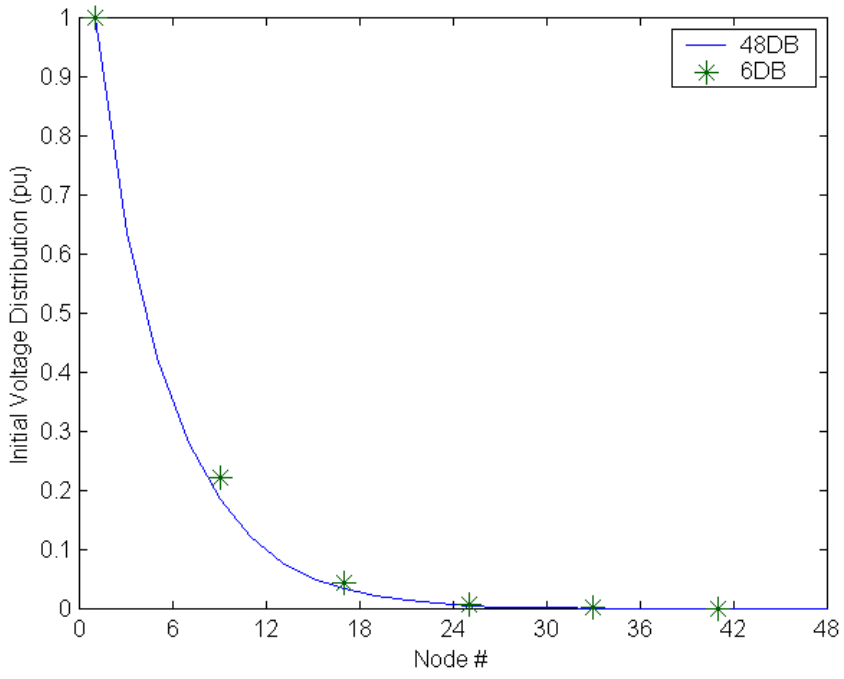

Figure IV.10: Initial Voltage Distribution of the Coil

IV.5. Transient Analysis Techniques in the Studied SMES Coil

One of the objectives of this study is to investigate the electromagnetic transient interactions between a superconducting coil and the power electronics interface for a Flexible AC Transmission Systems (FACTS) application. This study uses a 50MW, 100MJ, 12.5H SMES coil being built by BWX Inc. Technologies. Understanding the transient phenomena associated with a SMES system is essential in this investigation. The high power and high voltage DC interface of this particular design poses significant design challenges which need to be well understood and adequate solutions need to be proposed. As stated in early transient related works, large-scale SMES coils require special attention in their analysis of transient behavior and their protection to insulation damages. The following steps are to be taken in the transient modeling and simulation of the coil.

- Distributed electrical parameters are derived
- Simulation model is developed
- Frequency response of the coil is analyzed to evaluate the resonant frequencies that may excite the coil
- Voltage distribution of the coil is plotted under different operating conditions
- Filtering/surge capacitors can be used to make the voltage distribution uniform
- Metal oxide varistors can be connected to the terminal to terminal or terminal to ground of the coil to protect the coil against overvoltages.

These techniques are utilized in the next chapter to identify transient overvoltages, and recommend schemes to reduce these overvoltages.

CHAPTER V

TRANSIENT MODELING AND SIMULATION OF A SMES COIL AND ITS POWER ELECTRONICS INTERFACE

This chapter presents the modeling and simulation results of a superconducting magnetic energy storage (SMES) system for power transmission applications. This is the largest SMES coil ever being built for power utility applications, and has the following unique design characteristics: 50 MW (96 MW peak), 100 MJ, 24 kV DC interface. As a consequence of the high power and high voltage interface, special care needs to be taken with overvoltages that can stress the insulation of the SMES coil, especially in its cryogenic operating environment. The transient overvoltages impressed on the SMES coil are the focus of this investigation. Suppression methods were also studied to minimize transients. The simulation is based on detailed coil and multiphase GTO-based chopper models. The study was performed to assist in the design of the SMES coil insulation, transient protection, and the power electronics specification and interface requirements.

The purpose of this study is to investigate the electromagnetic transient interactions between a superconducting coil and the power electronics interface for a flexible ac transmission systems (FACTS) application. Transient overvoltages can endanger the insulation of a superconducting coil, especially in its cryogenic operating environment where the insulation characteristics are different from that at normal conditions. The transients may originate from normal or abnormal SMES switching operations, and/or faults or lightning and switching surges from the ac and dc systems. They usually take place for a very short time as compared to the steady state, but have the potential to stress the coil insulation. The understanding of the possible transient overvoltages the SMES coil will be subjected to is essential in the design of its insulation and transient suppression schemes. The high power and high voltage dc interface of this particular design poses significant design challenges which need to be well understood and adequate solutions need to be proposed.

The transients associated with a SMES coil, which is interfaced with a gate-turn-off thyristor (GTO) based chopper, were simulated using an electromagnetic transient program

EMTDC^{TM} (electromagnetic transients for dc) [Manit88]. The following transient suppression schemes were investigated to minimize the transient overvoltages: a) adding filtering/surge capacitor b) adding metal oxide varistor (MOV) elements, c) changing the current sharing inductances. Grounding resistors were used to reduce the terminal to ground voltage stress. In addition to these schemes, the impact of chopper parameters such as time delay between firing angles of the GTO branches and snubber circuits were studied. Potential alternative chopper designs were examined.

V.1. Modeling of the SMES Coil

This study is based on a 50 MW, 100 MJ SMES coil being built by BWX Technologies, Inc. for a FACTS/ energy storage application. The structure of the SMES coil is illustrated in Figure V.1 (a). The entire SMES coil has a width/ height ratio of 3.66 m (144 in) / 1.53 m (60 in) made of 48 double pancakes. Each double pancake has 40 turns. In order to reduce the computational burden, an equivalent circuit of the coil was represented by a 6-segment model comprised of self inductances, mutual couplings, ac loss resistances, and series and shunt capacitances, as shown in Figure V.1 (b). Including the mutual couplings between segments was to obtain more accurate frequency and voltage response [Abet53]. The procedure of calculating coil parameters is given in the previous chapter. The inductance and capacitance values for segments based on the previous design of the SMES coil provided by BWX Technologies. Turn-to-turn values were lumped to obtain the parameters for the 6 segment model. These parameters are used throughout the study presented in this chapter. The inductance matrix used in the simulation is as follows:

$$L_{Coil\_6segment} = \begin{bmatrix} 0.5806 & & & & & \\ 0.4308 & 0.5806 & & & & \\ 0.3064 & 0.4308 & 0.5806 & & & \\ 0.2360 & 0.3064 & 0.4308 & 0.5806 & & \\ 0.1885 & 0.2360 & 0.3064 & 0.4368 & 0.5806 & \\ 0.1539 & 0.1885 & 0.2360 & 0.3064 & 0.4368 & 0.5806 \end{bmatrix}$$

Frequency scan analysis was performed to predict resonant frequencies. The result showing the magnitude of the coil terminal voltage vs. frequency is given in Figure V.2. As can be seen, the coil has several resonance frequencies, parallel resonances at frequencies around 60Hz, 400Hz, 890Hz, and series resonances at 280Hz, 830Hz, which can lead to magnification of transients. Since the SMES coil has a rather high inductance of 12.5H, the resonance frequencies of the coil are relatively low.

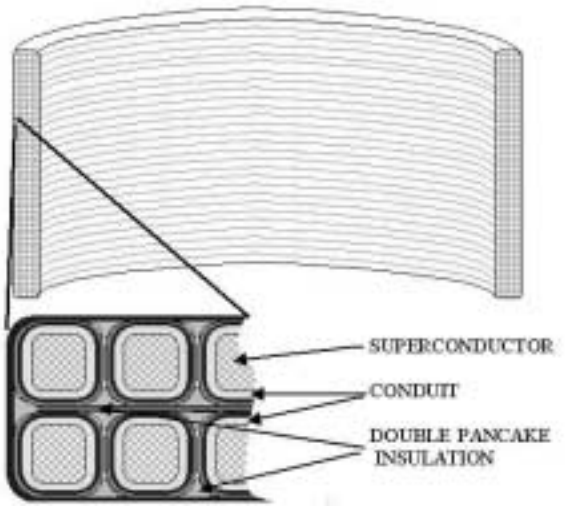

(a)

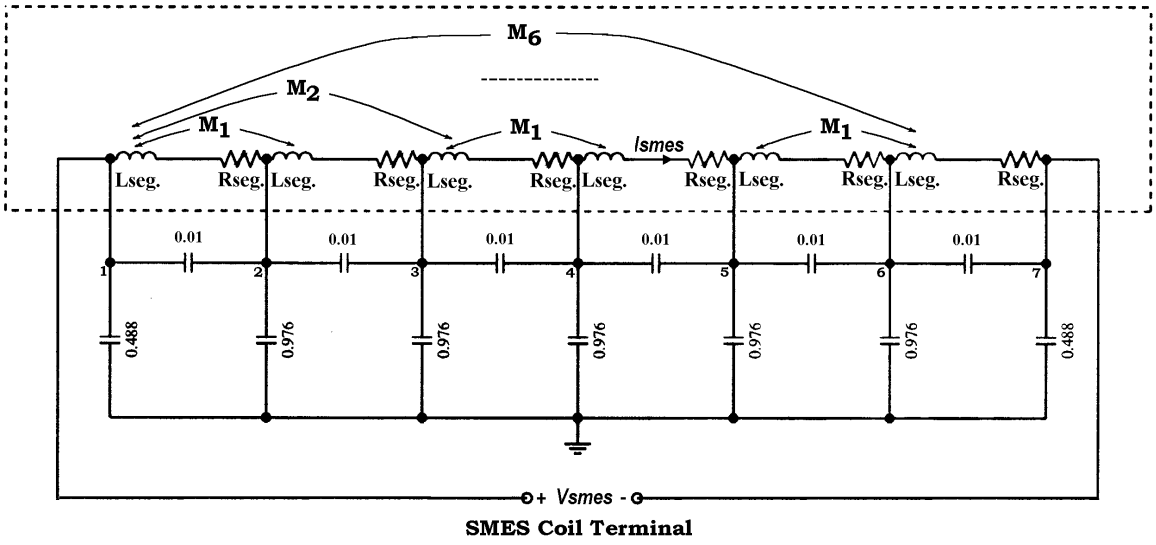

(b)

Figure V.1: (a) SMES coil (b) Simplified SMES coil model (Capacitance in μF)

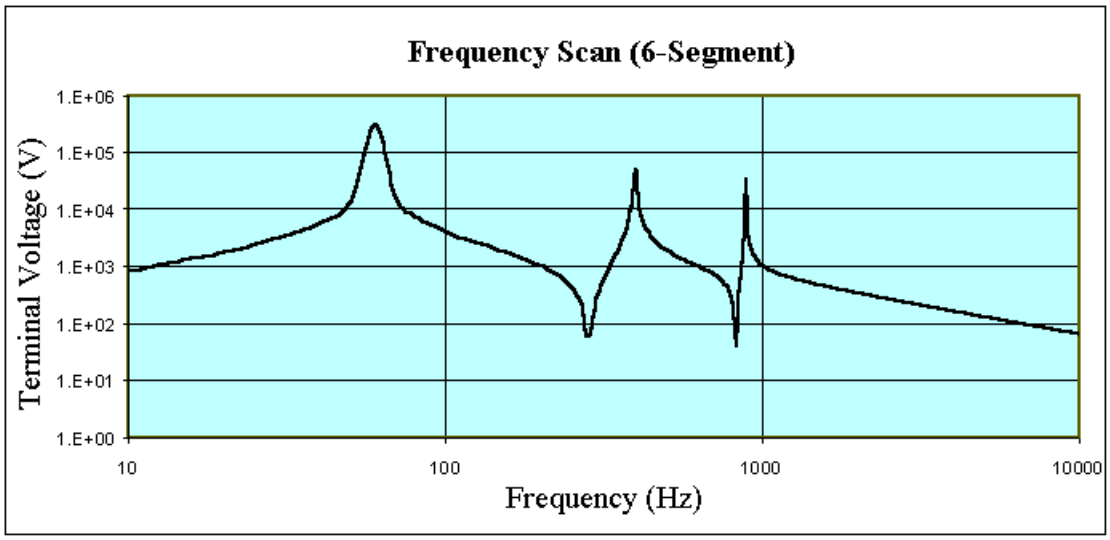

Figure V.2: Frequency Response of the 6-segment SMES Coil Model

V.2. Modeling of the Power Electronics Interface - A GTO-Based Chopper

A multiphase GTO-based chopper was modeled for the study as shown in Figure V.3. Components in dashed rectangles are for bypass switching and transient suppression purposes. A constant 24 kV dc voltage source represents the dc side of the chopper. In FACTS/ SMES applications, the dc-dc chopper is connected to a FACTS device through a dc link capacitor, which maintains constant dc voltage.

Operation principles of the multiphase dc chopper can be explained with the help of a single-phase dc chopper. For a single-phase dc chopper, the GTO firing signal is a square wave with a specified duty cycle. The average voltage and current of the SMES coil are related to the dc source voltage and average current by the duty cycle applied [Hassa93]. These relationships can be expressed as:

$$V_{smes\_av} = [1 - 2d]V_{dc\_av}$$
$$I_{dc\_av} = [1 - 2d]I_{smes\_av}$$

where V_{smes_av} is the average voltage across the SMES coil, I_{smes_av} is the average current through the SMES coil, V_{dc_av} is the average dc source voltage; I_{dc_av} is the average dc source current, and d is the duty cycle of the chopper (d = GTO conduction time/period of one switching cycle).

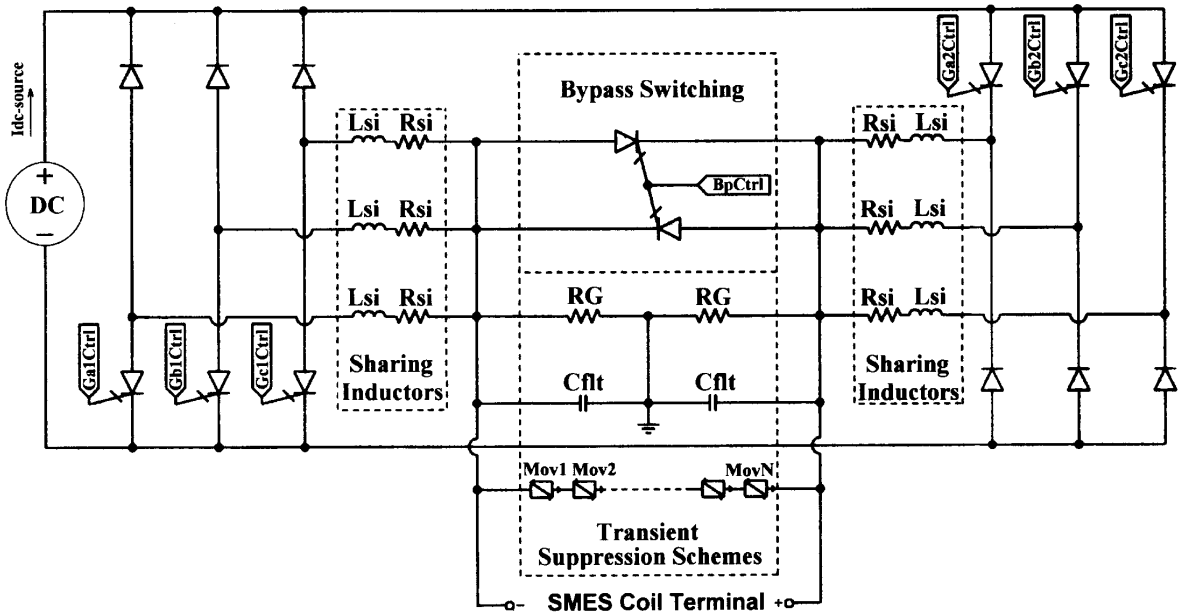

Figure V.3: Structure of a GTO-Based Chopper

It can be seen that there is no energy transferring at a duty cycle of 0.5, where the average voltage of the coil is zero and the average coil current is constant. In the cases of duty cycle being larger than 0.5 or less than 0.5, the coil is either charging or discharging, respectively. Adjusting the duty cycle of the GTO firing signals controls the rate of charging/discharging.

For an *n* phase dc chopper, the duty cycle of firing signals of each phase is 1/n of the total duty cycle. In the case of the 3-phase chopper used in this study, the duty cycle of each phase changes from 0 to 1/3, and the frequencies of the GTO firing signals are 100 Hz.

In Figure V.3, small inductors (*Lsi*) are placed at the output of each chopper phase for the purpose of current sharing and resistors (*Rsi*) represent the resistances of these inductors and the leads.

V.3. Examples of Transients seen by SMES Coil

Transients seen by the SMES coil can originate from ac or dc system faults/switchings. The normal switching operation of the devices generates periodic pulse sequences that may

be continuously applied to the SMES coil. In order to minimize the impact of the transients caused by the chopper switching, a bypass (or shorting) switch will be used to short the coil when power/energy exchange is not required. Operation of the bypass switch also introduces transients that may affect the coil.

This section presents the examples of transients that may be experienced by the coil. Section V.7 discusses the performance of some transient suppression schemes that will be attached to the SMES system. The simulation results given in the next few sections can be better understood, if one pays close attention to the measurement points indicated on the circuit diagrams in Figures V.1.(b) and 3.

V.3.1. Transients Generated by GTO Switching Under Normal Chopper Operation Condition

Under normal chopper operation condition, transient characteristics depend on the duty cycle and the average coil current. As an example, Figure V.4 gives the simulation results when duty cycle is 0.5 and average coil current is 0.4 kA.

The coil was charged at full speed (duty cycle equals to 1) from t=0 to t=0.22 sec. After 0.22 sec, the duty cycle was kept at 0.5 and the SMES system was in standby mode. Figure V.5.a shows the duty cycle for the time interval [0.22-0.28] sec. The SMES coil terminal voltage, V_{smes}, is shown in Figure V.4 (b) for the same time interval. An expanded inset of V_{smes} is also given in Figure V.4 (b-1) to show the high frequency components in detail. As can be seen, voltage transients appear after the duty cycle is changed to 0.5. The terminal voltage can easily go up to over 40 kV. It should be noted that the transitions of terminal voltages from negative to positive or vice versa have two transient processes. These are due to the delay of the two firing signals for the two GTO branches in the same phase. It is a common practice to keep this delay large enough so that the transitions do not cause high transients. For the studies presented in Section V.3 and V.4, this time delay was kept at about 0.41 msec that corresponds to 15 degrees for 100 Hz.

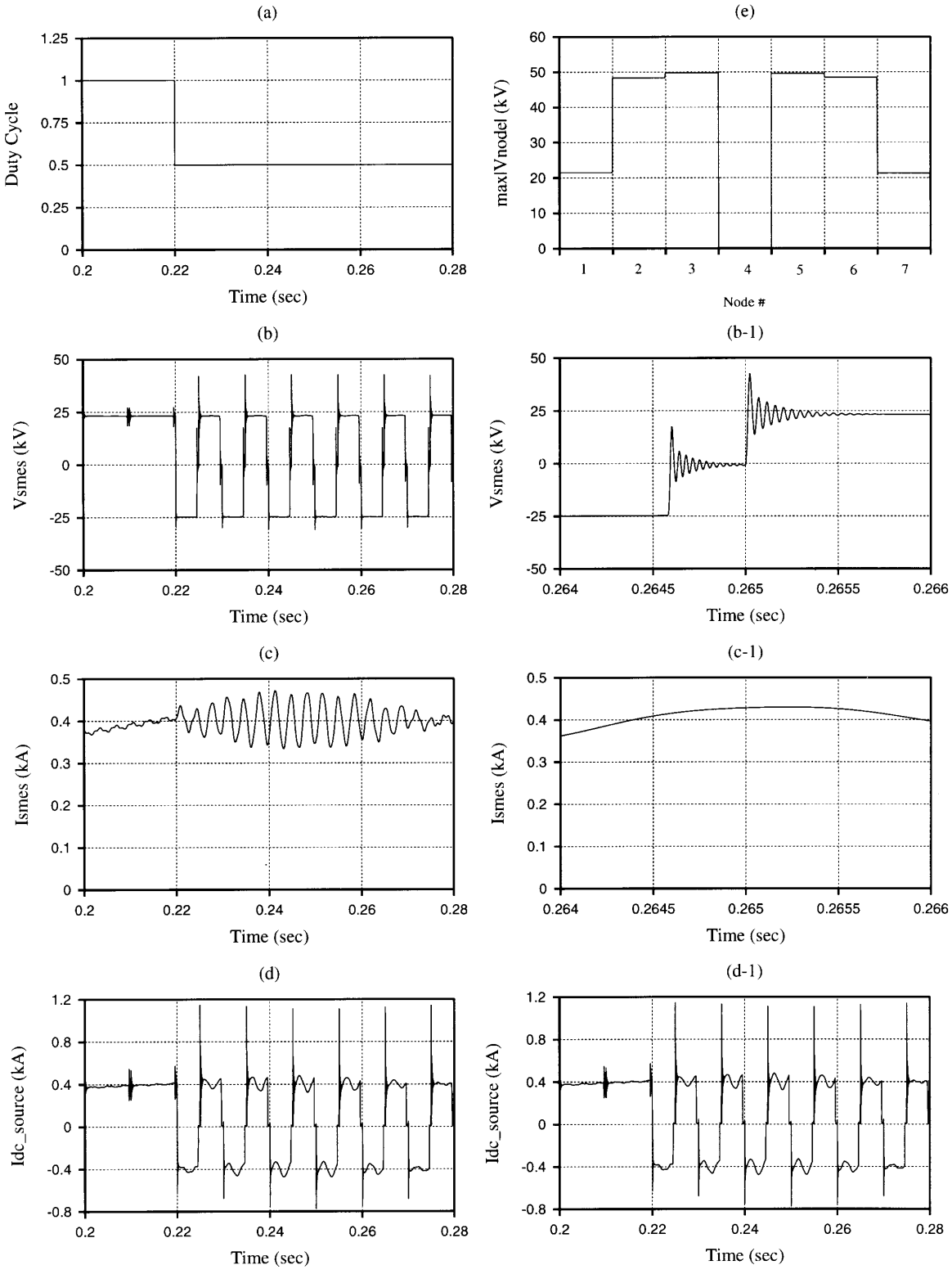

Figure V.4: Transients under Normal Operation Condition

Transients also appear in current waveforms. The plots of the coil current at the terminal, I_{smes}, and the source current, $I_{dc\text{-}source}$, along with their expanded insets are given in Figures V.4 (c), (d), (c-1), and (d-1), respectively.

Figure V.4 (e) shows the maximum voltage (to ground) at each node along the entire coil. Each data point was obtained by recording the maximum absolute value of the voltage at each node (V_{node}) within a period of time. In the case of 6-segment representation of the coil shown in Figure V.1 (b), there are 7 node voltages (5 internal nodes) that were monitored. As can be seen, the distribution of the maximum voltage is symmetrical (in magnitude) since the structure of the coil is symmetrical. Due to the symmetrical structure of the coil and the grounded mid-point of the distributed capacitors, the mid-point internal node voltage is almost zero. Also note that the voltage is applied to the terminal nodes of the coil. If it was applied to terminal to ground, the mid-point internal node voltage would not be zero. It is also important to note that the internal node voltages can be higher than terminal voltages due to partial winding resonances.

V.3.2. Transients Generated by Bypass Switch

The bypass switch that is used to isolate the coil also has the function of minimizing the chopper switching losses. This study used a back to back GTO switch as shown in Figure V.3. In standby mode operation, the bypass switch is turned on (closed) in advance before the chopper is turned off so that the coil is properly disconnected from the chopper. On the other hand, if the chopper needs to be reconnected to the coil, the chopper must be turned on before the bypass switch can be turned off (opened). The firing signals which controls bypass and chopper operations are shown in Figure V.5.a where “1” corresponds to ON and “0” corresponds to OFF for either bypass or chopper. Failure of this sequence and improper selected time delay between chopper and bypass switching may result in extremely high transient overvoltages. If these two aspects are properly considered, high transient voltages can be avoided as can be seen in Figure V.5 (b). It should be noted in Figure V.5 (b) that the voltage across its terminal is zero and voltage spike and transients seen in the voltage plot are due to the chopper switching when the coil is bypassed between 0.232 sec and 0.242 sec.

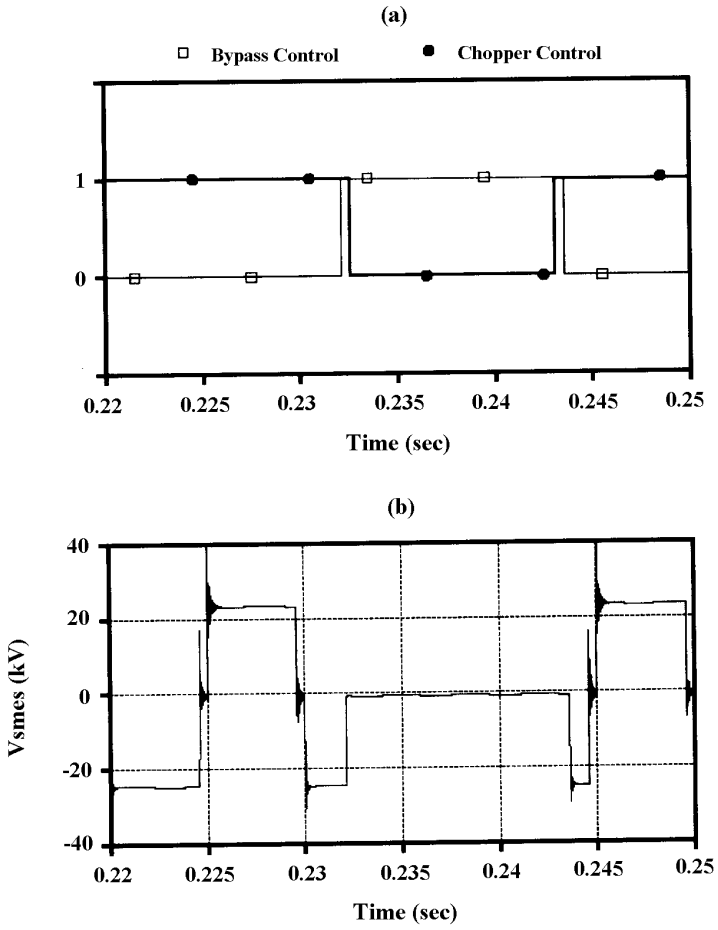

Figure V.5: SMES Transients under Bypass Switching

V.3.3. Transients Generated by GTO Faults

Figure V.6 gives the transients resulting from GTO faults. The faults are simulated by opening or short-circuiting one GTO branch at a specific time. The left column corresponds to the open-circuit case and the right column to the short-circuit case. The open-circuit fault was initiated when the GTO is conducting under normal chopper operation condition. Whereas, the short-circuit fault was created when the GTO is not conducting under normal chopper operation conditions. As expected, the open-circuit case results in higher transient voltages, while the short-circuit case causes increasing GTO current. As a consequence, the transient suppression schemes should be optimized to reduce voltage and current transients to acceptable levels.

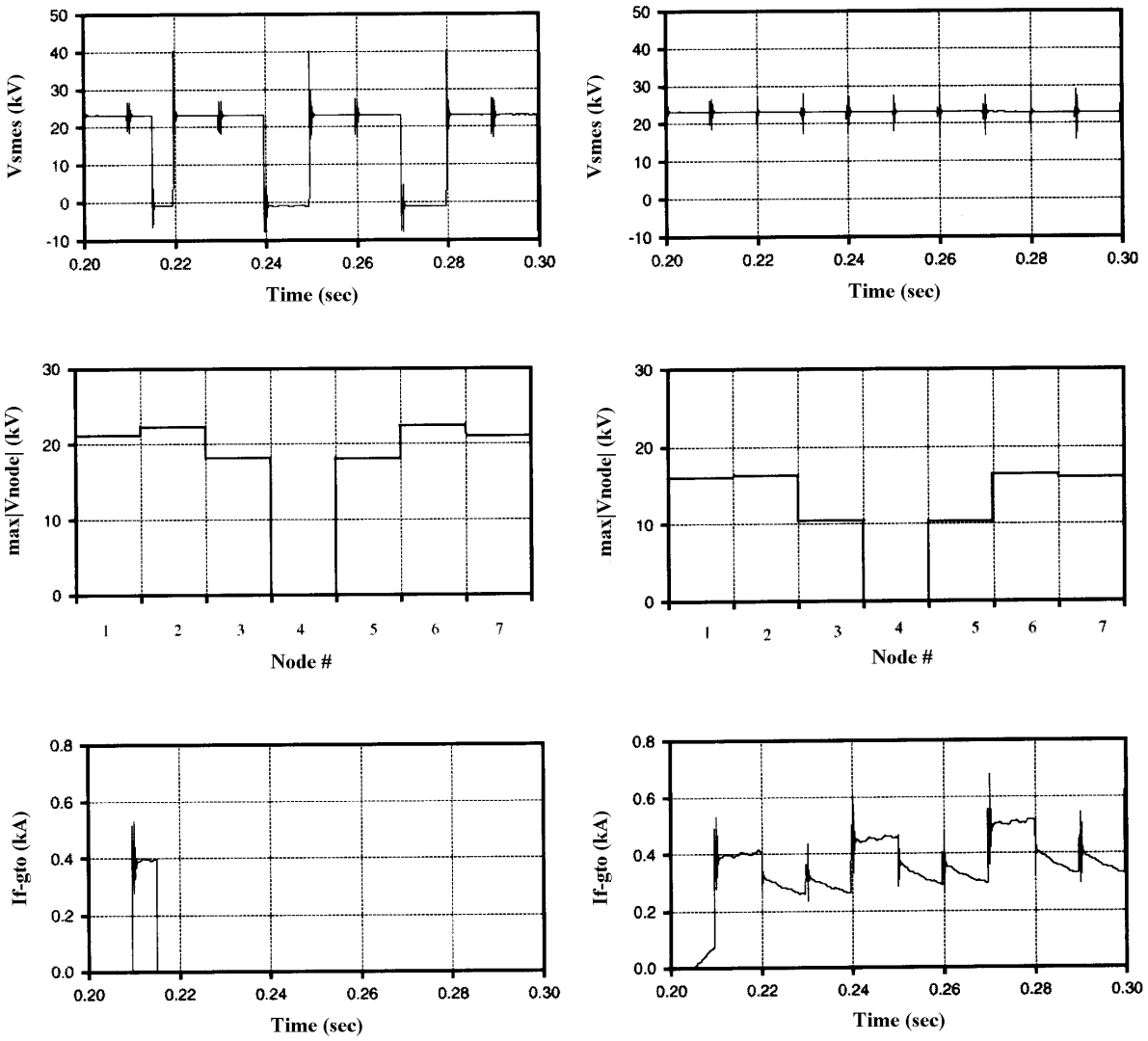

One GTO open after t = 0.215 sec. One GTO close after t = 0.205 sec

Figure V.6: SMES Transients due to GTO Faults

V.4. Performance of Transient Suppression Schemes

From Section V.3, we see that the transient voltages a SMES coil could experience in the normal operation condition can reach a very high level. If no transient suppression schemes are used, the coil insulation could be easily damaged. This section will discuss the performance of some transient suppression schemes.

V.4.1. Addition of Filtering/Surge Capacitors (*Cflt*) Together with Grounding Resistors (*RG*)

The effect of using filtering/ surge capacitors (*Cflt*) together with grounding resistors (*RG*) was studied. The location of *RG* and *Cflt* is shown in Figure V.3. Varying the value of Cflt shows different transient suppression performances. In this particular case, the function of the grounding resistors (*RG* = 25 kΩ) is to reduce the voltage stress (to ground) on the coil to half of the terminal to terminal voltage. On the other hand, the filtering/surge capacitors (*Cflt* = 5 μF) absorb some of the transient energy generated by switching actions. Figure V.7 shows the ratio of maximum internal node voltages to the first node voltage versus node number. As can be seen, the addition of surge capacitors reduces the internal node voltages of the coil.

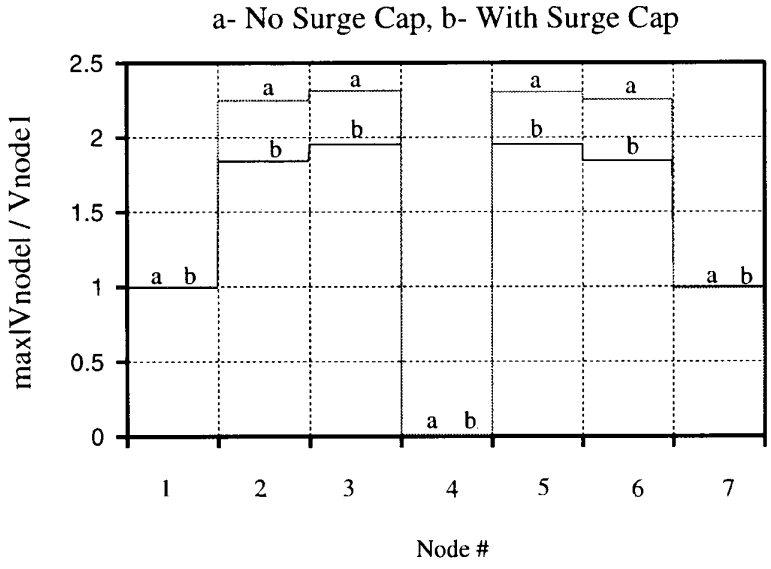

Figure V.7: Coil Voltage Distribution Ratio w/wo Surge Capacitors

V.4.2. Addition of MOV

In this study, the coil insulation design requires that the transient overvoltages be limited to below 37 kV (terminal to terminal). Having the rated coil terminal operating voltage of 24

kV (24 kV terminal to terminal and 12 kV terminal to ground) introduces a challenge to MOV application. In order to protect the coil from experiencing overvoltages above 37 kV, and in the mean time, to avoid significant MOV leakage current, the type and number of MOV stacking elements must be carefully selected. This study used the MOV component defined in EMTDC with the *V-I* characteristics given in Figure V.8.

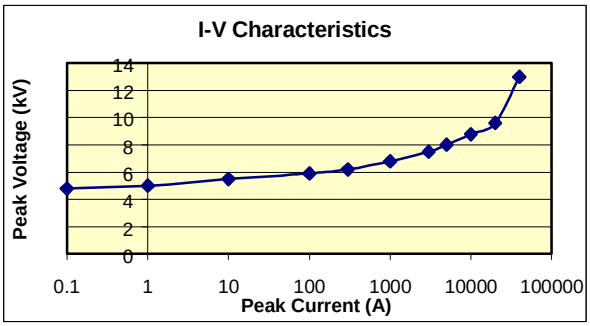

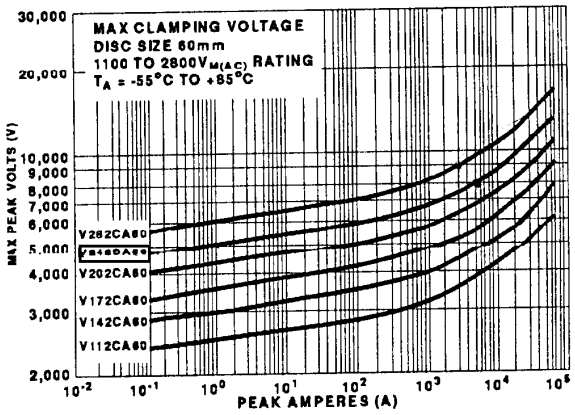

(a) **(b)**

Figure V.8: (a) Characteristics of One MOV Element Used in EMTDC
(b) Transient *V-I* Characteristics Curves in [Harri95]

The circled curve in (b) is used for the EMTDC simulation

In the preliminary study, a couple of approaches have been examined to determine the number of MOVs that need to be connected across the SMES coil terminal. Figure V.9 gives SMES terminal voltage and the energy absorbed by one MOV when the number of series MOVs (n) is five and eight respectively. It is apparent that the MOV energy is lower as the number of MOVs is increased. On the other hand, the overvoltages impressed across the SMES coil seems higher for n=8. Another approach was to vary the dc voltage applied to the terminal of SMES coil, and to observe the current flowing through one MOV. This observation is tabulated in Table V.1 for different number of series MOVs (n=5,6, and 8). It can be seen from this table that the current responses of five MOVs are much more sensitive to higher voltage levels than those of other MOVs.

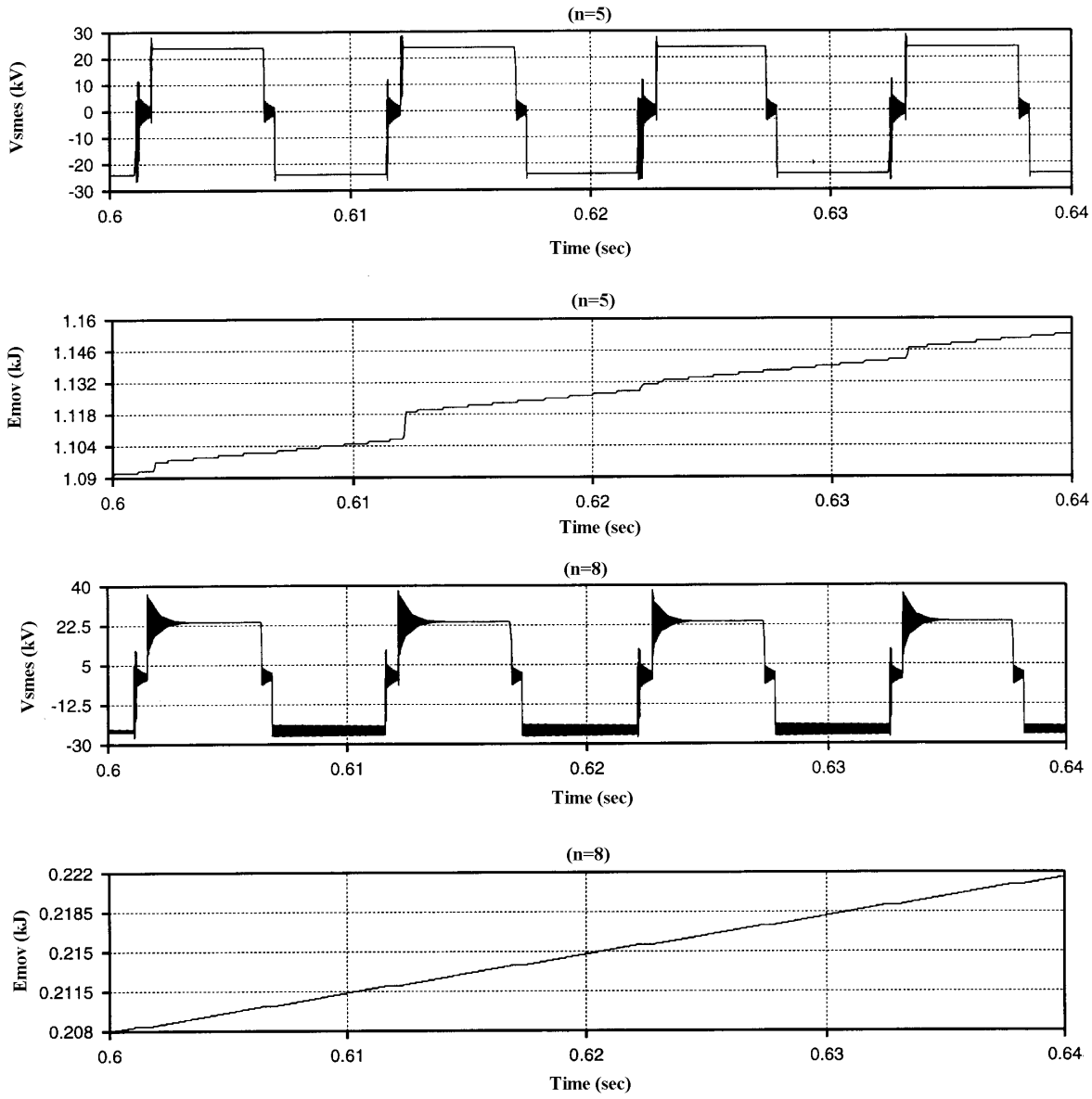

Figure V.9: MOV Implementation with n=5 and n=8

Table V. 1: MOV Current vs. dc Voltage Source

Vdc_source (kV)	*Imov(A) n=8*	*Imov(A) n=6*	*Imov(A) n=5*
24	0.125	0.167	0.2
30	0.156	1.99	330
37	0.193	552	5290
45	70	5880	22500

n= The Number of MOV Connected in Series Across the SMES Terminal

After this preliminary study, a scheme with five MOV components connected in series across the coil terminals was chosen. The voltage and current scales of each MOV component were adjusted to maintain the coil terminal voltage at the desired value. MOV conducts high current consequently absorbs energy to reduce transient overvoltages that occur during normal operating condition. This can be observed in Figure V.10. Transient voltages between SMES coil terminals are reduced as expected. The energy through one MOV component was recorded as 0.057 kJ per cycle for a normal switching transient case. Figures V.11 and V.12 show that the MOVs keep the SMES coil voltage below 37 kV.

Parallel branches of MOVs are utilized to meet the energy requirement. The number of parallel stacks of metal oxide discs can be increased according to transient energy levels the MOVs may experience. However, most of the temporary overvoltages coming from dc side are limited to only a few cycles by control and protection functions such as dc arresters, voltage clamps on the dc bus and overvoltage protection of the dc-dc chopper.

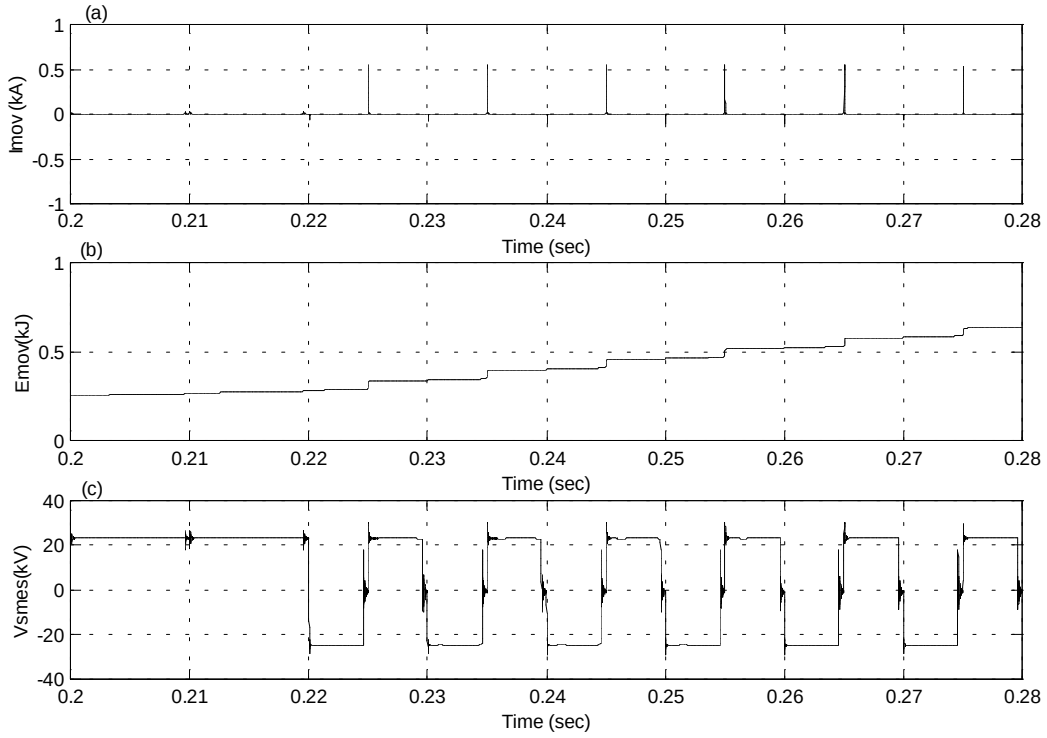

Figure V.10: (a) MOV Current, (b) Energy absorbed by MOV, (c) SMES Terminal Voltage

Consequently, the energy seen by the SMES side MOVs will be limited and they are mostly from chopper switching transients. Sustained faults in the SMES coil or the adjacent dc bus will be dealt with by a fast dump switch/resistor. Once the design of the dc-dc chopper is complete, additional simulations will be performed to verify the exact energy requirements of the MOV arresters.

V.4.3. Combination of *Cflt* and MOV

Based on the above simulation results, the combination of *Cflt* and MOV seems to provide the transient protection required. In the simulation, *RG* was also added to the combination of *Cflt* and MOV to reduce the terminal to ground voltage stress. The right part of Figure V.11 shows the results. The SMES terminal transient voltage was kept the same, but the internal node voltage and terminal current transients of the SMES coil were lowered. Therefore, the surge capacitors and MOVs demonstrate their effectiveness in suppressing the transients applied to the SMES coil.

The effectiveness of transient voltage suppressing measures can be shown when the coil is subjected to a different kind of transient voltage such as a standard lightning impulse voltage superimposed on the 24 kV dc voltage source. When no transient suppression is used, the magnitudes of the SMES terminal voltage and current will increase abruptly as a response of the coil to the impulse transient. This is illustrated in the left part of Figure V.12, where the first (upper left) plot corresponds to the impulse transient and the second and third ones to the SMES terminal voltage and current, respectively. The combination of *Cflt*, and MOV reduces the terminal voltage and current to acceptable levels as can be seen in the right part of Figure V.12. It should be noted that the SMES terminal voltage was kept below 37 kV due to the effect of the MOVs.

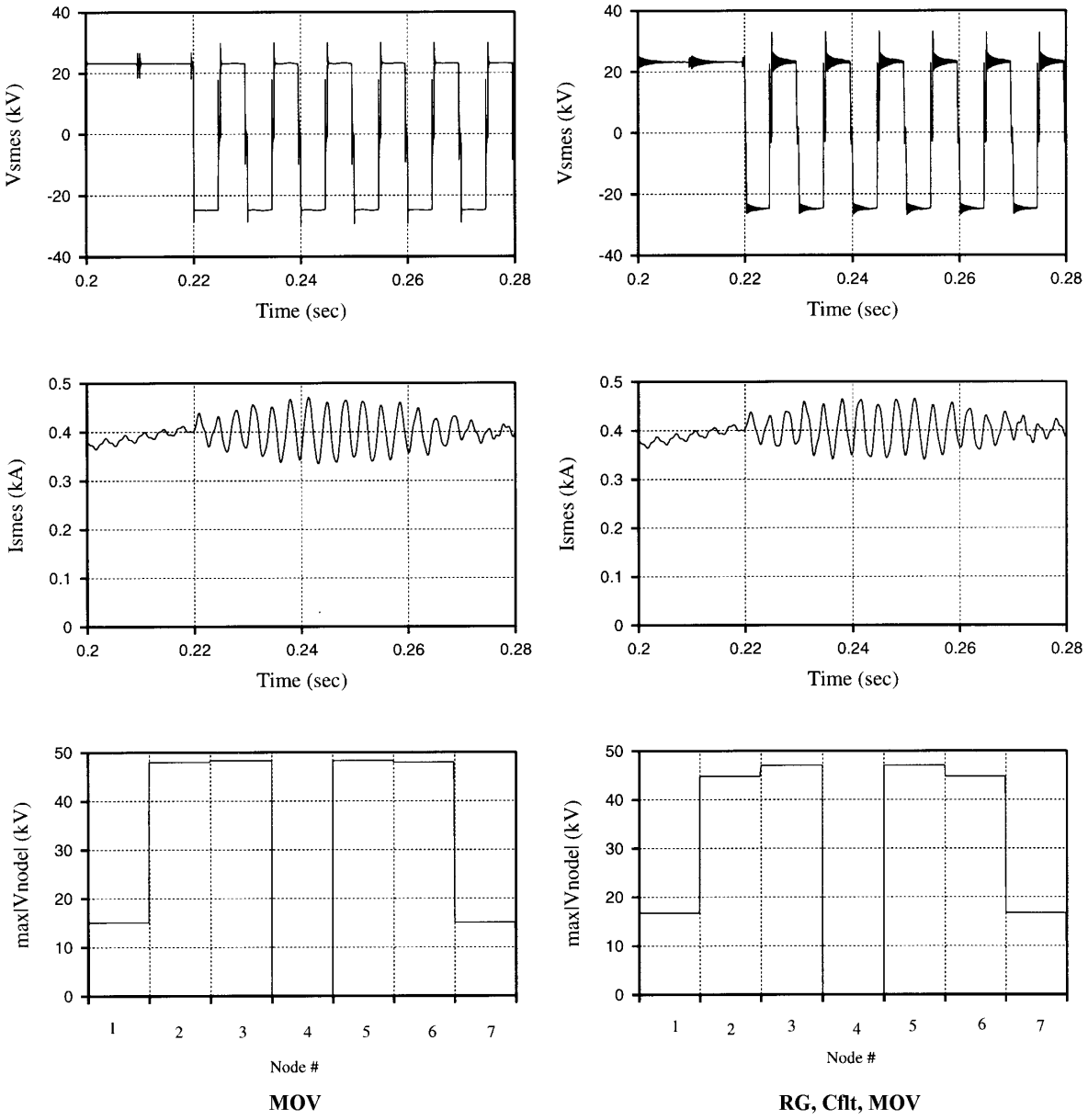

Figure V.11: Performance of SMES Transient Suppression Schemes

V.4.4. Tuning The Current Sharing Inductances

When *RG*, *Cflt* and MOV combination is applied, it was found that varying the sharing inductances *Lsi* can affect the terminal voltage under bypass switching conditions (the SMES coil was bypassed at t=0.228 sec. for 0.01sec). Figure V.13 gives the terminal voltage and

maximum internal voltages for two different values of *Lsi*. This figure clearly shows that the higher inductance value results in less high frequency voltage transients. This result was also observed in the SMES terminal current. This study can be carried out to determine the optimum value for *Lsi*.

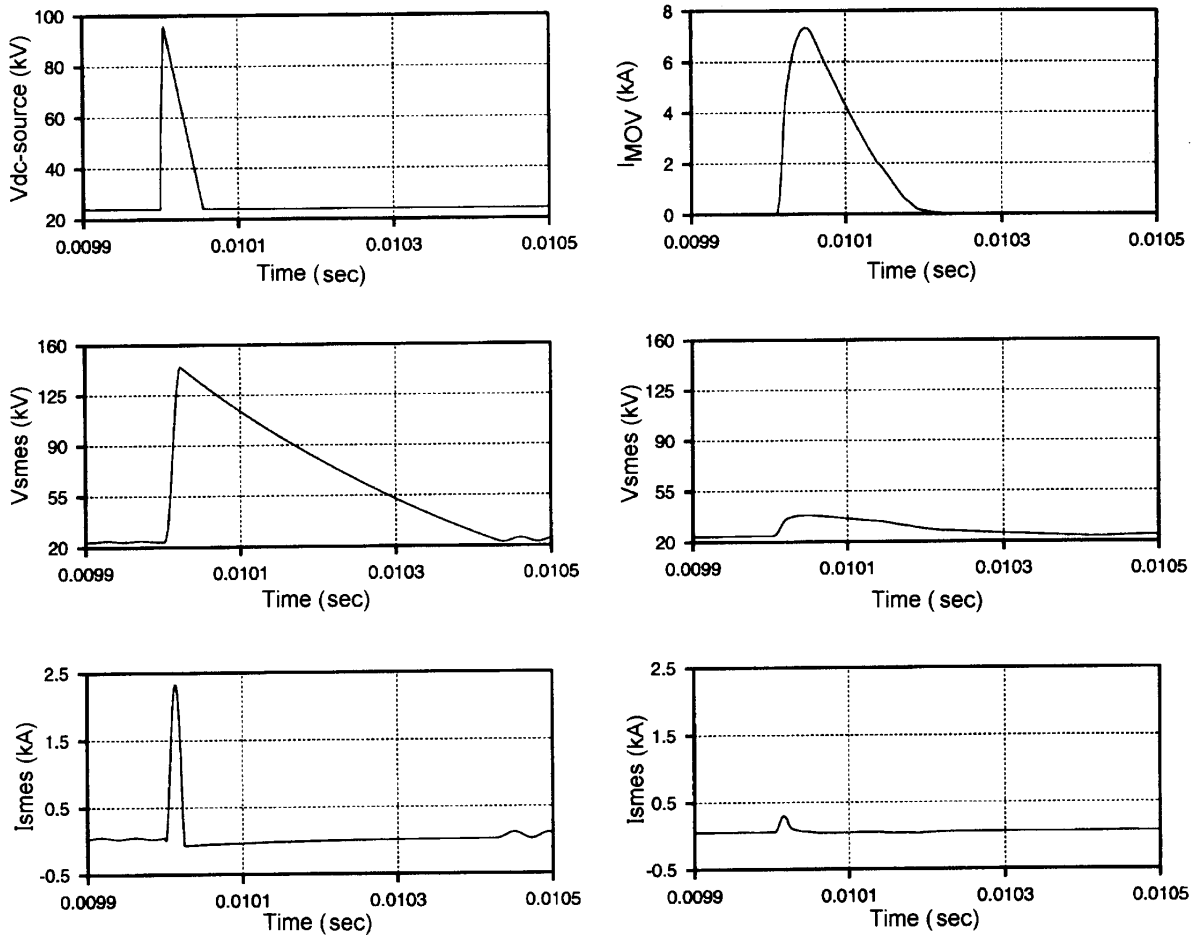

No Transient Suppression Full Transient Suppression

Figure V.12: Typical Lightning Impulse Responses of the SMES Coil w/wo Transient Suppression Schemes

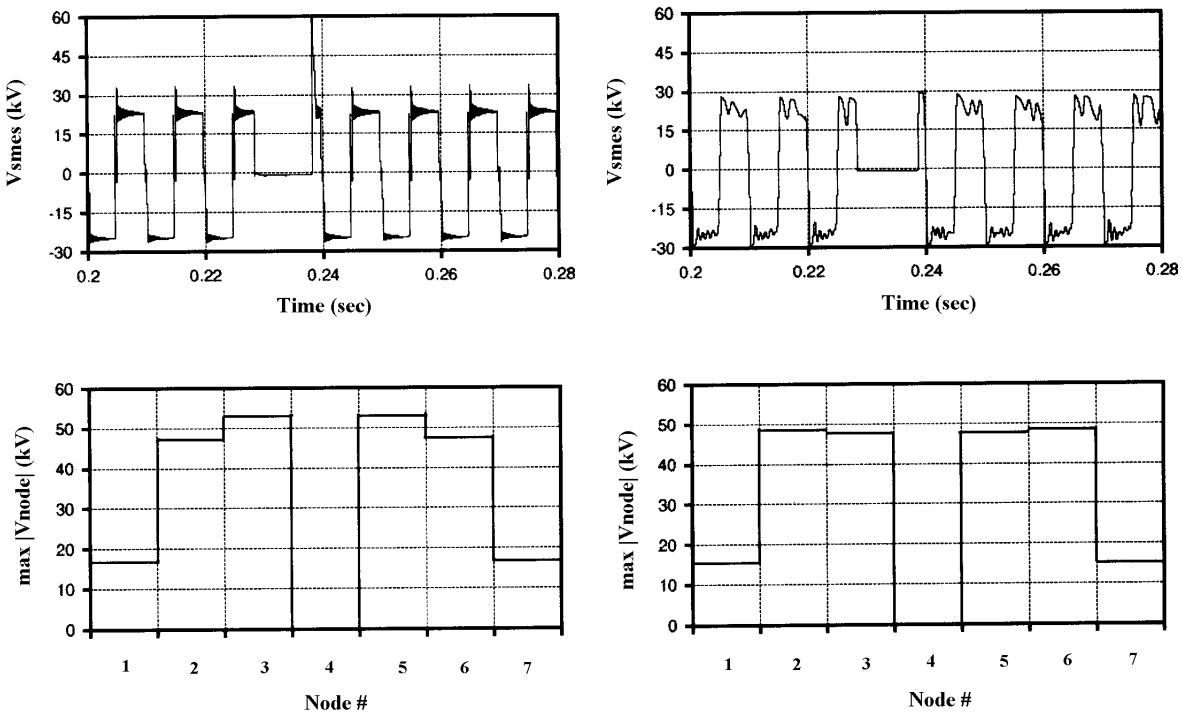

Lsi=0.1mH *Lsi*=10mH

Figure V.13: Influence of Sharing Inductances

V.5. The Impact of dc-dc Chopper Parameters on SMES Coil Transients

A dc-dc chopper is used to interface the SMES coil to a voltage source inverter. It controls the voltage across the coil. Section V.2 presented a chopper modeling based on a two quadrant 3-phase GTO configuration. The multi phase chopper design allows sharing the maximum coil current through the parallel paths. Due to the relationship given below, as the switching frequency of the chopper is low, the multi-phase approach is employed to eliminate the low order ripples that appears in the coil voltage or chopper output voltage.

Lowest ripple frequency = (Chopper Switching Frequency) x (Number of Phases)

GTOs have been widely accepted high power semiconductor devices used in high power converter designs. The chopper modeling of this study is also based on GTOs. In this section, several parameters of the GTO chopper, including time delay between GTO firing signals, switching frequency and snubber circuit, are modified to see its impact on SMES coil transients.

V.5.1. Snubber Circuit

GTO semiconductor devices utilize complex snubber circuits to reduce or limit the rate of di/dt during turn-on and dv/dt during turn-off. GTOs defined in EMTDC are ideal switches with a series R-C circuitry connected parallel with the switch. A series R-C along with a freewheeling diode was connected across the GTO device to enhance the default snubber circuit. The new snubber reduced the high frequency components of the SMES terminal voltage and current and decreased the maximum node voltage.

V.5.2. Time Delay between the Same Phase GTO Branches

The time delay between two GTOs of the same phase branches is varied at the same switching frequency (SF). The snubber circuit is added as presented in previous section. Its effect on the maximum internal node voltage is observed as given in Table V.2. It can be seen from the table that the internal maximum node voltages are very low when the delay angle is 180^o. Firing signals of the 3 phase choppers are shown in Figure V.14. Operating chopper at this angle has a considerable effect in reducing the maximum internal node voltages, and decreasing the terminal voltage and current transients.

The SMES terminal voltage and currents are plotted in Figure V.15 to when the delay angle is 15 and 180 degrees. No overvoltages occur across the SMES terminal, and current spikes become lower when the angle delay is set to 180 degrees. While keeping 180^o angle delay at the frequency of 100 Hz, the coil was charged for 0.22 sec, and the duty cycle has been changed varied between ¼ to ¾. The observed maximum node voltages are given in Figure V.16. Lower internal node voltages were obtained when the duty cycle is changed from one to half at t=0.22sec.

V.5.3. Switching Frequency

Since high power GTOs are operated at a low switching frequency, the switching frequency of a chopper has been selected 100 Hz. In order to see the effect of higher

switching frequency on transient overvoltages, the switching frequency was increased to 900Hz. Though, it may not be as high in practical consideration. With the higher GTO frequency, it was observed that terminal voltage transients are lower, but the magnitudes of internal node voltages and SMES terminal currents are about the same compared to the lower frequency case. Higher switching frequency, of course, will cause switching losses in the chopper.

Table V.2: Delay Angle Changes at SF=100Hz (Δt=10μsec)

Max|Vnode|/Δdelay	***0°***	***15°***	***30°***	***60°***	***90***	***120***	***150***	***180***
Vsmes1 (kV)	23.62	16.26	13.85	13.86	14.17	14.64	14.05	13.85
Vsmes2 (kV)	55.75	49.09	38.74	28.34	46.85	51.02	33.07	16.38
Vsmes3 (kV)	57.16	50.22	33.07	23.0	48.43	54.33	33.34	11.49
Vsmes4 (kV)	0	0	0	0	0	0	0	0
Vsmes5 (kV)	57.16	50.22	33.07	23.0	48.43	54.33	33.34	11.49
Vsmes6 (kV)	55.75	49.09	38.74	28.34	46.85	51.02	33.07	16.38
Vsmes7 (kV)	23.62	16.26	13.85	13.86	14.17	14.64	14.05	13.85

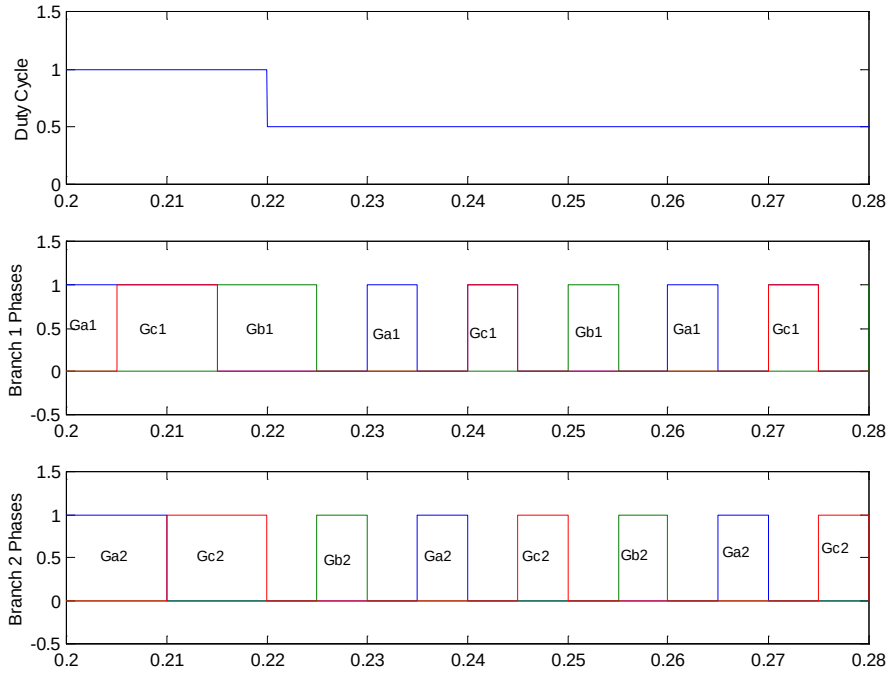

Figure V.14: Firing Signals of 3-phase GTO Chopper when the Delay Angle is 180°
Corresponding GTOs of firing signals for branch 1 (Ga1, Gb1, and Gc1) and branch 2 (Ga2, Gb2, Gc2) phases can be pointed in Figure V.3

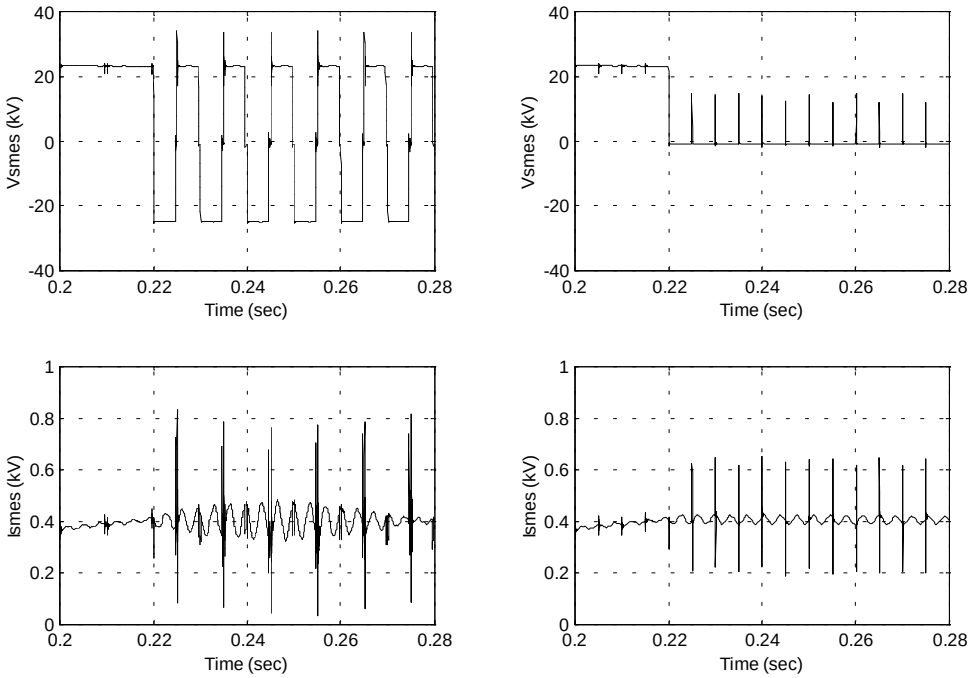

Figure V.15: SMES Terminal Voltage and Current Comparison for the Delay Angles of 15^{o} and 180^{o}

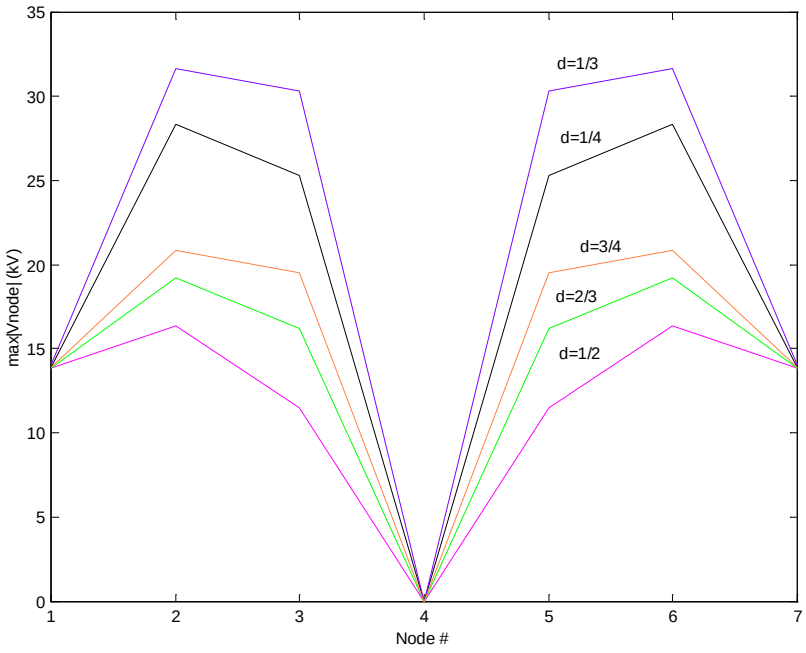

Figure V.16: Maximum Internal Node Voltages as Duty Cycle Changes at t=0.22 (Δt=10μsec).

V.6. Alternative Chopper Design

As stated before, the utilization of GTOs for high power converters have been well accepted. On the other hand, GTOs have low switching frequency capability that requires multi-pulse converter configurations. The advancements in IGBTs which are high switching frequency devices, and their availability for high power applications may introduce an alternative chopper design. Instead of having a 3-phase low frequency GTO chopper, a one-phase IGBT chopper can be considered for a SMES coil to interface with a voltage source inverter. Another approach could be replacing two level chopper with a three level chopper described by [Mao96]. These design approaches are simulated and given as subsections below.

V.6.1. Two Level One Phase IGBT Chopper

A two-level one –phase chopper is operated according to the four subtopologies shown in Figure V.17. The SMES coil is charged ($V_{smes}>0$) when subtopologies I, III, and IV are active, and it is discharged ($V_{smes}<0$) when subtopologies II, III, and IV are active. In previous cases, three-phase GTO choppers were utilized to eliminate the lower order harmonics since the switching frequency of GTOs was low. The chopper operation was also based on these subtopologies.

In this scenario, the use of IGBTs are recommended since they are higher switching frequency devices those do require neither snubber nor multi phase configuration. Distributed 6-segment SMES coil (defined in Section V.1) is connected to a two level one-phase IGBT chopper. The SMES terminal voltage, maximum internal node voltages and current are plotted in Figure V.18.

V.6.2. Three Level One-Phase IGBT Chopper

The SMES coil used in this study requires high power/voltage power electronics interface (96 MW/24kV). Special attention must be given on the performance parameters such as

switch voltage rating, current ripples and switching losses. A multilevel chopper approach introduced in [Mao96] shows that these parameters are reduced to 1/(k-1) in a k-level converter compared to in a traditional chopper. A three- level chopper is considered to be connected to the distributed SMES coil for its simplicity to compare its performance with the performance of two level choppers on the SMES transients.

A three level one- phase chopper connection to a SMES coil is illustrated in Figure V.19. Diodes DC1 and DC2 are used to clamp the maximum switch voltage at *Vdc*/2. As a matter of fact that all switches in this configuration only block the *Vdc*/2. This is very attractive for high power switches since a better voltage sharing achieved, consequently higher reliability and efficiency are obtained. This structure consists of nine subtopologies as shown in Figure V.20. A proper PWM scheme eliminates the redundant states and operates the chopper with the subtopologies that produce the voltage levels adjacent to SMES terminal voltage to reduce switching loss and current ripple. Table V.3 is generated to determine the switching strategies.

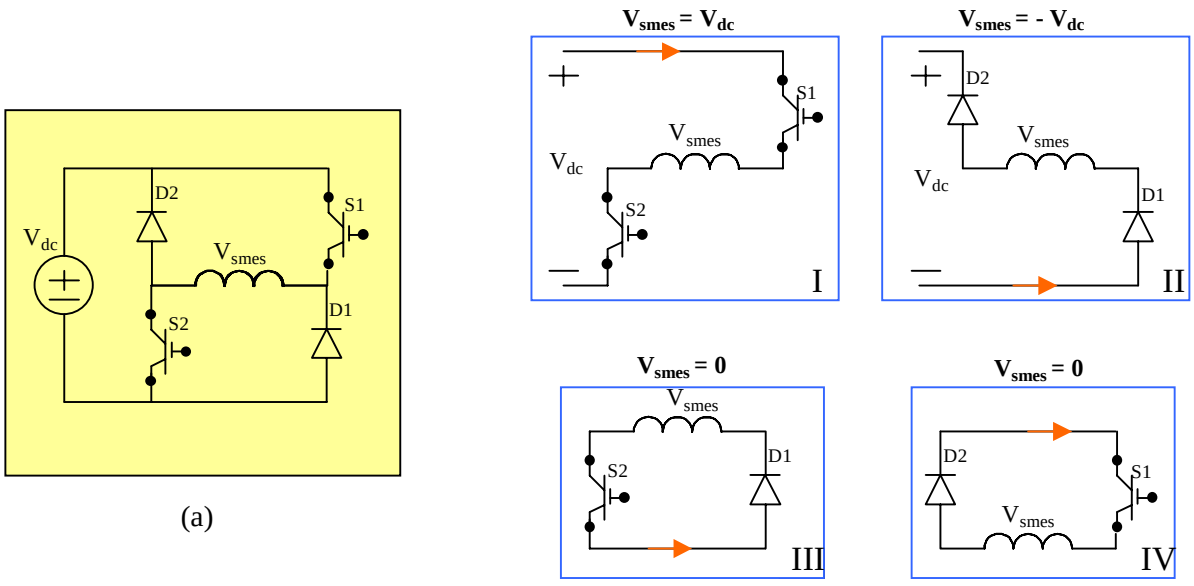

Figure V.17: (a) Two Level Two-Quadrant dc-dc Chopper (b) Subtopologies for the Chopper

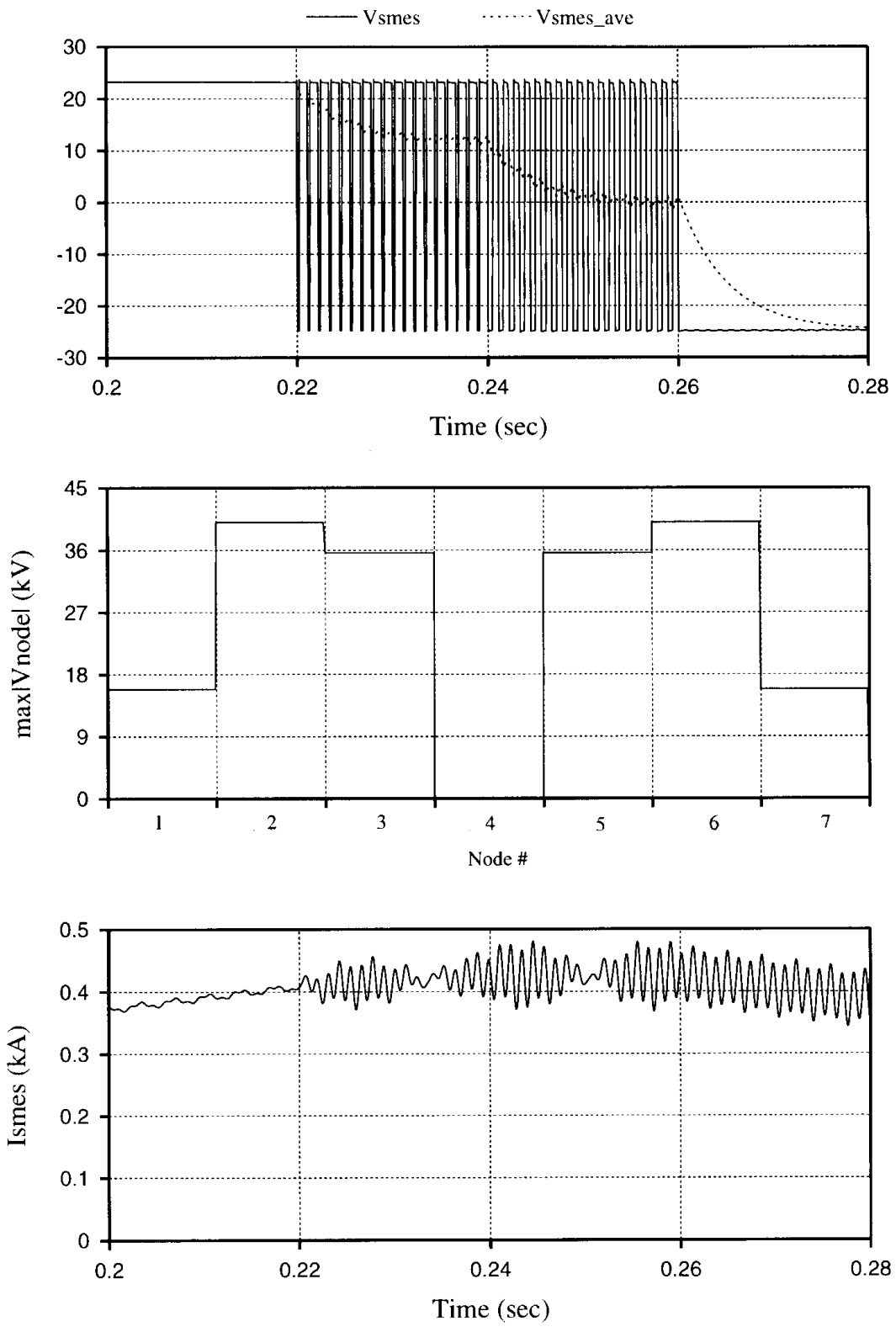

Figure V.18: SMES Current and Voltages when a SMES is Connected to a Two Level Chopper

With the switching strategy stated above, a three level one-phase IGBT chopper was designed and connected to the studied coil. The delay angle between S1 and S2 or S3 and S4. The coil was charged for 0.22 sec, then the voltage across the coil was varied three times in 0.6 sec. The results show that the magnitudes of voltage and current transients are reduced considerably. The SMES terminal voltage, maximum internal voltages and SMES currents are shown in Figure V.21. Compared to two-level one-phase chopper the transient overvoltages are lower.

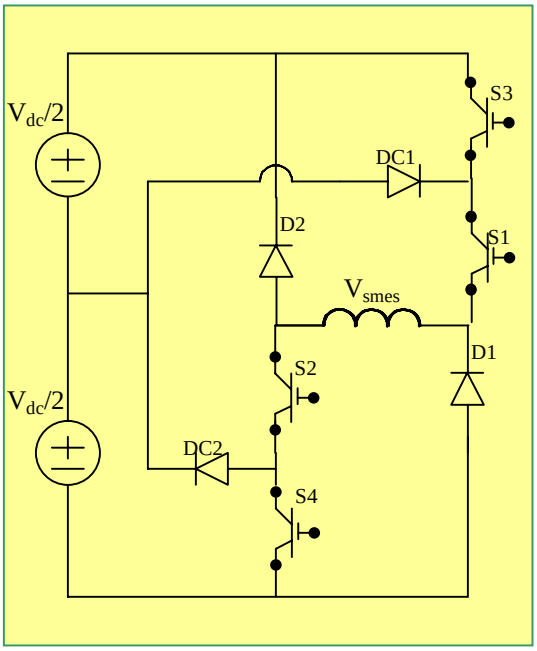

Figure V.19: Three Level One-Phase dc-dc Chopper

Maximum internal node voltages were compared when a distributed SMES coil is connected to a two-level and three-level one-phase IGBT chopper. The results are shown in Figure V.22.

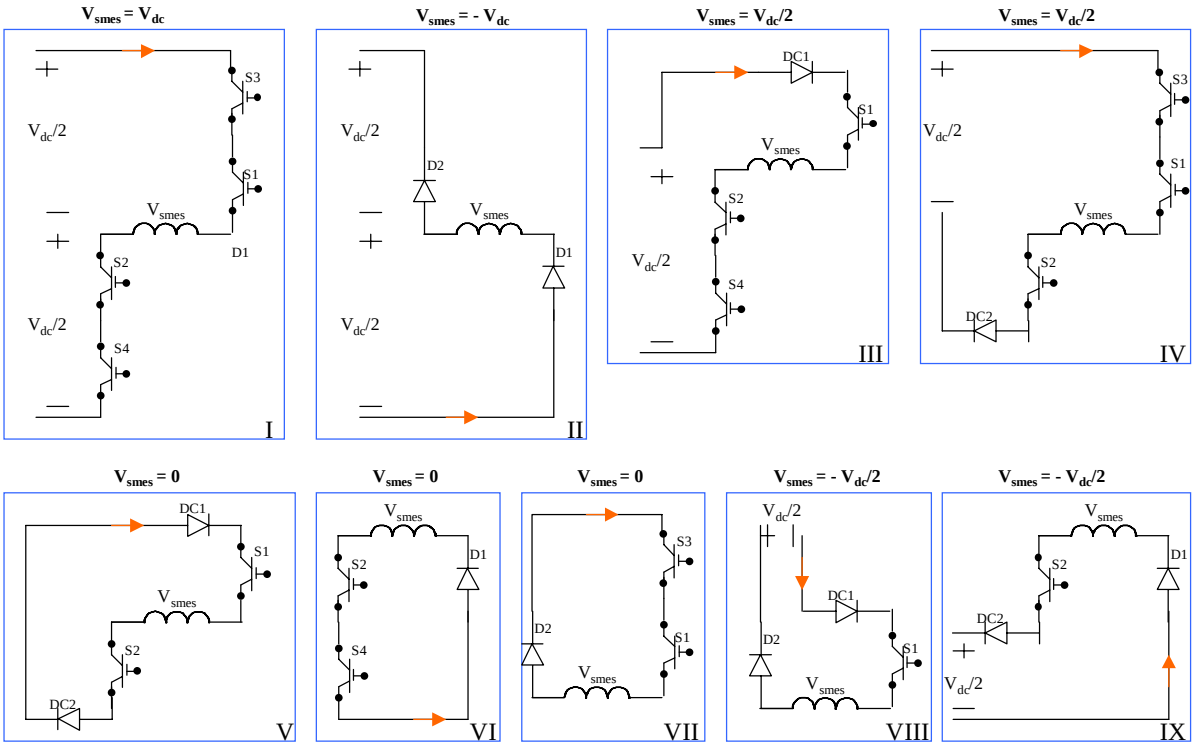

Figure V.20: Subtopologies of Three Level One-Phase Chopper

Table V.3: Three Level Chopper Switching Strategies

Operating Range	***Active Subtopologies***	***S1***	***S2***	***S3***	***S4***
1 > Vsmes/Vdc > 0.5	(I), (III), (IV)	on	on	d>0.5	d>0.5
0.5 > Vsmes/Vdc > 0	(III), (IV), (V)	on	on	d<0.5	d<0.5
0 > Vsmes/Vdc > -0.5	(VIII), (IX), (V)	d>0.5	d>0.5	off	off
-0.5 > Vsmes/Vdc > -1	(VIII), (IX), (II)	d<0.5	d<0.5	off	off

When two switches have the duty cycle (d) of being greater 0.5 or less than 0.5, there could be delay time between them. “On” means that the switch is always conducting,, and “off” means that the switch is not conducting.

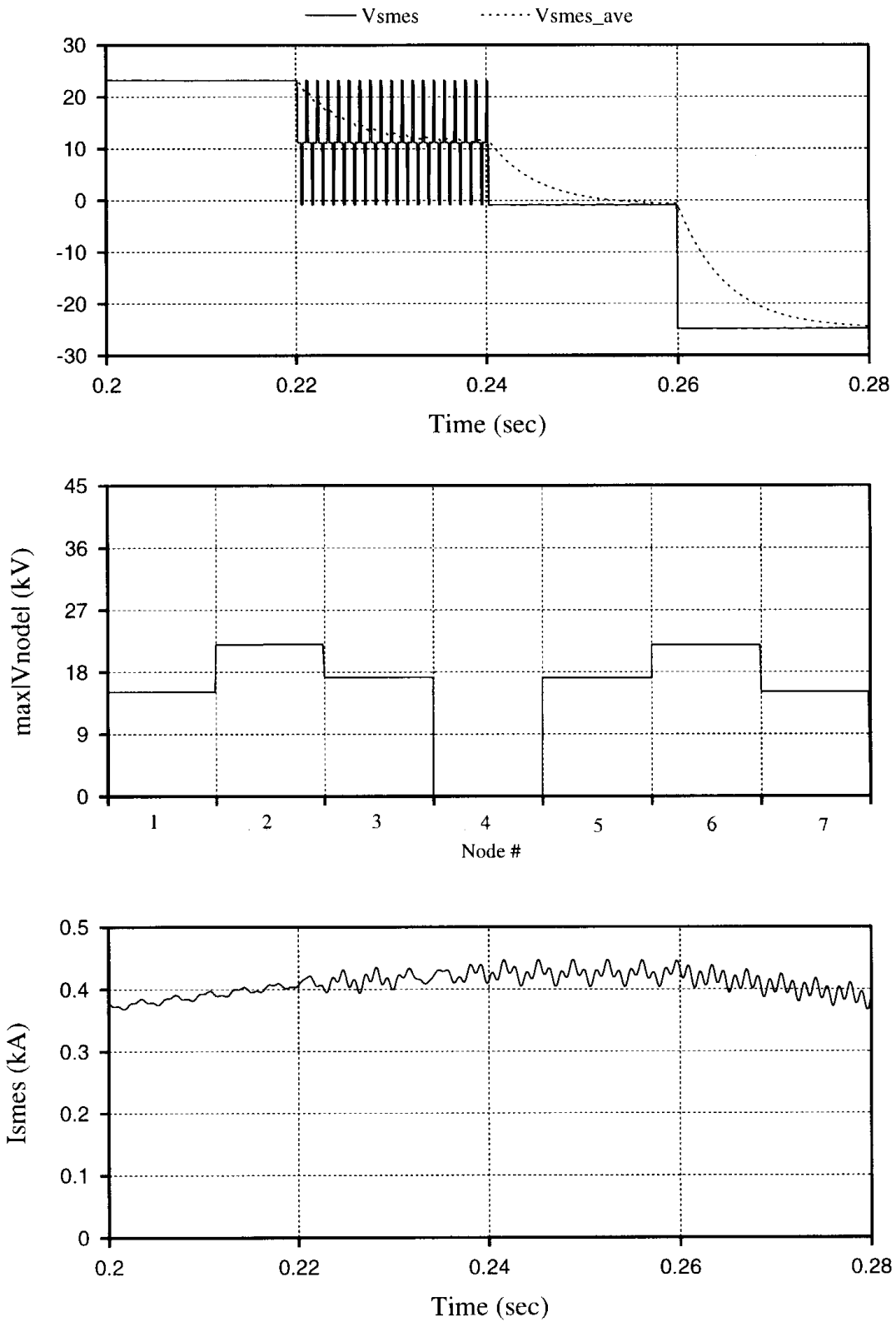

Figure V.21: SMES Current and Voltages when a SMES is Connected to a Three Level Chopper

V.7. Summary

The results of the electromagnetic transients and voltage suppression study of a 100MJ SMES system proposed for a FACTS/ energy storage applications are presented. This study aimed to better understand the transient processes and interactions between a high power and high voltage SMES coil and its power electronics interface, dc-dc chopper.

The simulation and integrated modeling of the SMES coil and associated power electronics have been performed using an electromagnetic transient program, PSCAD^{TM}/ EMTDC^{TM}. The simulation used detailed SMES coil and multiphase GTO-based chopper models. Transient voltages in the SMES coil include those generated by normal GTO, SMES system bypass switching, and those coming from the ac system. Transient suppression methods may include adding filtering capacitors, MOV elements, sharing inductances, changing the chopper switching frequency, and snubber circuit parameters. An alternative chopper design, three-level one-phase IGBT chopper, was recommended.

Although the electromagnetic interactions of a coil and the power electronics interface have been studied before, the high power and the high voltage level of this SMES application have presented new challenges to the coil and the power electronics interface designers. These simulations have helped to identify some areas that may be further investigated and optimized as the design of the system proceeds.

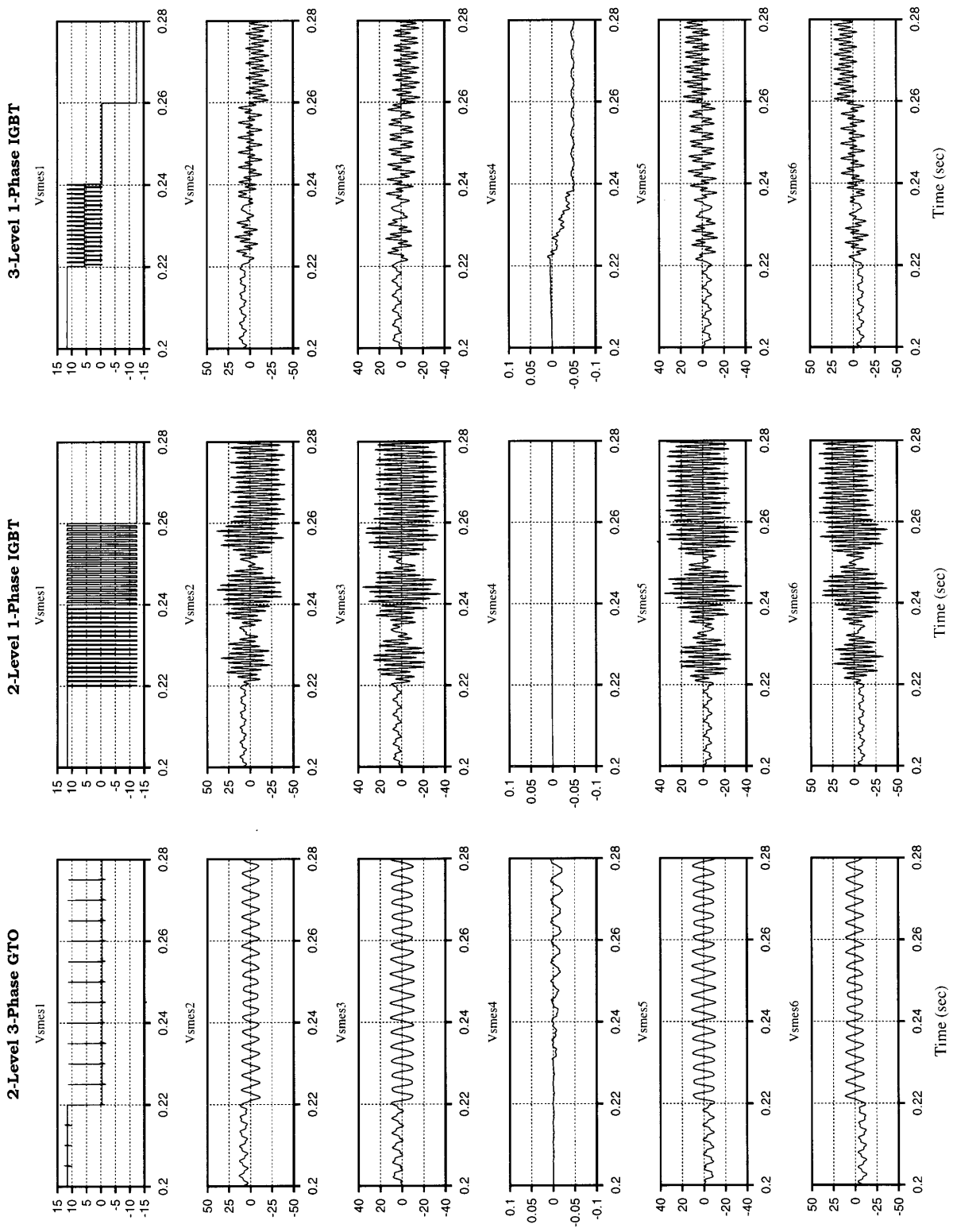

Figure V.22: Comparison of Internal Node Voltages for Different Chopper Topologies

CHAPTER VI

INTEGRATION OF SUPERCONDUCTING MAGNETIC ENERGY STORAGE WITH A STATIC SYNCHRONOUS COMPENSATOR

This chapter discusses the integration of a static synchronous compensator (StatCom) with the superconducting magnetic energy storage (SMES) system in damping power oscillations. The performance of the StatCom, a self-commutated solid-state voltage converter, can be improved with the addition of energy storage. In this study, a 100 MJ 96 MW (peak) SMES coil is attached to the voltage source inverter front end of a ±160 MVA StatCom via a dc-dc chopper. The real and reactive power responses of the integrated system to system oscillations are studied using an electromagnetic transient program PSCAD^{TM}/EMTDC^{TM}, and the findings are presented. The results show that, depending on the location of the StatCom-SMES combination, simultaneous modulation of real and reactive power can significantly improve the performance of the combined compensator. Some of these results are also presented in [Arsoy99a, Arsoy00a, Arsoy00b].

VI.1. Introduction

As expected and demonstrated in the past [Roger83], modulation of real power can have a more significant influence on damping power swings than can reactive power. Even without much energy storage, static compensators with the ability to control both reactive and real power can enhance the performance of a transmission grid.

A static synchronous compensator (StatCom), is a second generation flexible ac transmission system controller based on a self-commutated solid-state voltage source inverter. It has been used with great success to provide reactive power/voltage control and transient stability enhancement [Hingo00, Sen99, Schaud98, Patil98, Gyug94]. Currently, there are StatCom controllers installed in two substations, (one at Sullivan substation of Tennessee Valley Authorization, TVA, and the other one is at Inez substation of American Electric Power, AEP) [Schau95, Schau98]. A StatCom, however, can only absorb/inject

reactive power, and consequently is limited in the degree of freedom and sustained action in which it can help the power grid. The addition of energy storage allows the StatCom to inject and/or absorb active and reactive power simultaneously, and therefore provides additional benefits and improvements in the system. The voltage source inverter front-end of a StatCom can be easily interconnected with an energy storage source such as a superconducting magnetic energy storage (SMES) coil via a dc-dc chopper.

Advances in both superconducting technologies and the necessary power electronics interface have made SMES a viable technology for high power utility and defense applications [Karas99]. The characteristics of a SMES system such as rapid response (Mili-second), high power (multi-MW), high efficiency, and four-quadrant control can meet the power industry's demands for more flexible, reliable and fast active power compensation devices. SMES systems can provide improved system reliability, dynamic stability, enhanced power quality and area protection [Hasse83, Mitan89, Bonne90, Lasse91, Kral95], as its potential applications are shown in Figure VI.1 [Giese98]. The squared area indicates the possible cost effective SMES applications.

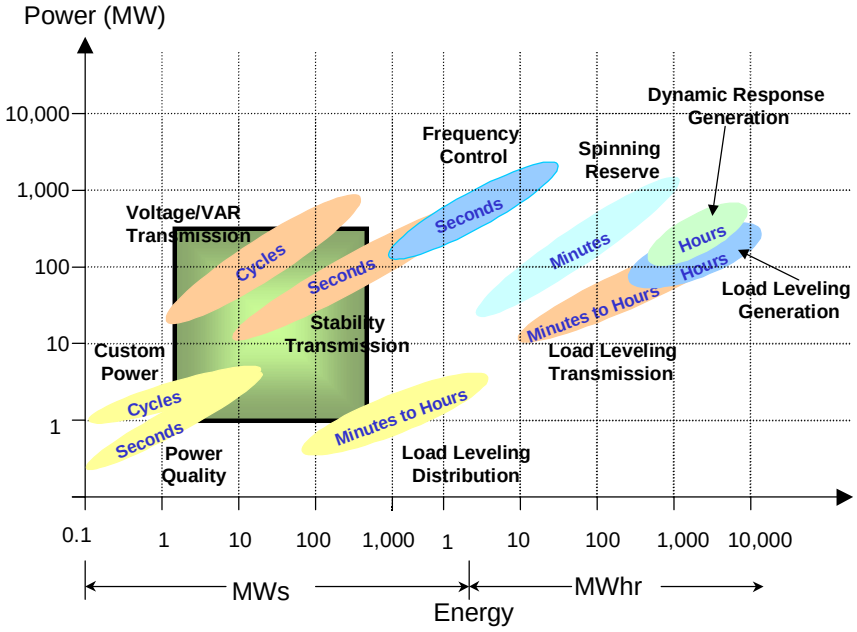

Figure VI.1: SMES Power and Energy Requirements for Potential Electric Utility Applications

Since SMES requires an ac/dc inverter, it can be attached to an existing StatCom [Schau98] unit via a dc-dc chopper to improve the operation of the StatCom. This work intends to model and simulate the dynamics of the integration of a ±160MVAR StatCom, and 100 MJ SMES coil (96MW peak power and 24 kV dc interface) which has been designed for a utility application. Modeling and control schemes utilized for the combined compensator are described first. Then, the impact of the location of the combined compensator on dynamic system response is discussed, and the findings are presented.

VI.2. Modeling and Control

A typical ac system equivalent was used in this study order to show the dynamic performance of the StatCom with a SMES coil. The circuitry simulated representing this integration is shown in Figure VI.2. The detailed representation of the StatCom, dc-dc chopper, and SMES coil is depicted in Figure VI.3. In the figures, the units of resistance, inductance, and capacitance values are Ohm, Henry, and micro-Farad, respectively.

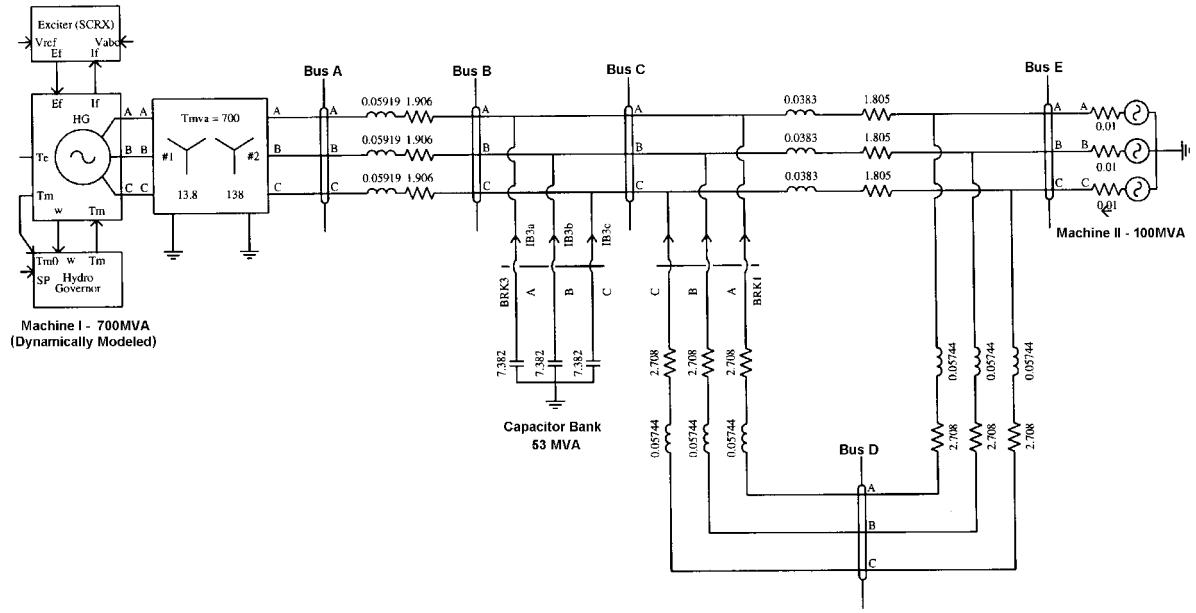

Figure VI.2: AC System Equivalent

VI.2.1. The AC Power System

The ac system equivalent used in this study corresponds to a two machine system where one machine is dynamically modeled (including generator, exciter and governor) to be able to demonstrate dynamic oscillations. Dynamic oscillations are simulated by creating a three-phase fault in the middle of one of the parallel lines at *Bus D* (Refer to Fig. 2). A bus that connects the StatCom-SMES to the ac power system is named a StatCom terminal bus. The location of this bus is selected to be either *Bus A* or *Bus B*.

VI.2.2. The StatCom

As can be seen from Figure VI.3, two-GTO based six-pulse voltage source inverters represent the StatCom used in this particular study. The voltage source inverters are connected to the ac system through two 80 MW coupling transformers, and linked to a dc capacitor in the dc side. The value of the dc link capacitor has been selected as 10mF in order to obtain smooth voltage at the StatCom terminal bus.

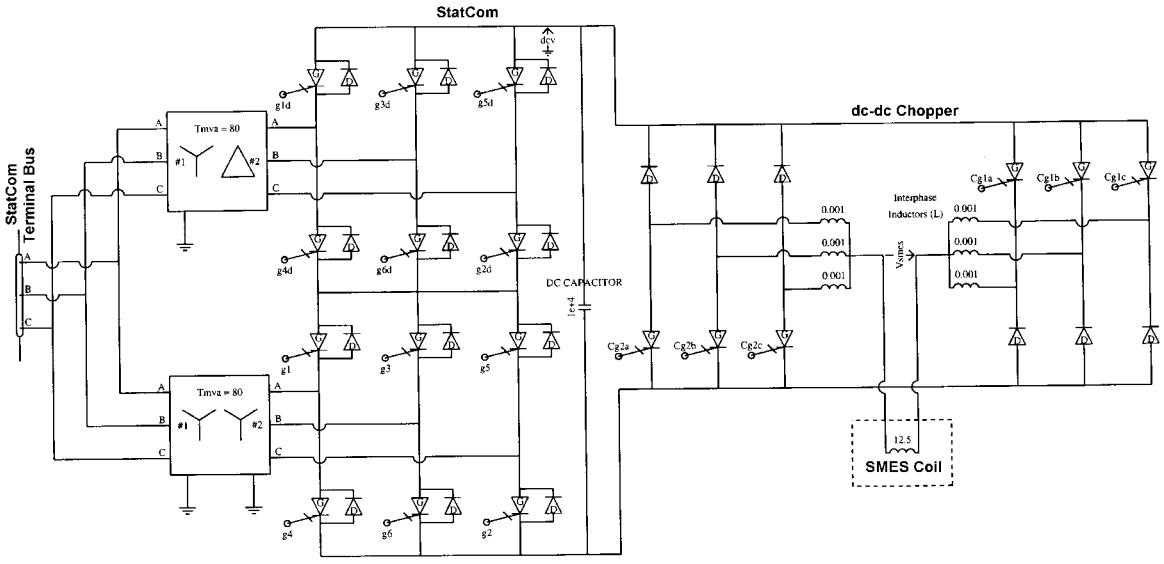

Figure VI.3: Detailed Representation of StatCom, dc-dc Chopper, and SMES Coil

As stated in [Hingo00, Sen99], a GTO based inverter connected to a transmission line acts as an alternating voltage source in phase with the line voltage, and, depending on the voltage produced by the inverter, an operation of inductive or capacitive mode can be achieved. It has also been emphasized that a dc link capacitor establishes equilibrium between the instantaneous output and input power of the inverter.

The primary function of the StatCom is to control reactive power/voltage at the point of connection to the ac system. Figure VI.4 shows the control diagram of the StatCom used in the simulation. The control inputs are the measured StatCom injected reactive power (*SQstat*) and the three-phase ac voltages (*Va*,*Vb* and *Vc*) and their per unit values measured at the StatCom terminal bus. The per unit voltage is compared with base per-unit voltage value (1pu). The error is amplified to obtain reference reactive current which is translated to the reference reactive power to be compared with *SQstat*. The amplified reactive power error-signal and phase difference signal between measured and fed three phase system voltages are passed through a phase locked loop control. The resultant phase angle is used to create synchronized square waves.

To generate the gating signals for the inverters, line to ground voltages are used for the inverter connected to the Y-Y transformer, whereas line to line voltages are utilized for the inverter connected to the Y-D transformer. This model and control scheme is partly based on the example case given in the UNIX Version of EMTDC^{TM}/PSCAD^{TM} simulation package, though some modifications have been made to meet the system characteristics. These modifications include change in transformer ratings and dc capacitor rating, tuning in control parameters and adding voltage loop control to obtain reference reactive power. It should be noted that the StatCom control does not make use of signals such as deviation in speed or power to damp oscillations, rather it maintains a desired voltage level at the terminal bus that the StatCom is connected to.

In the initial phase of this study, the StatCom was controlled so that it can regulate the desired reactive power flow at the StatCom terminal. Compared to the control presented in Figure VI.4, there was no output voltage control loop to obtain the reference reactive power (*Qref*). This value is entered as desired, and it was compared to the measured reactive power

flow at the StatCom ac terminal rather than the injected StatCom reactive power. The simulation results including this type of control is presented in [Arsoy99b].

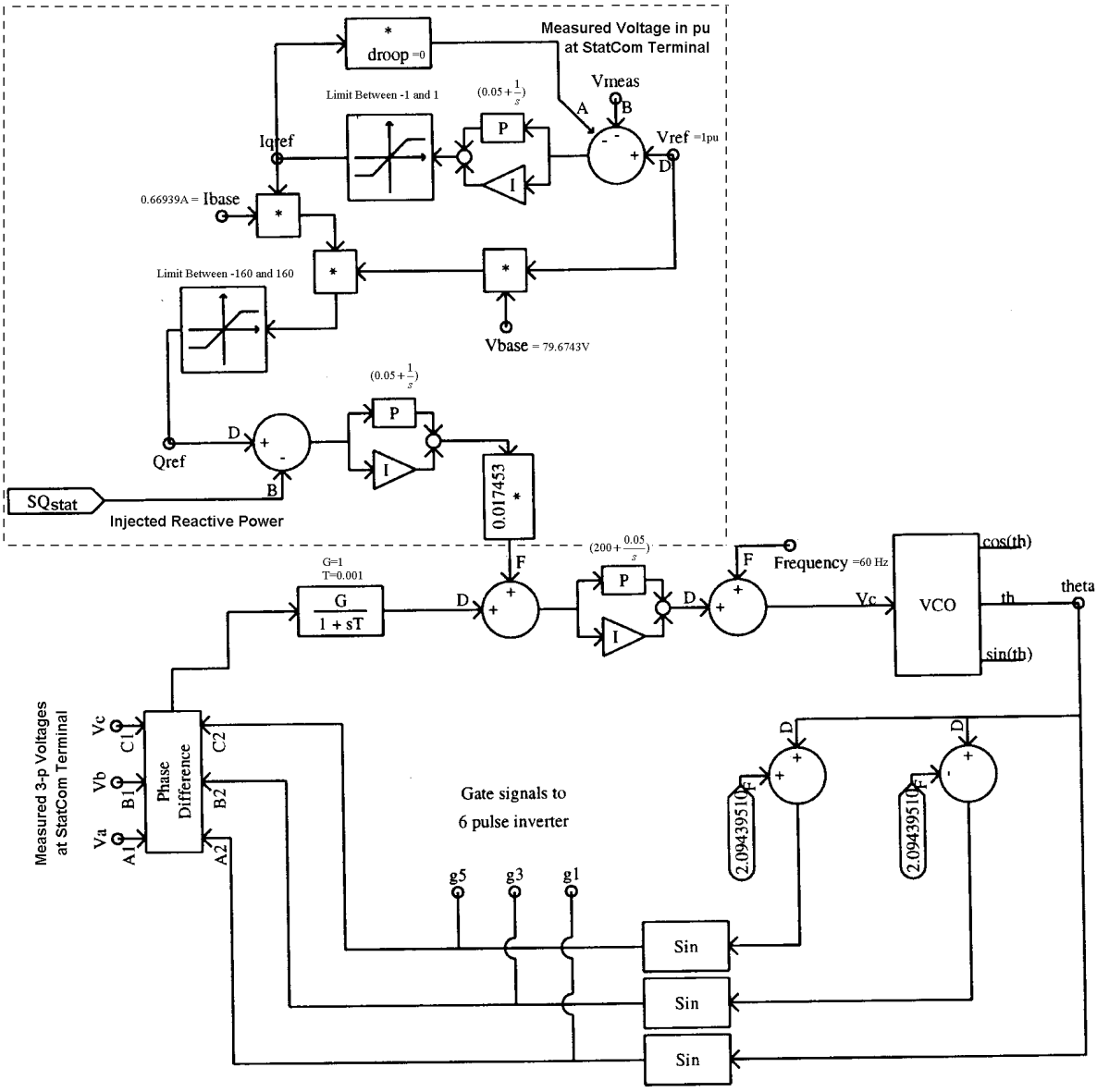

Figure VI.4: StatCom Control

PSCAD StatCom Control Approach: The area in the dashed rectangular generates the order angle. Without this signal, the rest represents a phase locked loop control so that the StatCom terminal voltage and the StatCom output voltages are synchronized. The relationship between input and output of VCO (Voltage controlled oscillator) is given with the simple equation of $th(t) = th(t - dt) + 2\pi dtVc$ where *th* is the output in radians, *dt* is the time step of simulation, Vc is the input. As the result, a ramp output from zero to 2π is obtaine. When *th* is equal to 2π, the output is reseted, and a saw tooth function with values from 0 to 2π where the width of the ramp is one cycle. Three signals created based on *th* is compared to the measured StatCom terminal 3-phase voltages. The average value of the phase difference is smoothed by real pole, and fed into a PI controller. By adding system frequency to the output of the PI controller, the input to VCO is varied around system frequency which creates the angle *th* in sawtooth waveform synchronized with StatCom terminal voltage *A*. With the addition of angle order created by the reactive power control, the output of VCO, *th*, is synchronized to voltage *A* and shifted by the ordered angle so that the desired reactive output is obtained.

VI.2.3. The DC-DC Chopper and SMES Coil

A SMES coil is connected to a voltage source inverter through a dc-dc chopper. It controls dc current and voltage levels by converting the inverter dc output voltage to the adjustable voltage required across the SMES coil terminal. The purpose of having inter-phase inductors is to allow balanced current sharing for each chopper phase.

A two-level three-phase dc-dc chopper used in the simulation has been modeled and controlled according to [Arsoy98, Arsoy99a]. The phase delay was kept 180 degrees to reduce the transient overvoltages. The chopper's GTO gate signals are square waveforms with a controlled duty cycle. The average voltage of the SMES coil is related to the StatCom output dc voltage with the relationship of $V_{SMES-av} = (1 - 2d)V_{dc-av}$ where $V_{SMES\text{-}av}$ is the average voltage across the SMES coil, $V_{dc\text{-}av}$ is the average StatCom output dc voltage, and *d* is duty cycle of the chopper (GTO conduction time/period of one switching cycle) [Hassa91].

This relationship states that there is no energy transferring (standby mode) at a duty cycle of 0.5, where the average SMES coil voltage is equal to zero and the SMES coil current is constant. It is also apparent that the coil enters in charging (absorbing) or discharging (injecting) mode when the duty cycle is larger or less than 0.5, respectively. Adjusting the duty cycle of the GTO firing signals controls the rate of charging/discharging.

As shown in Figure VI.5, the duty cycle is controlled in two ways. Three measurements are used in this chopper-SMES control: SMES coil current (*CIsmes*); ac real power (*SPmeas*) measured at the StatCom terminal bus; and dc voltage (*dcvolt*) measured across the dc link capacitor. The SMES coil is initially charged with the first control scheme, and the duty cycle is set to 0.5 after reaching the desired charging level. The second control is basically a stabilizer control that orders the SMES power according to the changes that may happen in the ac real power. This order is translated into a new duty cycle that controls the voltage across the SMES coil, and therefore the real power is exchanged through the StatCom.

VI.3. Case Studies

In order to demonstrate the effectiveness of the StatCom-SMES combination, several cases are simulated. These cases are given as subsections here. A three-phase fault is created at *Bus D* of Figure VI.2 to generate dynamic oscillations in each case. The plot time step is 0.001 sec for all the figures given in these cases.

VI.3.1. AC Oscillations and StatCom-Only Mode

A two-machine ac system is simulated. The inertia of the machine I was adjusted to obtain approximately 3 Hz oscillations from a three phase fault created at time=3.1 sec and cleared at time=3.25sec. When there is no StatCom -SMES connected to the ac power system, the system response is depicted in the first column of FigureVI.6 in the interval of 3 to 5 sec where first and second rows correspond to the speed of Machine I and ac voltage at *Bus B*, respectively. When a StatCom-only is connected, the response is given in the second

column of Figure VI.6. Since the StatCom is used for voltage support, it may not be as effective in damping oscillations.

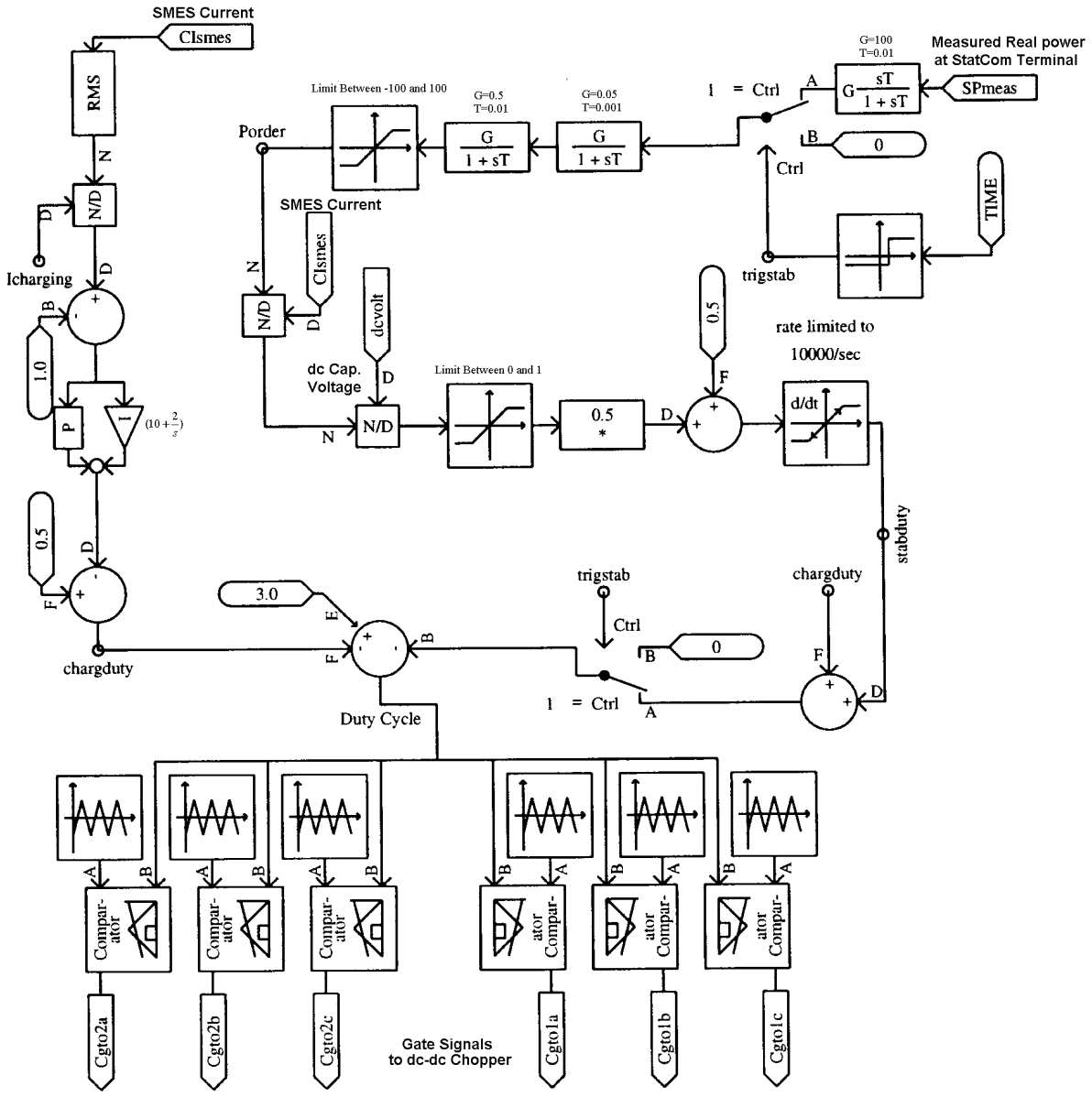

Figure VI.5: SMES and Chopper Control

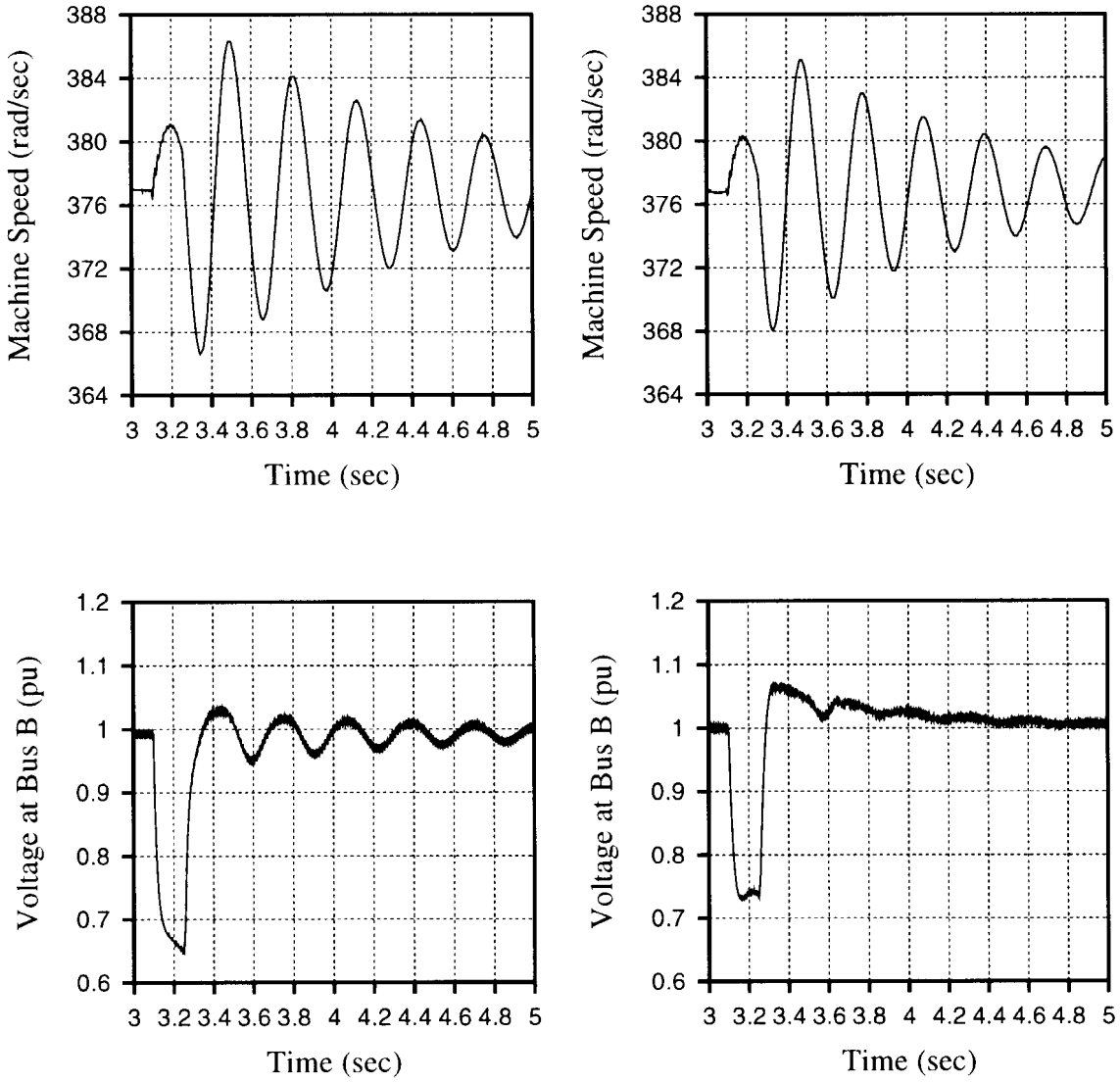

No StatCom-SMES StatCom-only *at Bus B*

Figure VI.6: Dynamic Response to AC System Oscillations

VI.3.2. StatCom-SMES Located at Bus B

Now, the 100MJ-96MW SMES coil is attached to a 160MVAR StatCom through a dc-dc chopper at *Bus B*. The SMES coil is charged by making the voltage across its terminal positive until the coil current becomes 3.6kA. Once it reaches this charging level, it is set at the standby mode. In order to see the effectiveness of the StatCom-SMES combination, the

SMES activates right after the three-phase fault is cleared at 3.25sec. The dynamic response of the combined device to ac system oscillation is depicted in the first column of Figure VI.7. The first plot shows the machine frequency, the next two gives the real and reactive power injected or absorbed by the StatCom-SMES device, and the fourth one gives the StatCom terminal voltage in pu. In these figures, negative real and/or reactive power values represent the injected power from the device to the ac system. When compared to no compensation and StatCom-only cases shown in FigureVI.6, both frequency and voltage oscillations were damped out faster.

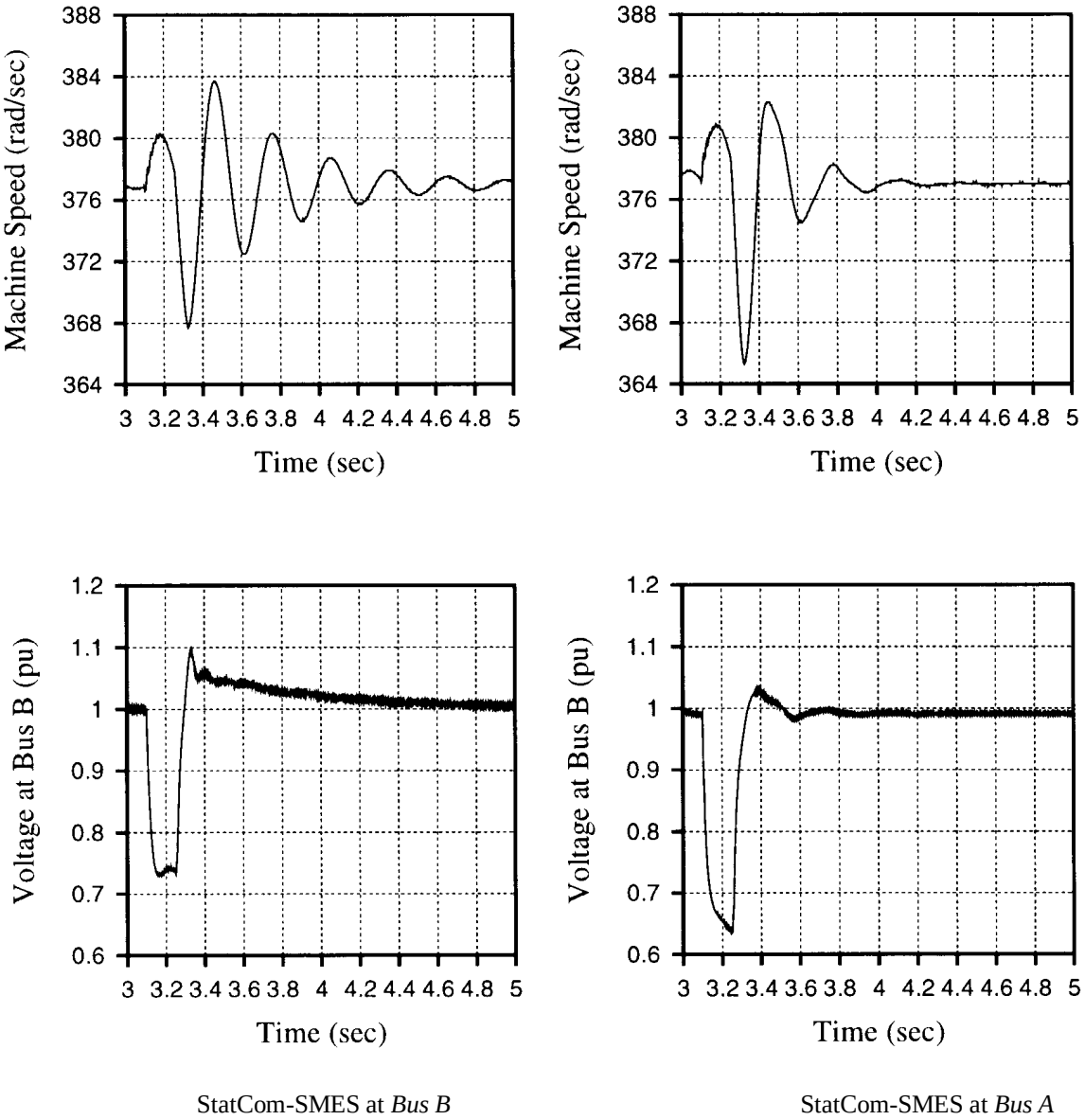

StatCom-SMES at *Bus B* StatCom-SMES at *Bus A*

Figure VI.7: Dynamic Response of StatCom-SMES to AC System Oscillations

VI.3.3. StatCom-SMES Located at Bus A

The StatCom -SMES combination is now connected to the ac power system at a bus near the generator bus. The same scenario drawn in Section VI.3.2 applies to this case. The results are shown in the second column of Figure VI.7. Compared to other two cases, StatCom-SMES connected to a bus near the generator shows very effective results in damping electromechanical transient oscillations caused by a three-phase fault.

VI.3.4. The Performance of StatCom-SMES at Different Locations

The real and reactive power responses of the compensator to oscillations are compared for different locations Figure VI.8 compares the StatCom real and reactive power responses for these previous cases (StatCom-SMES at *Bus B* and StatCom-SMES at *Bus A)*. When the StatCom-SMES is located at *Bus B*, it provides a voltage support by injecting approximately 50MVA., and damps the oscillations. When the combined compensator is located at *Bus A*, no reactive power injection is necessary since *Bus A* voltage is fixed by the exciter of Machine I.

As a response to system oscillations, the operation of SMES is also compared for different locations as shown in Figure VI.9. From top to bottom, SMES current, SMES terminal voltage, dc capacitor voltage and SMES energy are plotted. SMES current hence energy does not change abruptly, which is expected. Otherwise, transient overvoltages are observed at the terminal of SMES. SMES terminal voltage changes its polarity as the coil charges or discharges. The positive SMES voltage charges the SMES coil, which absorbs power from the ac system. Any variation on the StatCom ac terminal voltage is reflected to the dc capacitor voltage or the input voltage to the dc-dc chopper as shown in the 3rd row of Figure VI.9.

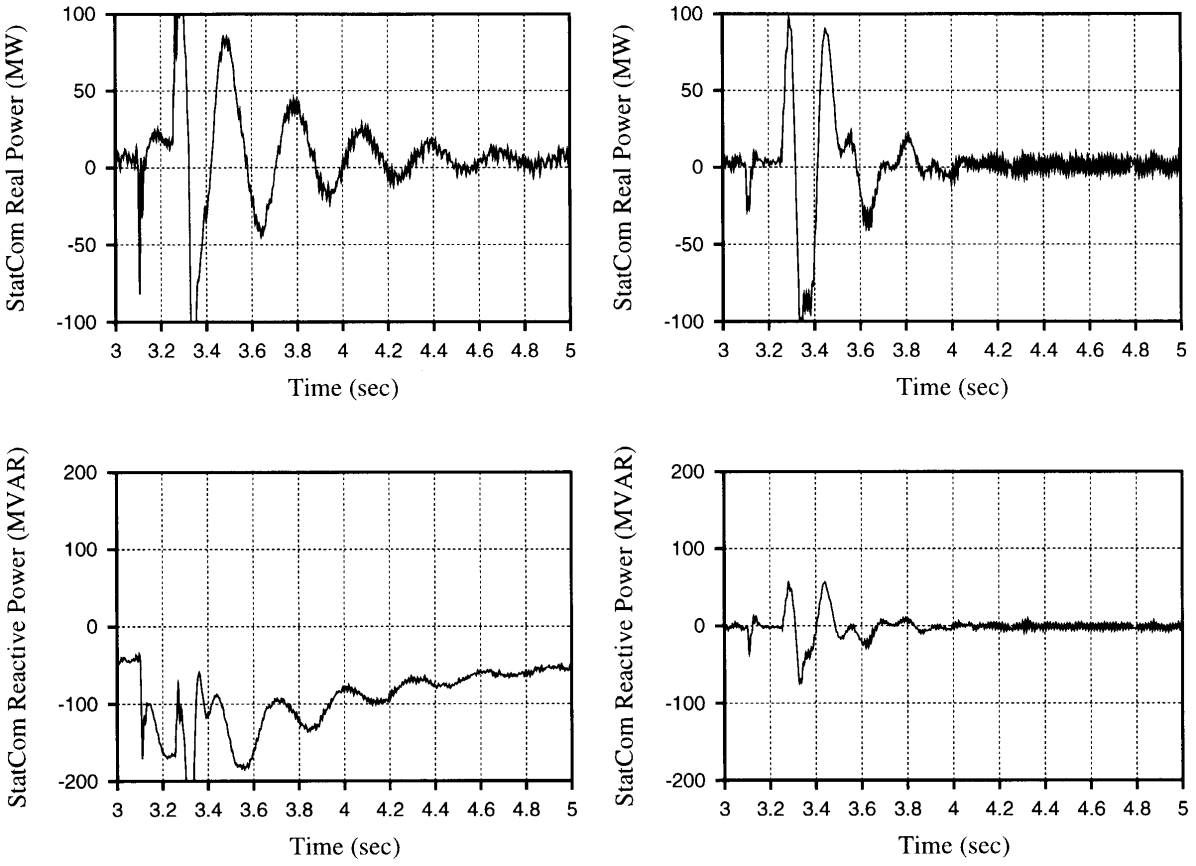

Figure VI.8: Real and Reactive Power Responses of StatCom-SMES

VI.3.5. Adding Load at Bus B

In this case, the performance of the combined compensator was studied when a 100 MVA load at power factor of 0.85 is connected to *Bus B*. The existence of the load forced the controller to be operated closer to its maximum rating.

The performance of the compensator to ac system oscillations showed similar results as obtained in previous two cases. The dynamic response of the StatCom-SMES is shown in Figure VI.10. The first row correspond to the speed of the machine, the second and third row correspond to real and reactive power injection of StatCom to the ac system. The voltage at *Bus B* is plotted in the last row of Figure VI.10. The voltage at *Bus B* of the second column is

not supported well since the StatCom-SMES compensator is located at *Bus A*. On the other hand, it shows better damping performance.

The location of the load was changed to *Bus E*, where the load rating was varied. At this loading condition, a three-phase fault was created. It was observed that the SMES-StatCom compensator responded as if there is no load in the system regardless of the location of the compensator. The reason is that the load variation was taken under control by Machine II.

VI.3.6. Reduced Rating in StatCom-SMES

While keeping the compensator location at *Bus B*, the performance of StatCom-only at full rating is compared to the performance of StatCom-SMES at reduced rating. The power rating of the SMES and StatCom was reduced to half of its original ratings (80MVAR, 50MW peak). The energy level of SMES was kept the same, however the real power capability of SMES was decreased. The SMES coil was charged until it reaches the desired charging current level, which took twice the time since the terminal voltage was lower. A three-phase fault is created at 5.6sec for .15 sec, and the responses of the StatCom-SMES versus StatCom-only to the power swings are compared in Figure VI.10.

This comparison shows that StatCom-SMES at the reduced rating can be as effective as a StatCom at the full rating in damping oscillations. On the other hand, the terminal voltage has not been improved. This requires higher reactive power support, but not as high as the full rating. Adding energy storage therefore can reduce the MVA rating requirements of the StatCom operating alone.

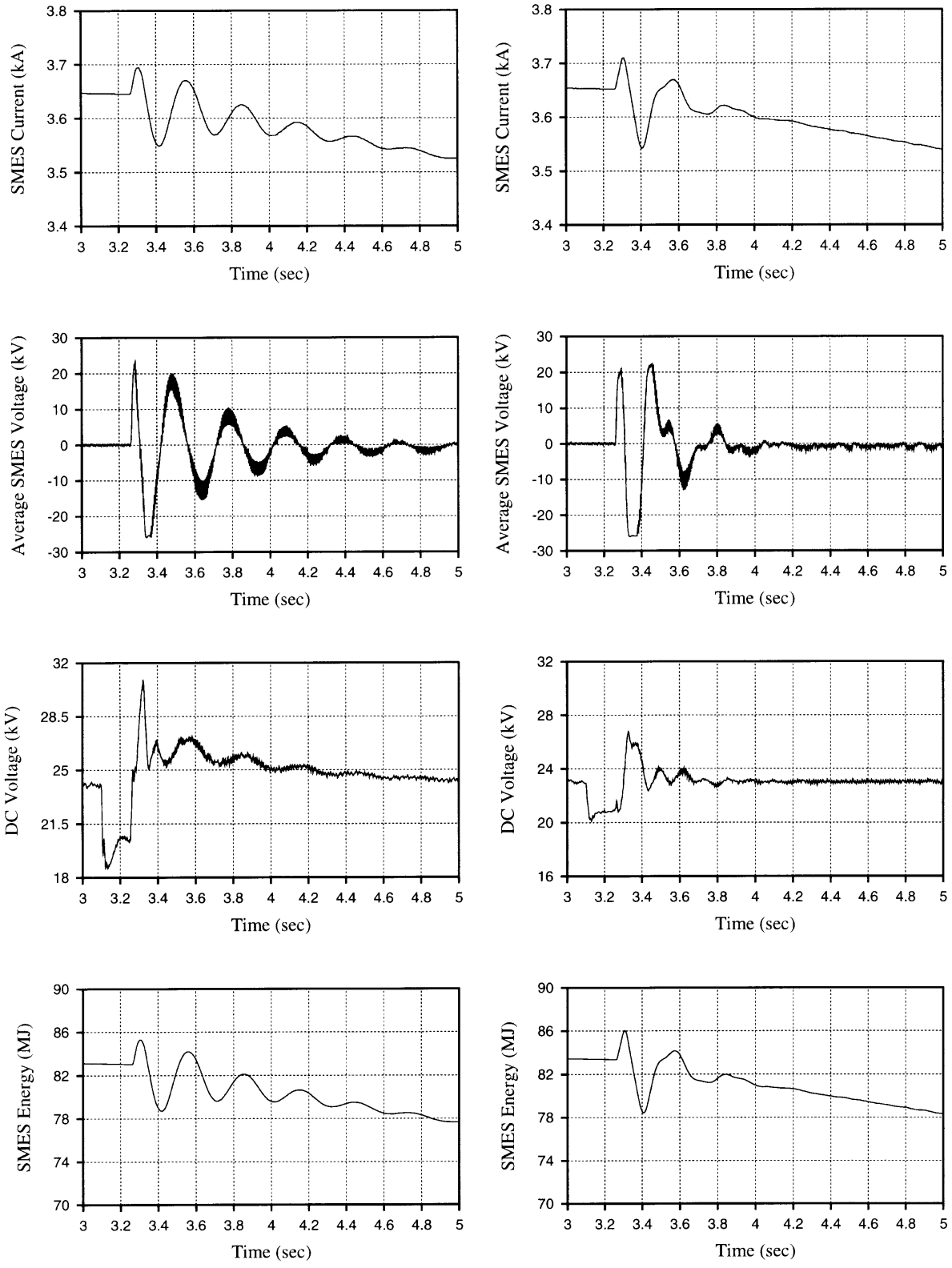

StatCom-SMES at *Bus B* StatCom-SMES at *Bus A*

Figure VI.9: SMES Operation as Response to AC System Oscillations

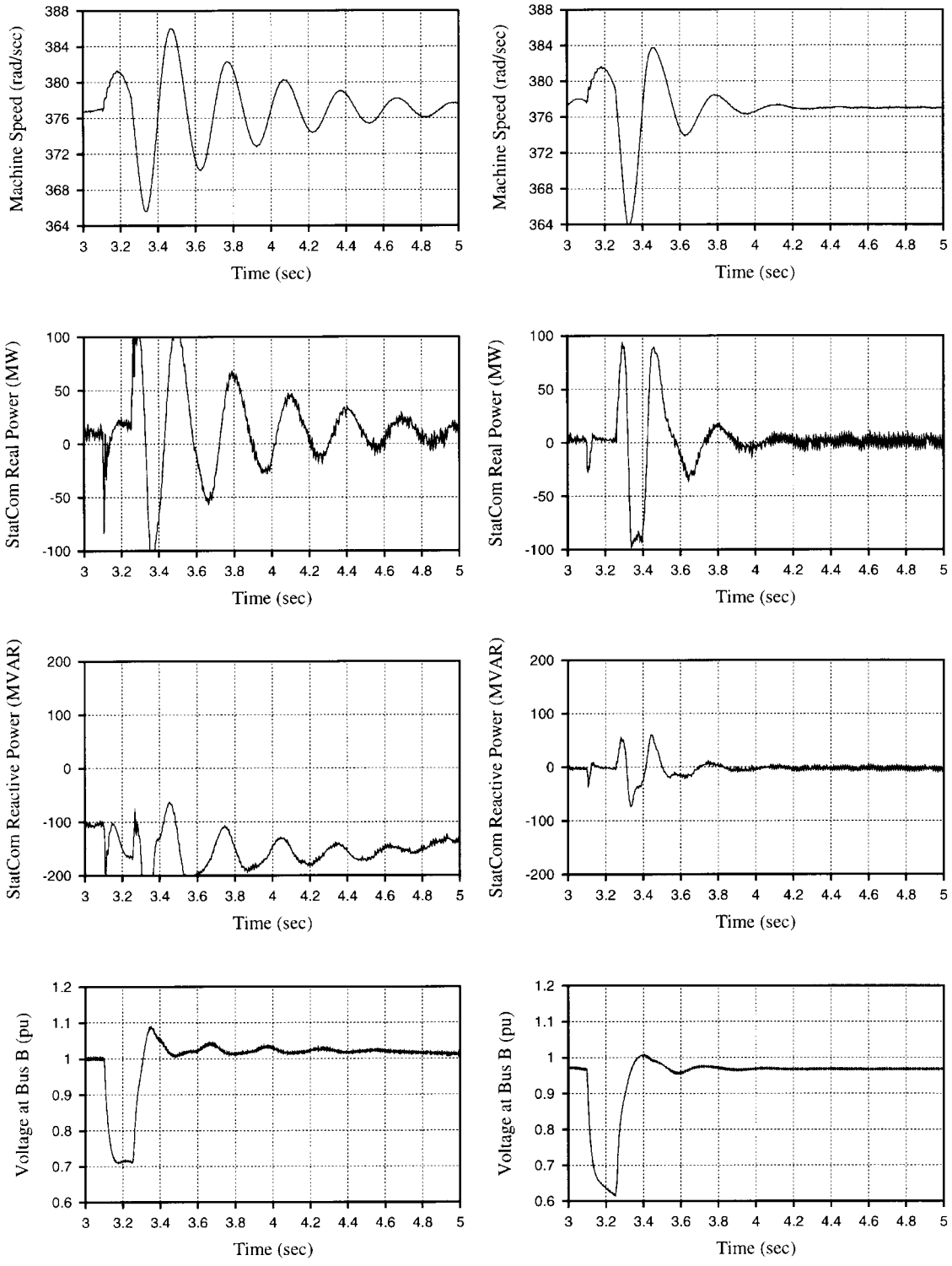

StatCom-SMES at *Bus B* StatCom-SMES at *Bus A*

Figure VI.10: Dynamic Response of StatCom-SMES when a 100 MVA load is added

VI.4. Real Power vs. Reactive Power in Damping Oscillations

Low frequency oscillations following disturbances in the ac system can be damped by either reactive power or real power injection/absorption. However, the reactive power injected to the system is dependent on the StatCom terminal voltage. On the other hand, the SMES is ordered according to the variation of the real power flow in the system. Damping power oscillations with real power is more effective than reactive power since it does not effect the voltage quality of the system. Better damping dynamic performance may be obtained if SMES is connected to the ac system through a series connected voltage source inverter (Static Synchronous Series Compensator) [Larse92] rather than a shunt connected voltage source inverter. However, this is not a justifiable solution since it involves more cost.

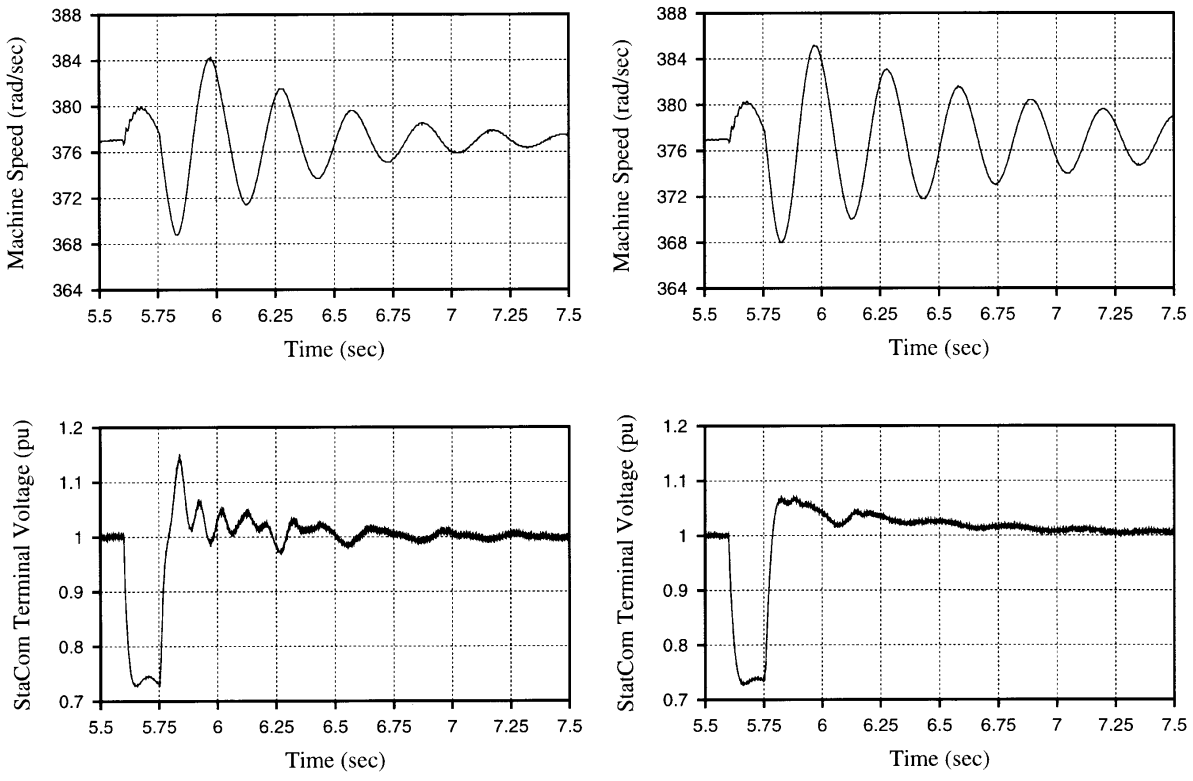

80 MVA StatCom + 50MW SMES at *Bus B* 160 MVA StatCom at *Bus B*

Figure VI.11: Comparison between 160MVA StatCom and 80MVA StatCom+ 50MW SMES

VI.5. Summary and Discussion

This chapter presents the modeling and control of the integration of a StatCom with SMES, and its dynamic response to system oscillations caused by a three-phase fault. It has been shown that the StatCom-SMES combination can be very effective in damping power system oscillations. Adding energy storage enhances the performance of a StatCom and possibly reduces the MVA ratings requirements of the StatCom operating alone. This is important for cost/ benefit analysis of installing flexible ac transmission system controllers on utility systems.

It should be noted that, in this study, the StatCom provides a real power flow path for SMES, but the SMES controller is independent of the StatCom Controller. While the StatCom is ordered to absorb or inject reactive power, the SMES is ordered to absorb/inject real power.

It was also observed that the location where the combined compensator is connected is important for improvement of the overall system dynamic performance. Although the use of a reactive power controller seems more effective in a load area, as stated in [Larse92], this simulation study shows that a StatCom with real power capability can damp the power system oscillations more effectively, and therefore stabilize the system faster if the StatCom - SMES controller is located near a generation area rather than a load area.

Control Parameters: The control parameters in this study were tuned so that the desired performance was obtained. The objective was to show a successful operation of the StatCom-SMES integration in damping power swings. In order to determine the optimal range of each control gain, a small signal stability and eigenvalue analysis can be performed. Several papers in the literature have used this analysis for a specific application of StatCom. [Patil98, Passe97]. Thorough information on eigenvalue analysis can be found in [Kundu94, Sauer98].

Credibility of the software: The simulation software program (EMTDC/PSCAD) utilized in this study is a commercial product that has been used for various purposes of power system studies. This program has many built-in models, some of which were employed in the studied model.

Fault Insertion Testing: As several fault cases were simulated in the model, it was observed that the output was as expected. Most of the fault cases simulated are electrical short circuit fault that produced zero voltage and high fault current where the fault is applied.

Comparison with Literature Results, Engineering Judgment: Several output of this simulation study can be compared to the studies presented in the literature. For instance, the result of SMES located near generator behaves more effective in damping oscillations was also obtained in this study. The results are acceptable based on engineering judgment.

CHAPTER VII

SUMMARY, CONCLUSIONS, AND FUTURE WORK

This chapter first summarizes the procedure and the findings of the modeling and simulation studies presented in this dissertation. It includes the studies of electromagnetic transient interaction between a SMES coil and its power electronics interface, and integration of a StatCom with SMES for dynamic oscillation damping. Then, the contributions of this work and the main conclusions are presented. Finally, future work is recommended following the conclusions.

VII.1. Electromagnetic Transient Interaction between a SMES Coil and dc-dc Chopper

As SMES devices involve power electronics switches, the SMES coil is subject to switching transient overvoltages that can stress its insulation. Therefore, the electromagnetic transient interaction between the coil and its immediate power electronics interface needs to be explored.

This investigation considered a transient modeling of a SMES coil and the chopper. The SMES coil was modeled as distributed sections where each section was represented with its series capacitance, shunt capacitance, self and mutual inductances to other sections. The calculations of these parameters are based on the coil dimension information provided by BWX Inc. Technologies. The computation of the parameters are performed in turn to turn level, then lump section models were developed to represent the entire coil.

A dc-dc chopper was modeled as a GTO-based 2-level 3-phase power electronics configuration. While the chopper output was connected to the SMES coil, the chopper input was fed by a dc voltage source representing the rest of the system.

Several transient overvoltages are identified. These are due to the normal chopper operation, open or short circuit fault in one of the chopper GTOs, bypass switching operation and impulse voltage from the dc source. Several transient suppression schemes were

developed to reduce the overvoltages. Among these are a) connecting surge filters across the coil terminal to distribute the voltage distribution evenly along the coil, b) connecting metal oxide varistors to reduce the overvoltages to a desired value, and c) varying the value of inter-phase sharing inductors.

To reduce overvoltages, variation in chopper parameters such as snubber circuit and time delay between phases were also simulated. Different configurations for the chopper were examined. The configurations of two-level one-phase IGBT based chopper and three-level one-phase IGBT choppers were selected. The performances of these configurations were compared with the one initially used. three-level one-phase IGBT based chopper shows reduced overvoltages during normal chopper operation.

VII.2. Integration of SMES with a StatCom

A StatCom injects/ absorbs only reactive power. It can mitigate only voltage related transmission level problems by providing reactive power/voltage support and transmission stability enhancement. On the other hand, the problems such as uneven real power flow, transient and dynamic stability, subsynchronous oscillations and power quality issues can be impacted more effectively if energy storage can be integrated to an existing StatCom. This will provide much needed flexibility to overcome the transmission level problems.

In this part of the study, the incorporation of a SMES coil into an existing StatCom is explored in damping power oscillations. The StatCom has been modeled as a 12-pulse voltage source inverter connected to a generic power system equivalent through two 80 MVA transformers, and linked to a dc capacitor in the dc side. The dc link capacitor ties the dc-dc chopper to the voltage source inverter. The SMES coil is represented with a lumped inductor.

The StatCom is controlled so that it can provide necessary reactive power (inject/absorb) to maintain desired voltage level. It also allows a real power path to charge and discharge the coil. The coil is initially charged. It is controlled so that it reacts when there exists a deviation in the real power flow on the transmission system due to a three-phase fault disturbance.

A number of simulation studies were performed. The operation of SMES modes (charging, discharging and standby) are successfully achieved with the entire integration. It was realized that the addition of SMES into a StatCom improves the performance of the StatCom in damping power swings following a three-phase fault. This improvement is better if the StatCom-SMES is located near generator side. Adding energy storage can possibly reduce the MVAR rating requirements of the StatCom operating alone.

VII.3. Conclusions

Distinct contributions of this work can be listed as follows:

- A state of the art review of SMES was performed. Past and present applications were discussed, and cost effective SMES applications were identified.
- Based on coil dimensions, disk type SMES coil model parameters were derived. Turn to turn coil parameters were lumped to sections to reduce computational effort.
- An electromagnetic transient interaction modeling between a SMES coil and a dc-dc chopper was developed, simulation studies were carried out to determine switching transient overvoltages.
- Transient suppression schemes were developed.
- Different chopper topologies were compared in reducing overvoltages.
- An integration of a StatCom with a SMES coil was explored in damping electromechanical oscillations following a three-phase fault.

The first two sections of this chapter summarized and stated the conclusions of the simulation and modeling studies. Overall concluding remarks of this work can be listed as follows:

- Currently, the cost effective SMES applications include frequency control, transmission stability and power quality.

- The cost factor is the main constraint of a SMES device being a commercially available product. Incorporation of a SMES coil into an existing static synchronous compensator can reduce the power electronics-based cost, and also can improve the performance of the compensator by adding another power dimension.

- Transient overvoltages to SMES coil are generated during normal chopper operation, any open or short circuit fault on the chopper GTOs, and the bypass switch operation.

- Metal oxide varistors can be utilized to reduce the transient overvoltages that can affect the coil insulation.

- A three-level one-phase IGBT chopper is preferred as a power electronics interface to a SMES coil since its normal operation does not generate high switching transient overvoltages.

- An integration of a StatCom with SMES coil is very effective in damping power oscillations.

- When StatCom-SMES is located near a generator, it shows better performance in damping oscillations.

VII.4. Recommended Future Work

This work can be extended in several ways:

- Different power electronics topologies can be explored such as the use of 6 pulse PWM inverter instead of multi-pulse synchronized inverters, 3 level inverters in place of 2 level inverters.

- Although it is not cost effective, the integration of SMES to a series static synchronous compensator or a unified power flow controller can be investigated.

- The control issues can be redefined. Eigenvalue analysis can be utilized to obtain optimum range for control gain parameters.

- The impact of SMES in mitigating other transmission level problems such as transient stability, damping inter-area oscillatory modes, power quality can be studied further.

APPENDIX A

LITERATURE REVIEW OF SMES TECHNOLOGY

Paper	***content***	***Important Remarks***
[1] [Luong96]	Reviews the developments in the US SMES program, SMES related activities around the world, and points out trends, applications and development of SMES	• Although SMES was envisioned as a load leveling device, it is now seen a tool to help in power system operation • SMES has not fully emerged from developmental stage to commercial stage
[2] [Karas99]	Reviews the possible utility applications of SMES, discusses a number of technical issues and trade-offs including conductor design options, system configuration, insulation issues, power electronics circuit topology and devices, and cost issues.	• In the process of the deregulation of power utility industry, SMES devices will become an attractive option as opposed to constructing new lines. • SMES inverter and FACTS inverter are similar, attachment of SMES to facts controller is a logical approach, since it enhances the overall controllability. • Cable in conduit conductor (CICC) is a preferred design approach • Surge capacitors, MOVs can protect the coil against the transient overvoltages that can be generated through normal chopper switching surges or surges coming from AC network • Four-quadrant power control can be achieved through the use of GTO, IGBT or IGCTs. GTOs have been preferred for power utility applications due to their high power ratings.

Paper	***content***	***Important Remarks***
[3] [Boom72]	Discusses the use of large superconducting inductors as an alternate to pumped energy storage, gives a preliminary analysis for a 400MW-10,000MWh unit	• Energy storage by SC is a realistic possibility for power systems • Overwhelming structure requirements is more important than optimization of the superconducting material. • Electromechanical oscillations can be damped with proper design
[4] [Roger79] [5] [Roger83]	Reviews the 30MJ SMES program with design, fabrication, installation and the preliminary experimental operation of the system	• Design parameters of the coil and the SMES system are given • A small scale SMES device can be to damp low frequency oscillations due to its feature of fast response. • Such a system can successfully interface with an electrical network and alter the power transmission
[6] [Hasse83] [7] [Hasse89]	Presents historical development of superconductivity, describes the design and functions of the SMES components of an engineering reference design for 1GWh SMES unit, presents rationale for energy storage on utility systems, describes the general technology of explains the chronological development of the technology, and explains the impact of high TC materials on SMES	• SMES has the potential of becoming an economical means of load leveling. • If its price can be brought down with continued research and development, the SMES technology will become more attractive and competitive with other storage technologies • High temperature SMES can be advantageous over Low Temperature ones • Reinforced structure of the SMES coil is expensive
[8] [Peter75]	Presents the steady-state operating characteristics of SMES Inductor-Converter units, and some simulation results to show possible benefits of such units protection and capital cost issues.	• SMES can provide electromechanical damping and improved transient stability • SMES can have significant electromechanical damping capability even with a smaller size inductor

Paper	***content***	***Important Remarks***
[9] [Hassa93]	Presents the 22MWh ETM SMES system, describes the SMES operation during charging and discharging, explores the feasibility of the PCS and overall behavior of the system under fault conditions.	• Voltage source inverters are most cost effective than current sourced ones • GTO based VSI is capable of four quadrant operation of independent control of real and reactive power • Surge suppressers are required to protect the SMES coil against transients
[10] [Ise86]	Presents simultaneous real and reactive power flow control using 6 and 12-pulse GTO converters	• A voltage clipper circuit was adopted to handle energy stored in the leakage inductances of the transformer. • SMES systems which employ GTOs can be used as a power system stabilizer as well as minimizing the reactive power requirement
[11] [Lasse91a] [12] [Lasse91b]	Presents hybrid CSI and VSI power conditioning systems for SMES, and gives the study results of the dynamic responses of these two conditioners to load change, three phase fault and start-up.	• Both PCSs provide and independent control of real and reactive power. • The transformer rating is lower in the case of CSI. • Hybrid CSI is easier to control, but VSI allows better control of harmonics.
[13] [Han93]	Presents a 12 pulse GTO converter and an electronically controlled tap changing transformer, gives operational analysis and system interaction analysis.	• The proposed PCS offers reduction of system rating as well as independent control of powers

Paper	***content***	***Important Remarks***
[14][Shira94]	Presents a new type gate pulse generator (GPG) to give GTO based 6 pulse CSI quick response firing angle control and PWM control functions.	• The developed GPG provides a quick response firing angel control function and PWM control function • A SMES system with the GPG for its GTO conversion unit shows an effective way in suppressing the voltage disturbance following a load step change.
[15][Jiang96]	Presents an analysis of the power control of a SMES unit employing PWM switching control for the CSI conditioner, describes a criteria for executing a power limit scheme to maintain power flows within their controllable range, and presents two experimental example results.	• An optimal PWM algorithm should satisfy 1) low frequency device switching for high power GTOs, separate and linear modulation depth and angle control, minimal low order harmonic generation into the ac network, and providing a continuous path on the dc side. • P priority control scheme plays important role in P-Q regulation of a SEMS unit.
[16][Rahim96]	Proposes a control strategy for a SMES system to damp subsynchronous resonant oscillations, presents the test results of applying the proposed control on the IEEE second benchmark model.	• The control strategy requires the measurement of ac terminal voltage and the variation of real and reactive power. • Unstable subsynchronous modes can be canceled through the current injection from SMES.
[17][Skile96]	Presents the lab test results of a VSI/Chopper power conversion system to demonstrate the SMES operation as a static var compensator, low frequency modulator of the real power, and the SMES speed of response.	• By different control schemes, a SMES system can provide and independent real/reactive power control, can operate as an SVC, and respond in 2-3 cycles • Response time depends on several things such as the size of the dc capacitor, the state of charge of the SMES coil.
[18][Mitan88]	Proposes SMES control schemes for a 4-quadrant simultaneous real and reactive power for stabilization, discusses effective locations and necessary capacities for	• The location of SMES depends on its application. Near the generator to improve damping by means of real power, at the center of transmission line to improve voltage control by means of reactive power and at the demand side for load leveling application.
[19][Baner90]	Presents the application of a small-size energy storage capacity to damp electromechanical oscillations in a power system.	• The control takes the area control error as its input and uses inductor current deviation feedback

Paper	***content***	***Important Remarks***
[20][Tam90]	Introduces a new SMES scheme, SMES/dc link for energy storage and control of power, presents its operation and benefits, and also demonstrates SMES' positive impacts on transmission systems.	• SMES functioning as diurnal load leveling can reduce the transmission line loading and associated transmission losses during heavy load hours. • SMES/dc link can minimize loop flow, reduce transmission losses and costs, and enhance the utilization of existing transmission networks.
[21][Kral95	Describes the 1800MJ, 50MW SMES system that planned to be installed in Alaska, discusses its possible applications in the utility and its cost.	• Planned SMES system services include: frequency support, damping transmission line oscillations, voltage support and automatic generation control.
[22][Huang95	Describes the 1800MJ SMES system's magnet and conductor design, its utility applications and discusses ac losses	• Governing criteria for conductor design include reliability cost and transportability • Ac losses generated during charge and discharge include eddy current losses in the aluminum stabilizer, hysterisis losses in the superconducting filament and coupling losses in the strands
[23][Pariz97]	Discusses requirements and configurations of the use of a small-scale SMES operating in 15kV substations to solve power quality problems for substation applications	• A lower energy stored SMES is capable of providing higher than specified power for a short time.
[24][Feak97]	Presents the results of a study assessing the benefits of SMES.	• Two stability related case study showed that SMES provided an effective mean of stabilizing, but neither case supported the selection of a SMES option while there is a cheaper alternative to do that.
[25][Kral97]	Explains the need for installing an 1800MJ SMES system in Alaska, reviews conductor configuration and characteristics, describes winding pack, presents magnet quench and protection, discusses cryostat design, and presents overall magnet system thermal and structural characteristics.	• Identified three SMES system performance modes include spinning reserve or frequency support mode (≤60sec), system stabilization or frequency stabilization mode (<20sec), and voltage support or variable VAR compensation mode (continuous)

Paper	***content***	***Important Remarks***
[26] [Johns97]	Presents a scheme to attach a SMES coil into a LVdc transmission system, and discusses required modifications for this incorporation.	• A SMES coil incorporate to LVdc system do not require a complex power conversion unit, and its control is easier. It can be connected to the LVdc mesh either by a dc-dc chopper or directly. • Rectifier voltage regulation schemes control the charging and discharging of the coil
[27] [Ngamr99] [28] [Kamol99] [29] [Ise99]	Introduces the Super SMES concept where it is composed of inverters connected in series and parallel to a power system, presents control schemes for different applications.	• A SuperSMES can be a power quality controller, a power system stabilizer and a load frequency controller • As a power system stabilizer, location does not matter since the controller uses both generator terminal and local signals
[30] [Rehta99]	Proposes a multifunctional control concept	• A multifunctional SMES should have a dimension between mid and large storage levels. • The sequential tasks of an integrated SMES control with fuzzy set theory includes 1) short term dynamic, 2) Second reserve power, 3) Voltage stability and 4) Voltage control
[31] [Borga99]	Discusses the problem being experienced in WPS system, and how a portable SMES units can provide solutions to the problem considering their performance and cost attributes.	• Placing multiple micro-SMES units at key substation locations of WPS system can solve the instability problems, and provide voltage support. • Distributed SMES can respond to voltage sags faster than the other options, and more economic than the options considered. Its modularity makes it easier to site, reconfigure or change to other locations
[32] [Masud87]	Describes a 5GWh SMES design study, discusses conductor, structure and refrigeration system of the design	• Coil parameters are : 5GWh stored energy, 8.4 T peak filed at a rated current of 707 kA, 71.8 H coil inductance, 376m mean diameter and 18m height solenoid coil

Paper	***content***	***Important Remarks***
[33] [Schoe93]	Presents a conceptual design requirements for SMES using HTS conductors.	• The use of HTS materials for SMES has several advantages such as less expensive cryogen, higher refrigeration efficiency higher reliability as well as disadvantages such as lower critical current density, therefore lower energy density and easier brittleness.
[34] [Lieur95]	Presents design and cost studies for mid-size (1-5MWh) SMES systems using alternative configurations such as solenoid, toroid and race track coil configuration	• The cost of solenoid and toroid magnet configurations are comparable for 1MWh systems • Customer requirements determine the specific configuration for a given application
[35] [Tomin]	Describes the design and test results of a 1MJ SMES system that has been built and tested in Japan	• Coil parameters are : 1 MJ stored energy, 4.2 T peak filed at a rated current of 1kA, 2H coil inductance, 550mm mean diameter and 667mm height solenoid coil
[36] [Luongo95]	Reviews the evolution of SMES efforts taken by Bechtel Corp., and describes a 1MWh/500MW CICC based SMES for a utility demonstration	• The most important change introduced to the coil pack design was to combine most structural, electrical and thermal functions into a single dump shunt • Self supporting coil pack design is cheaper than the earth supported one. • A SMES demonstration unit will be located at SDG&E utility site to increase simultaneous load transfer
[37] [Wohlw95]	Summarizes the design requirements of US ITER magnet, and illustrates the manufacturing methods	• Coil parameters are : 600 MJ stored energy, 13 T peak filed at a rated current of 46 A, 568 H coil inductance, 2.6m mean diameter and 1.775m height solenoid coil • The turn-turn insulation is Kapton/ fiberglass/ epoxy.
[38] [Bauti97]	Describes the design and manufacturing of a 25kJ superconducting coil and its structure, and presents a PWM low switching frequency controlled power converter topology	• Coil parameters are : 25 kJ stored energy at a rated current of 115 A, 3.8 H coil inductance, 127mm mean diameter and 123mm height solenoid coil

Paper	***content***	***Important Remarks***
[39] [Kusto91]	Presents SCR/GTO based inverter circuit topologies, switching schemes, control of real and reactive power and shorting switch	• Hybrid SCR/GTO can reduce the reactive power requirement • PWM scheme reduces the ac current harmonics • A mechanical switch can be used to bypass the coil at current zero
[40] [Schoe96]	Presents the benefit/cost results for the electric energy storage technologies considered for small, medium and large scale systems	• For small and medium scale cases, SMES could be cost effective with its operating benefits.
[41] [Scwe87]	Reviews and summarizes the dielectric properties of all kinds of insulation materials for insulation design of superconducting coils	• The voltage withstand requirements of a particular system strongly influenced by the application • As far as electrical stresses are concerned, the room temperature tests may be the worst condition that the magnet ever experience and may determine the insulation design. • Based on literature, safety factors range from 2 to 5.
[42] [Bauma92]	Presents environmental and energy conservation benefits of SMES systems supplementing already identified benefits of SMES.	• SMES can be recognized as energy and environmental technology and tool
[43] [Mitsu94]	Summarizes electrical insulation technology for superconducting magnets in Japan. Endure	• Electrical insulation of superconducting magnets should be able to withstand a variety of voltages under normal operating condition, during coil quenching, and at withstand voltage tests. • In the manufacturing of a 1 MJ SMES coil, double pancake winding with cooling channels in the horizontal and vertical directions were adopted to improve cooling efficiency, vertical and horizontal spacers were used to increase the coil stiffness, and the selection of the coil structural objects was made to decrease the ac losses.

Paper	***content***	***Important Remarks***
[44] [Thero93]	Presents the results of economical and technical evaluations of SMES in industrial applications, and compares this evaluations with battery systems.	• For the applications of smoothing of short power interruptions and smoothing of varying loads, batteries are not desired since they do not have satisfactory rapid storage recovery cycles and require oversize with respect to the needed energy.
[45] [Lee99]	Proposes a simultaneous active and reactive power control scheme for a SMES unit where control parameters are determined by pole assignment method, and validates the proposed controller with eigenvalue analysis and time domain digital simulation	• SMES is connected to the ac system through a 12 pulse current source inverter, and the system model for the SMES unit is a single machine infinite bus model, where the machine is dynamically modeled including exciter, governor and turbine system. • Takes speed deviation as a feedback to provide satisfactory damping capability and enhance system stability with various load characteristics where a composite load model including dynamic and static load models.
[46] [Miri95] [47] [Miri98]	Introduces the use of superconducting magnets in fusion experiment, presents a method to calculate transient voltages in superconducting magnets	• The SMES coil model can be obtained by deriving self and mutual inductances, serial and transverse capacitances from the design drawings, and effective resistances from Eddy-current losses. • The calculation of the system response is based on the frequency domain analysis. • Coils with grounded shear plates have a high ratio of turn-ground capacity, which may cause large internal voltage oscillations. • The damping of the transient oscillations at cryogenic temperature is weaker than in the normal conducting coil.
[47] [Hayas99]	Presents an analytic analysis of an insulation breakdown for the KYU-Japan SMES.	• Current limiting resistors are proposed to protect the coil against lead wire short-circuits.

APPENDIX B

CAPACITANCE MEASUREMENT OF THE SAMPLE COIL

A sample of the 100 MJ SMES coil shown in Figure B.1 is used to perform capacitance measurement. The length/width/height of the sample coil is approximately 207mm, 95mm, and 98mm, respectively. The dimensions of each turn are considered as the same as the dimensions of the designed actual SMES coil. The dimensions of the turn will be given when the theoretical capacitance calculation is made later.

Figure B.1. Sample Coil

B.1. Test Setup

A transmission/reflection test kit is connected to a Network/Spectrum/Impedance analyzer (HP 4395A). Analyzer type was selected as network analyzer. Measurement setup was made as B/R (transmitted/incident) to obtain the transmission characteristics of the tested device, then conversion function was selected to convert B/R to impedance. The measurement format was linear. After calibration, the sample coil is connected to the analyzer as shown in Figure B.2. In transmission measurement, R end is connected to one turn and B end is connected to the other turn. The screen of the analyzer was captured to show the graphics of impedance vs. frequency for different frequency ranges.

Impedance measurements between turns M and N are given in Figure B.3 for the frequency ranges of [5-10kHz], [10Hz-500kHz], [10Hz-1MHz], and [10Hz-500MHz].

Figure B.2: Sample Coil Connected to the Network Analyzer

B.2. Capacitance Measurement and Calculations

From Figure B.3, it can be seen that there are so many resonant points when the frequency range is enlarged. It seems that the two points from which the measurement was taken represents a distributed model consisting of many L and Cs. To make the capacitance calculation simple, this model is assumed to be a parallel L and C circuit. Based on, this assumption following derivation is made.

$$z = \frac{jwL\dfrac{1}{jwC}}{jwL + \dfrac{1}{jwC}} \Rightarrow \quad |z| = Z = \frac{wL}{1 - w^2 LC} \quad or \quad \frac{Z}{wL} = 1 + ZwC \Rightarrow L = \frac{Z}{w(1 + wZC)}$$

$$at\ w = w1, \quad Z = Z_1$$

$$at\ w = w_2, \quad Z = Z_2$$

$$\frac{\dfrac{Z_1}{w_1 L}}{\dfrac{Z_2}{w_2 L}} = \frac{1 + Z_1 w_1 C}{1 + Z_2 w_2 C} \Rightarrow \frac{w_2 Z_1}{w_1 Z_2} = \frac{1 + Z_1 w_1 C}{1 + Z_2 w_2 C} \Rightarrow \quad C = \frac{w_1 Z_2 - w_2 Z_1}{Z_1 Z_2 (w_2{}^2 - w_1{}^2)}$$

Another approach is based on the assumption that the impedance values we measure are directly the ohmic values of the capacitance at particular frequency. $C=1/(2\pi fZ)$ gives the Farad value of the capacitance. Let's call this assumption to be assumption II. While two frequency points are needed for assumption I, one frequency point is sufficient for assumption I to calculate the capacitance value between two turns for assumption II. The following table gives the selected frequencies and measured impedance between turns M-N, M-P, M-R, and M-T in the selected frequency range.

	Frequency (kHz)	Z_{M-N} (Ω)	Z_{M-P} (Ω)	Z_{M-R} (Ω)	Z_{M-T} (Ω)
Frequency range of 5-10kHz	5	190k	221k	314k	458k
	5.5	233k	216k	360k	384k
	6	244k	234k	248k	353k
	6.5	251k	237k	412k	447k
	7	225k	217k	429k	534k
	7.5	230k	238k	350k	400k
	8	215k	251k	328k	596k
	8.5	167k	210k	280k	388k
	9	183k	201k	258k	379k
	9.5	148k	200k	285k	371k
	10	141k	157k	298k	340k
Frequency Range of 250	250	6610	6970	11200	14500
	300	5540	5680	9500	11400
	400	4290	4110	6900	8390
	750	2260	2230	3720	4550
	900	1880	1890	3030	3640

Between two turns, the final capacitance values were calculated as follows.

i.e. $C_{M-N}= Avg(C_{250-300kHz}+C_{250-400kHz}+.....+ C_{400-750kHz} + C_{750-900kHz})$.

These capacitance values for selected turns are:

Z Model	Frequency Range	C_{M-N} (pF)	C_{M-P} (pF)	C_{M-R} (pF)	C_{M-T} (pF)
Z=L // C	Range 5-10kHz	93	71	42	33
	Range 250-900kHz	93	95	58	49
Z=C	Range 5-10kHz	107	100	62	52

The following observations were made throughout the measurement.

- As the distance between turns gets larger, higher noise components existed.
- As the frequency range was decreased, higher noise components existed.
- To reduce the noise, BW was decreased.
- As the frequency range was decreased, an overload on R (incident) input was observed. The source power decreased to avoid this caution.

B.3. Theoretical Capacitance Compared to Measured Capacitance

Theoretical capacitance calculation assumes that two turns can be represented as two parallel plates. Given the actual coil dimension:

Conduit dimension: 14.70mm vertical, 10.90mm radial; length: 207mm

Spacing: 0.254mm (ε_1=3.5)+ 2*0.4064mm (ε_2=4.5) +0.254mm (ε_1=3.5) both radial and vertical.

where ε is dielectric constants of each insulation. (ε_0=8.854*1e-12)

$C=\varepsilon A_{t1\text{-}t2}/d$

$\varepsilon/d= (1/(1/(\varepsilon_1\varepsilon/0.254e\text{-}3)+ 1/(\varepsilon_2\varepsilon/(2*0.4064e\text{-}3))+1/(\varepsilon_1\varepsilon/0.254e\text{-}3)))= 2.7179e\text{-}008$

$A_{M\text{-}N}=14.70*207/1e+6= 3e\text{-}3m^2$ $A_{M\text{-}P}=10.90*207/1e+6= 2.3e\text{-}3m^2$

$C_{M\text{-}N}=83pF$

$C_{M\text{-}P}=61.32pF$

Theoretical and measured capacitance values are in the same magnitude.

a) Z_{M-N} [5-10kHz]

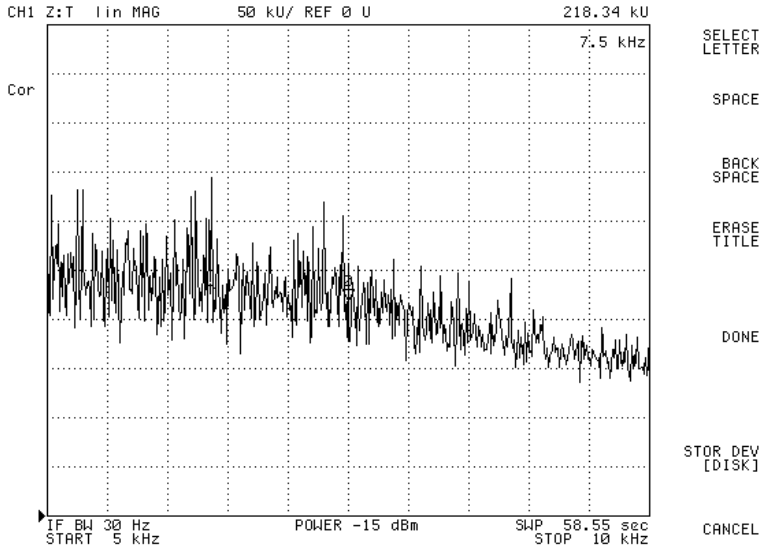

b) Z_{M-N} [10Hz-500kHz]

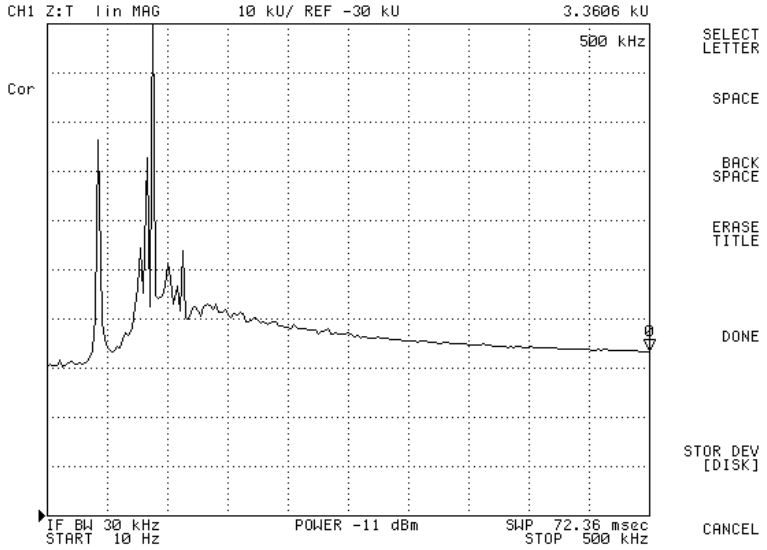

Figure B.3: Impedance vs. Frequency

c) Z_{M-N} [10Hz-1MHz]

d) Z_{M-N} [10Hz-500MHz]

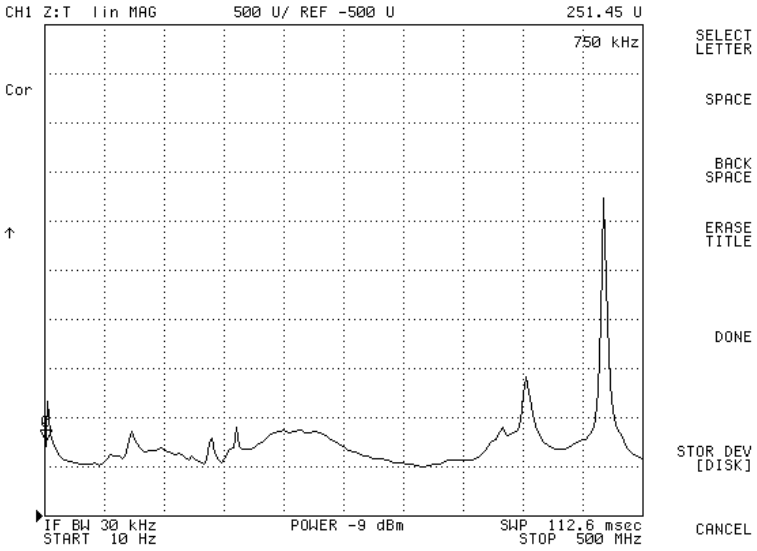

Figure B.4: Impedance vs. Frequency (cont.)

APPENDIX C

MATLAB CODE TO CALCULATE COIL PARAMETERS

```
%%%%%%%%%%%%%%%%%%%%%%%%%%%%%%%%%%%%%%%%%%%%%%%%%%%%%%%%%%%%%%%%%%%%%%%%%%%%%%%%
%% This is a program to calculate self and mutual and series and shunt  %%
%% capacitance values when the dimensions of the coil are given         %%
%% The coil is assumed to be a disk type coil. The number of turns      %%
%% (N) in a single pancake are the same for the other pancakes          %%
%% The total number of double pancakes is Ndp                           %%
%%%%%%%%%%%%%%%%%%%%%%%%%%%%%%%%%%%%%%%%%%%%%%%%%%%%%%%%%%%%%%%%%%%%%%%%%%%%%%%%
clear

disp(' Enter the requested dimensions in inches')

%%% DIMENSIONS
% conductor width and height are given including the stainless steel
conduit

wc  = input('Enter the width of the conductor of the turn: ')
hc  = input('Enter the height of the conductor of one turn: ')
cwt = input('Enter the thickness of the conduit of one turn: ')
vs  = input('Enter the vertical conduit spacing of one turn: ')
rs  = input('Enter the radial conduit spacing of one turn: ')
ti1 = input('Enter the thickness of the first insulation:')
ti2 = input('Enter the thickness of the second insulation')
do  = input('Enter the outer diameter of the magnet coil: ')
di  = input('Enter the inner diameter of the magnet coil: ')
oi  = input('Enter the thickness of the outer insulation wrap: ')
N   = input('Enter the number of turns in one single pancake: ')
Ndp = input('Enter the number of double pancakes in the coil: ')

% No spacing or insulation is between pancakes are considered. An
% insulation between "insn" number of single pancakes is allowed

insn  = input('Enter the number of single pancakes for extra insulation')
inst  = input('Enter the thickness of the extra insulation')

dp1=2*oi+hc*2+vs*2

%%% CONSTANTS
mu0= 4*pi*1e-7; eps0 = 8.854*1e-12;

%% Calculating outer, inner and median diameter for each turn in a single
pancake
  for i=1:N
     R1(i) = (do/2 - oi-rs/2)-(i-1)*(wc+rs);
     R2(i) = R1(i)-(wc+rs);
     Rm(i) = (R1(i)+R2(i))/2;
     count(i)=i;
  end
  rad_t=[R1',Rm',R2']; rad_tinch=rad_t;
%%
```

```
%%Converting units in inches to meters
inch_m=0.0254
wc=wc*inch_m;    hc=hc*inch_m;   vs=vs*inch_m;      rs=rs*inch_m;
do=do*inch_m;    di=di*inch_m;   cwt=cwt*inch_m;    oi=oi*inch_m;
R1=R1*inch_m;    R2=R2*inch_m;   Rm=Rm*inch_m;      rad_t=rad_t*inch_m;
ti1=ti1*inch_m;  ti2=ti2*inch_m; inst=inst*inch_m;
%%
%%Displaying Results
matris=[wc,hc,vs,rs,do,di,cwt,ti1,ti2]
%%%

hf=hc-2*cwt;
wf=wc-2*cwt;
b1=hc;c1=wc; beta=sqrt((b1^2-c1^2)/12);


%%%%%%%%%%%%%%%%%%%%%%%%%%%%%%%%%%%%%%%%%%%%%%%%%%%%%%%%%%%%%%%%%%%%%%%%%%%%%%%
%%%%%%%%%%%%%            CAPACITANCE CALCULATIONS        %%%%%%%%%%%%%%%%%
%% C = (eps*A)/d, where A is the surface area between turns (conductors)%%
%% or turn to ground, d is the distance between bare conductors          %%
%% Once the capacitance values are obtained for one single pancake,      %%
%% the capacitances for the second one in a double pancake will be the   %%
%% same where the first turn in the first single pancake corresponds to  %%
%% the last turn in the second single pancake                            %%
%% Equation 5 of Chapter IV is used for capacitance calculations         %%
%% The concept in Figure IV.6 is used to calculate capacitances for a    %%
%% double pancake                                                        %%
%%%%%%%%%%%%%%%%%%%%%%%%%%%%%%%%%%%%%%%%%%%%%%%%%%%%%%%%%%%%%%%%%%%%%%%%%%%%%%%
%% Calculating Equivalent dielectric constant
eps1 = input('Enter the dielectric constant of the first insulation')
eps2 = input('Enter the dielectric constant of the second insulation')
eps3 = input('Enter the dielectric constant of outer insulation wrap')
eps1=eps1*eps0;   eps2=eps2*eps0;eps3=eps3*eps0;
eps_dv_d = (1/(1/(eps1/ti1)+ 1/(eps2/(2*ti2))+1/(eps1/ti1)));
%%
%% Capacitance between two turns in a single pancake
   for i=1:N
       Cadj(i) = eps_dv_d*2*pi*(hc)*R2(i);
%% Capacitance between two axially seperates turns in a single pancake
       Cax(i)  = eps_dv_d*2*pi*(wc)*Rm(i);
%% Capacitance between turn to ground for the first and last single
pancake
         Cg11  = eps1*2*pi*wc*Rm(i)/ti1;
         Cg12  = eps2*2*pi*(wc)*Rm(i)/(ti2);
         Cg13  = eps3*2*pi*(wc)*Rm(i)/(oi);
       Cg1(i)  = 1/(1/Cg12+1/Cg11+1/Cg13);
   end
      Cadj(N)=0;
Capac=[count',rad_tinch,rad_t,Cadj',Cax',Cg1']
%%
%% The capacitances between the outer turn and ground in each single
pancake
         Cg21      = eps1*2*pi*hc*(R1(1)-ti2-ti1/2)/ti1;
         Cg22      = eps2*2*pi*(hc)*(R1(1)+ti2/2)/(ti2);
         Cg23      = eps3*2*pi*(hc)*(R1(1)+oi/2)/oi;
         Cg2       = 1 / (1/Cg21 + 1/Cg22 + 1/Cg23);
%%
```

```
%% The Capacitances between the inner turn and ground in each single
pancake
         Cg31      = eps1*2*pi*hc*(R2(N)+ti2+ti1/2)/ti1;
         Cg32      = eps2*2*pi*(hc)*(R2(N)+ti2/2)/(ti2);
         Cg33      = eps3*2*pi*(hc)*(R2(N)-oi/2)/oi;
         Cg3       = 1 / (1/Cg31 + 1/Cg32 + 1/Cg33);

%% Series Capacitance Calculation -
%% -combining axial capacitances to the adjacent capacitance
      tsum=0;
      for i1=1:N;
         fama(i1)=(2*N-(i1*2-1))* Cax(i1) ;
         famb(i1)=(2*i1-1)*Cax(i1);
      end
      famab(1)=fama(1); sumab(1)=famab(1)+Cadj(1);rsumab(1)=1/sumab(1)
      for i2=2:2*N
         if i2<21
            famab(i2)=famab(i2-1)+fama(i2);
            sumab(i2)=famab(i2)+Cadj(i2);
         else
            famab(i2)=famab(i2-1)+famb(2*N-i2+1)-fama(2*N-i2+1);
               if i2~=2*N
                  sumab(i2)=famab(i2)+Cadj(2*N-i2);
               else
                  sumab(i2)=famab(i2)*2;
               end
            end
            rsumab(i2)=1/sumab(i2);
         end
         Cs_dpo=1/sum(rsumab)
         Cs_dpi=1/(rsumab(N)+2*sum(rsumab(N+1:2*N-1))+2*rsumab(2*N))
%%  Series Capacitance Calculation by Karasev and Bulgakov
% The average capacitance between adjacent turns = Ct
% The average capacitance between axially seperated turns = Cat
      Ct=(sum(Cadj)-Cadj(N))/(N-1);
      Cat=sum(Cax)/(N);
   Cs_karasev=(N*Cat/2)*[1+(1/N)*sqrt(Ct/Cat)*coth(N*sqrt(Cat/Ct))]
   Cs_Bulgakov=(N*Cat/2)*[1+(1/N)*sqrt(Ct/Cat)]
      thp=acosh(1+Cat/Ct);
      th=acosh(1+2*Cat/Ct);
      Cep=Cat*[1+coth((N-1)*thp)*coth(thp/2)];Cep1=2*Cat/(1-
cosh(thp)+(sinh(thp))*coth(N*thp));
      Ce=Cat*[1+coth((N-1)*th)*coth(th/2)];Ce1=2*Cat/(1-
cosh(th)+(sinh(th))*coth(N*th));
   Cs_Chowduri_gal_noshield= Cep/2
   Cs_Chowduri_cap_noshield= Cep1/2
   Cs_Chowduri=Ce
   Cfs=(Cs_karasev+Cs_Bulgakov+Cs_Chowduri_cap_noshield)/3
%%
%% Equivalent Ground Capacitance
      Cgidp         = 2*(Cg2+Cg3)
      Cgodp         = sum(Cg1(1:N))+2*(Cg2+Cg3)
      Cgtot         = (2*Ndp)*(Cg2+Cg3)+2*sum(Cg1(1:N))



 %%
```

```
%%%%%%%%%%%%%%%%%%%%%%%%%%%%%%%%%%%%%%%%%%%%%%%%%%%%%%%%%%%%%%%%%%%%%%%%%%%%
%%%%%%%%%%%%%%%          INDUCTANCE CALCULATIONS          %%%%%%%%%%%%%%%%%
%%             Self Inductance Calculation Formula (by Miki et all.)     %%
%%                  L=mu0*R*N^2(ln(8R/R1-2)  Equation 1 of Chapter IV    %%
%% Mutual Inductance Calculation Formula (By Maxwell), modified by Lyle %%
%%               M=(N^2)*mu0*sqrt(R1R2)[(2/k- k )K(k)- (2/k) E(k)]       %%
%% Equations 3 and 4 of Chapter IV are used to calculate the turn to    %%
%% mutual inductances                                                   %%
%%%%%%%%%%%%%%%%%%%%%%%%%%%%%%%%%%%%%%%%%%%%%%%%%%%%%%%%%%%%%%%%%%%%%%%%%%%%

a   = hc;  % The height of the turn including insulation wrap
Nt  = 1 ;  % The number of the turn
b=wc;      %abs(R1(itr)-R2(itr));

%% Grover's Formula
for itg=1:N
    C1(itg)=b/(2*Rm(itg)); C2(itg)=a/b;
    if C1<0.2
Pp= 4*pi*(0.5*(1+C1(itg)^2/6)*log(8/C1(itg)^2)-0.84834 +0.2041*C1(itg)^2);
Lt_grover(itg)= 1e-7*Rm(itg)*Nt^2*Pp;
    end
end
%%
%% Calculating self and mutual inductances of a single pancake
%% (Constructing 20x20)
 for itr=1:N
    for itc=1:N
        if itr==itc
           tm1  = 0.5*log(a^2+b^2);
           tm2  = (b^2/(12*a^2))*log(1+a^2/b^2);
           tm3  = (a^2/(12*b^2))*log(1+b^2/a^2);
           tm4  = (2*b/(3*a))*atan(a/b);
           tm5  = (2*a/(3*b))*atan(b/a);
           lnR1 = tm1 - tm2 - tm3 +  tm4 + tm5 -25/12;
           L1dp(itr,itr)= mu0*Rm(itr)*Nt^2*(log(8*Rm(itr)) - lnR1 -2);
        elseif itr~=itc
           d(itr,itc)=0;
kt=sqrt(((4*Rm(itr)*Rm(itc))/((Rm(itr)+Rm(itc))^2+(d(itr,itc))^2)));
K, E]= ellipke(kt^2);
M1=(Nt^2)*mu0*sqrt(Rm(itr)*Rm(itc))*((2/kt-kt)*K-2/kt*E);
d(itr,itc)=2*beta;
kt=sqrt(((4*Rm(itr)*Rm(itc))/((Rm(itr)+Rm(itc))^2+(d(itr,itc))^2)));
K, E]= ellipke(kt^2);
M2=(Nt^2)*mu0*sqrt(Rm(itr)*Rm(itc))*((2/kt-kt)*K-2/kt*E);
L1dp(itr,itc) =(2*M1+2*M2)/4;
end
      end
 end
   id=1 ;dd(1)=vs+hc;for id1=2:2*Ndp-1
     if id1~=insn*id;
        dd(id1)=dd(id1-1)+(vs+hc);
     else dd(id1)=dd(id1-1)+(vs+hc)+inst; id=id+1,
     end
  end
%%
%% Mutual inductance Calculation between the first single pancake to
others.
```

```
 for it1=1:2*Ndp-1
    for itr1=1:N
           for itc1=1:N
                r1=Rm(itr1)*(1+c1^2/(24*(Rm(itr1))^2));
                r2=Rm(N+1-itc1)*(1+c1^2/(24*(Rm(N+1-itc1))^2));
                d1(it1,1)=dd(it1)-2*beta;
                for lyl=1:3
                kt=sqrt(4*r1*r2/((r1+r2)^2+d1(it1,lyl)^2));
                [K, E]= ellipke(kt^2);
                M(lyl)=(Nt^2)*mu0*sqrt(r1*r2)*((2/kt-kt)*K-2/kt*E);
                d1(it1,lyl+1)=d1(it1,lyl)+2*beta;
             end
             L1dp(it1*N+itc1,itr1) =  (M(1)+2*M(2)+M(3))/4;
          end
       end
  end
%%
%% (N+1)x(2NNdp),1xN matrix has been constructed.
 for k=1:2*Ndp
   sumt(k)=sum(sum(L1dp(N*(k-1)+1:N*k,1:N)));
end
Lcoil(1,1)=2*sumt(1)+2*sumt(2);
for l=2:2:2*(Ndp-1); Lcoil(l/2+1,1)=sumt(l)+2*sumt(l+1)+sumt(l+2); end

Lcoil(1,1)=Lcoil(1,1)/2;
% The diagonal term was divided by two. The exact term
% will be obtained when the transpose of the matrix is added to itself.

%% Constructing the NdpxNdp matrix using the first column of the matrix
for c1=2:Ndp
   for r1=c1:Ndp
      if r1==c1
         Lcoil(c1,c1)=Lcoil(1,1);
      elseif c1<r1
         Lcoil(r1,c1)=Lcoil(r1-1,c1-1);
      end
   end
end
Lcoil=Lcoil+Lcoil';
```

APPENDIX D

TURN-TO-TURN COIL PARAMETERS

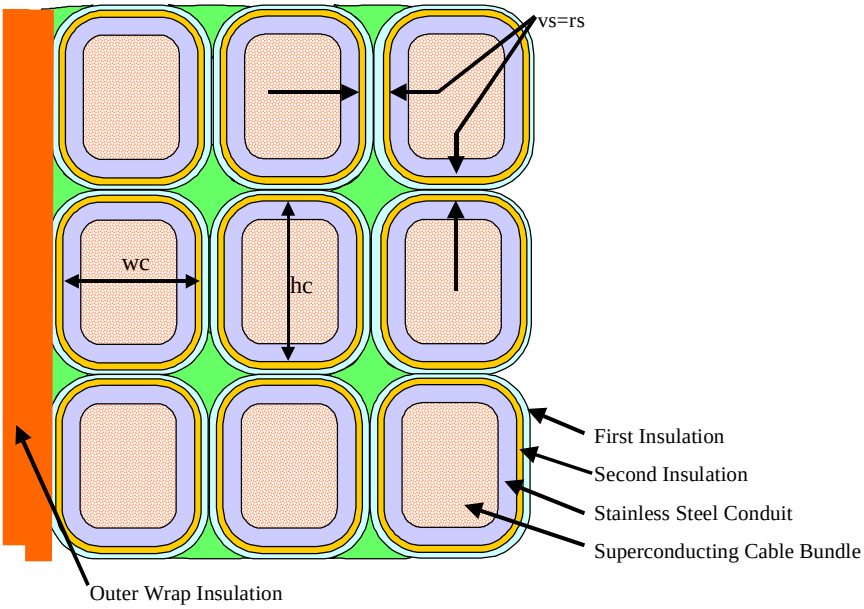

Figure D.1: Representation of Turns (Provided by BWX Technologies Inc.)

INPUT VARIABLES

wc = 0.4292;	the width of the conductor of one turn
hc = 0.5788;	the height of the conductor of one turn
cwt = 0.065;	the thickness of the conduit of one turn
vs = 0.052;	the vertical conduit spacing of one turn
rs = 0.052;	the radial conduit spacing of one turn
ti1 = 0.010;	the thickness of the first insulation
ti2 = 0.016;	the thickness of the second insulation
do = 144;	the outer diameter of the magnet coil (corresponds to R1 in Figure IV.3.a)
di = 122.6;	the inner diameter of the magnet coil (corresponds to R2 in Figure IV.3.a)
oi = 0.5;	the thickness of the outer wrap insulation
N = 20;	the number of turns in one single pancake
Ndp = 48;	the number of double pancakes in the coil
eps1 = 3.5;	the dielectric constant of the first insulation (Kapton Wrap)
eps2 = 4.5;	the dielectric constant of the second insulation (S glass Wrap)
eps3 = 5;	the dielectric constant of outer insulation wrap (G10-CR Module Wrap)

RESULTS:

Capacitance

Turn #	R1(inch)	R2(inch)	Rm(inch)	R1(m)	R2(m)	Rm(m)	Cadj	Cax	Cg
1	71.4740	71.2334	70.9928	1.8154	1.8093	1.8032	4.527E-09	3.368E-09	4.060E-10
2	70.9928	70.7522	70.5116	1.8032	1.7971	1.7910	4.496E-09	3.346E-09	4.032E-10
3	70.5116	70.2710	70.0304	1.7910	1.7849	1.7788	4.466E-09	3.323E-09	4.005E-10
4	70.0304	69.7898	69.5492	1.7788	1.7727	1.7665	4.435E-09	3.300E-09	3.978E-10
5	69.5492	69.3086	69.0680	1.7665	1.7604	1.7543	4.404E-09	3.277E-09	3.950E-10
6	69.0680	68.8274	68.5868	1.7543	1.7482	1.7421	4.374E-09	3.255E-09	3.923E-10
7	68.5868	68.3462	68.1056	1.7421	1.7360	1.7299	4.343E-09	3.232E-09	3.895E-10
8	68.1056	67.8650	67.6244	1.7299	1.7238	1.7177	4.312E-09	3.209E-09	3.868E-10
9	67.6244	67.3838	67.1432	1.7177	1.7115	1.7054	4.282E-09	3.186E-09	3.840E-10
10	67.1432	66.9026	66.6620	1.7054	1.6993	1.6932	4.251E-09	3.164E-09	3.813E-10
11	66.6620	66.4214	66.1808	1.6932	1.6871	1.6810	4.220E-09	3.141E-09	3.786E-10
12	66.1808	65.9402	65.6996	1.6810	1.6749	1.6688	4.190E-09	3.118E-09	3.758E-10
13	65.6996	65.4590	65.2184	1.6688	1.6627	1.6565	4.159E-09	3.095E-09	3.731E-10
14	65.2184	64.9778	64.7372	1.6565	1.6504	1.6443	4.128E-09	3.073E-09	3.703E-10
15	64.7372	64.4966	64.2560	1.6443	1.6382	1.6321	4.098E-09	3.050E-09	3.676E-10
16	64.2560	64.0154	63.7748	1.6321	1.6260	1.6199	4.067E-09	3.027E-09	3.648E-10
17	63.7748	63.5342	63.2936	1.6199	1.6138	1.6077	4.036E-09	3.004E-09	3.621E-10
18	63.2936	63.0530	62.8124	1.6077	1.6015	1.5954	4.005E-09	2.982E-09	3.594E-10
19	62.8124	62.5718	62.3312	1.5954	1.5893	1.5832	3.975E-09	2.959E-09	3.566E-10
20	62.3312	62.0906	61.8500	1.5832	1.5771	1.5710	0.000E+00	2.936E-09	3.539E-10

Cadj = Capacitance Between Adjacent Turns
Cax = Capacitance Between Axially Separated Turns
Cg = Capacitance Between Turns to Ground in the First and Last Single Pancake
Cgi = Capacitance Between Inner Turn in Single Pancakes to Ground = 2.0494e-9F.
Cgo = Capacitance Between Outer Turn in Single Pancakes to Ground = 9.6479e-9F.

Inductance Matrix for a Double Pancake (Columns 1-10)

	1	2	3	4	5	6	7	8	9	10
1	1.33E-05	1.14E-05	9.85E-06	8.92E-06	8.24E-06	7.71E-06	7.27E-06	6.90E-06	6.57E-06	6.28E-06
2	1.14E-05	1.32E-05	1.13E-05	9.77E-06	8.84E-06	8.17E-06	7.64E-06	7.21E-06	6.83E-06	6.51E-06
3	9.85E-06	1.13E-05	1.31E-05	1.12E-05	9.69E-06	8.77E-06	8.10E-06	7.57E-06	7.14E-06	6.77E-06
4	8.92E-06	9.77E-06	1.12E-05	1.30E-05	1.11E-05	9.61E-06	8.69E-06	8.03E-06	7.50E-06	7.07E-06
5	8.24E-06	8.84E-06	9.69E-06	1.11E-05	1.28E-05	1.10E-05	9.53E-06	8.61E-06	7.95E-06	7.44E-06
6	7.71E-06	8.17E-06	8.77E-06	9.61E-06	1.10E-05	1.27E-05	1.09E-05	9.44E-06	8.54E-06	7.88E-06
7	7.27E-06	7.64E-06	8.10E-06	8.69E-06	9.53E-06	1.09E-05	1.26E-05	1.08E-05	9.36E-06	8.46E-06
8	6.90E-06	7.21E-06	7.57E-06	8.03E-06	8.61E-06	9.44E-06	1.08E-05	1.25E-05	1.07E-05	9.28E-06
9	6.57E-06	6.83E-06	7.14E-06	7.50E-06	7.95E-06	8.54E-06	9.36E-06	1.07E-05	1.24E-05	1.06E-05
10	6.28E-06	6.51E-06	6.77E-06	7.07E-06	7.44E-06	7.88E-06	8.46E-06	9.28E-06	1.06E-05	1.23E-05
11	6.02E-06	6.22E-06	6.45E-06	6.71E-06	7.01E-06	7.37E-06	7.81E-06	8.39E-06	9.20E-06	1.06E-05
12	5.79E-06	5.96E-06	6.16E-06	6.39E-06	6.65E-06	6.94E-06	7.30E-06	7.74E-06	8.31E-06	9.12E-06
13	5.57E-06	5.73E-06	5.91E-06	6.11E-06	6.33E-06	6.58E-06	6.88E-06	7.23E-06	7.67E-06	8.24E-06
14	5.37E-06	5.51E-06	5.67E-06	5.85E-06	6.05E-06	6.27E-06	6.52E-06	6.81E-06	7.17E-06	7.60E-06
15	5.18E-06	5.32E-06	5.46E-06	5.62E-06	5.79E-06	5.99E-06	6.21E-06	6.46E-06	6.75E-06	7.10E-06
16	5.01E-06	5.13E-06	5.26E-06	5.41E-06	5.56E-06	5.74E-06	5.93E-06	6.15E-06	6.40E-06	6.69E-06
17	4.85E-06	4.96E-06	5.08E-06	5.21E-06	5.35E-06	5.51E-06	5.68E-06	5.87E-06	6.09E-06	6.33E-06
18	4.69E-06	4.80E-06	4.91E-06	5.03E-06	5.16E-06	5.30E-06	5.45E-06	5.62E-06	5.81E-06	6.03E-06
19	4.55E-06	4.64E-06	4.75E-06	4.86E-06	4.98E-06	5.10E-06	5.24E-06	5.40E-06	5.57E-06	5.75E-06
20	4.41E-06	4.50E-06	4.59E-06	4.70E-06	4.81E-06	4.92E-06	5.05E-06	5.19E-06	5.34E-06	5.51E-06
21	4.40E-06	4.49E-06	4.59E-06	4.69E-06	4.80E-06	4.91E-06	5.04E-06	5.18E-06	5.33E-06	5.49E-06
22	4.54E-06	4.64E-06	4.74E-06	4.85E-06	4.97E-06	5.09E-06	5.23E-06	5.38E-06	5.55E-06	5.73E-06
23	4.69E-06	4.79E-06	4.90E-06	5.02E-06	5.15E-06	5.29E-06	5.44E-06	5.61E-06	5.79E-06	6.00E-06
24	4.84E-06	4.95E-06	5.07E-06	5.20E-06	5.34E-06	5.49E-06	5.66E-06	5.85E-06	6.06E-06	6.30E-06
25	5.00E-06	5.12E-06	5.25E-06	5.39E-06	5.55E-06	5.72E-06	5.91E-06	6.12E-06	6.36E-06	6.64E-06
26	5.17E-06	5.30E-06	5.45E-06	5.60E-06	5.78E-06	5.97E-06	6.18E-06	6.42E-06	6.70E-06	7.03E-06
27	5.36E-06	5.50E-06	5.66E-06	5.83E-06	6.02E-06	6.24E-06	6.48E-06	6.77E-06	7.10E-06	7.49E-06
28	5.56E-06	5.71E-06	5.89E-06	6.08E-06	6.30E-06	6.55E-06	6.83E-06	7.16E-06	7.56E-06	8.06E-06
29	5.77E-06	5.95E-06	6.14E-06	6.36E-06	6.61E-06	6.89E-06	7.23E-06	7.63E-06	8.13E-06	8.76E-06
30	6.00E-06	6.20E-06	6.42E-06	6.67E-06	6.96E-06	7.30E-06	7.70E-06	8.21E-06	8.84E-06	9.61E-06
31	6.26E-06	6.48E-06	6.73E-06	7.02E-06	7.37E-06	7.77E-06	8.28E-06	8.92E-06	9.69E-06	1.02E-05
32	6.54E-06	6.80E-06	7.09E-06	7.43E-06	7.85E-06	8.35E-06	9.00E-06	9.78E-06	1.03E-05	9.69E-06
33	6.86E-06	7.15E-06	7.50E-06	7.92E-06	8.43E-06	9.07E-06	9.86E-06	1.04E-05	9.78E-06	8.92E-06
34	7.22E-06	7.57E-06	7.99E-06	8.50E-06	9.15E-06	9.95E-06	1.05E-05	9.86E-06	9.00E-06	8.28E-06
35	7.64E-06	8.06E-06	8.58E-06	9.23E-06	1.00E-05	1.06E-05	9.95E-06	9.07E-06	8.35E-06	7.77E-06
36	8.13E-06	8.65E-06	9.31E-06	1.01E-05	1.06E-05	1.00E-05	9.15E-06	8.43E-06	7.85E-06	7.37E-06
37	8.73E-06	9.39E-06	1.02E-05	1.07E-05	1.01E-05	9.23E-06	8.50E-06	7.92E-06	7.43E-06	7.02E-06
38	9.47E-06	1.03E-05	1.08E-05	1.02E-05	9.31E-06	8.58E-06	7.99E-06	7.50E-06	7.09E-06	6.73E-06
39	1.04E-05	1.09E-05	1.03E-05	9.39E-06	8.65E-06	8.06E-06	7.57E-06	7.15E-06	6.80E-06	6.48E-06
40	1.10E-05	1.04E-05	9.47E-06	8.73E-06	8.13E-06	7.64E-06	7.22E-06	6.86E-06	6.54E-06	6.26E-06

Inductance Matrix for a Double Pancake (Columns 10-20)

11	12	13	14	15	16	17	18	19	20
6.02E-06	5.79E-06	5.57E-06	5.37E-06	5.18E-06	5.01E-06	4.85E-06	4.69E-06	4.55E-06	4.41E-06
6.22E-06	5.96E-06	5.73E-06	5.51E-06	5.32E-06	5.13E-06	4.96E-06	4.80E-06	4.64E-06	4.50E-06
6.45E-06	6.16E-06	5.91E-06	5.67E-06	5.46E-06	5.26E-06	5.08E-06	4.91E-06	4.75E-06	4.59E-06
6.71E-06	6.39E-06	6.11E-06	5.85E-06	5.62E-06	5.41E-06	5.21E-06	5.03E-06	4.86E-06	4.70E-06
7.01E-06	6.65E-06	6.33E-06	6.05E-06	5.79E-06	5.56E-06	5.35E-06	5.16E-06	4.98E-06	4.81E-06
7.37E-06	6.94E-06	6.58E-06	6.27E-06	5.99E-06	5.74E-06	5.51E-06	5.30E-06	5.10E-06	4.92E-06
7.81E-06	7.30E-06	6.88E-06	6.52E-06	6.21E-06	5.93E-06	5.68E-06	5.45E-06	5.24E-06	5.05E-06
8.39E-06	7.74E-06	7.23E-06	6.81E-06	6.46E-06	6.15E-06	5.87E-06	5.62E-06	5.40E-06	5.19E-06
9.20E-06	8.31E-06	7.67E-06	7.17E-06	6.75E-06	6.40E-06	6.09E-06	5.81E-06	5.57E-06	5.34E-06
1.06E-05	9.12E-06	8.24E-06	7.60E-06	7.10E-06	6.69E-06	6.33E-06	6.03E-06	5.75E-06	5.51E-06
1.22E-05	1.05E-05	9.04E-06	8.16E-06	7.53E-06	7.03E-06	6.62E-06	6.27E-06	5.97E-06	5.70E-06
1.05E-05	1.21E-05	1.04E-05	8.96E-06	8.09E-06	7.46E-06	6.96E-06	6.56E-06	6.21E-06	5.91E-06
9.04E-06	1.04E-05	1.20E-05	1.03E-05	8.87E-06	8.01E-06	7.39E-06	6.90E-06	6.49E-06	6.15E-06
8.16E-06	8.96E-06	1.03E-05	1.19E-05	1.02E-05	8.79E-06	7.94E-06	7.32E-06	6.83E-06	6.43E-06
7.53E-06	8.09E-06	8.87E-06	1.02E-05	1.18E-05	1.01E-05	8.71E-06	7.86E-06	7.25E-06	6.76E-06
7.03E-06	7.46E-06	8.01E-06	8.79E-06	1.01E-05	1.17E-05	1.00E-05	8.63E-06	7.79E-06	7.18E-06
6.62E-06	6.96E-06	7.39E-06	7.94E-06	8.71E-06	1.00E-05	1.16E-05	9.92E-06	8.55E-06	7.71E-06
6.27E-06	6.56E-06	6.90E-06	7.32E-06	7.86E-06	8.63E-06	9.92E-06	1.15E-05	9.83E-06	8.47E-06
5.97E-06	6.21E-06	6.49E-06	6.83E-06	7.25E-06	7.79E-06	8.55E-06	9.83E-06	1.14E-05	9.74E-06
5.70E-06	5.91E-06	6.15E-06	6.43E-06	6.76E-06	7.18E-06	7.71E-06	8.47E-06	9.74E-06	1.13E-05
5.68E-06	5.88E-06	6.11E-06	6.38E-06	6.70E-06	7.08E-06	7.54E-06	8.13E-06	8.85E-06	9.32E-06
5.94E-06	6.17E-06	6.45E-06	6.76E-06	7.14E-06	7.62E-06	8.21E-06	8.93E-06	9.41E-06	8.85E-06
6.24E-06	6.51E-06	6.83E-06	7.21E-06	7.69E-06	8.29E-06	9.02E-06	9.50E-06	8.93E-06	8.13E-06
6.57E-06	6.90E-06	7.28E-06	7.76E-06	8.37E-06	9.10E-06	9.58E-06	9.02E-06	8.21E-06	7.54E-06
6.96E-06	7.35E-06	7.84E-06	8.44E-06	9.19E-06	9.67E-06	9.10E-06	8.29E-06	7.62E-06	7.08E-06
7.42E-06	7.91E-06	8.52E-06	9.27E-06	9.76E-06	9.19E-06	8.37E-06	7.69E-06	7.14E-06	6.70E-06
7.98E-06	8.60E-06	9.35E-06	9.85E-06	9.27E-06	8.44E-06	7.76E-06	7.21E-06	6.76E-06	6.38E-06
8.68E-06	9.44E-06	9.94E-06	9.35E-06	8.52E-06	7.84E-06	7.28E-06	6.83E-06	6.45E-06	6.11E-06
9.52E-06	1.00E-05	9.44E-06	8.60E-06	7.91E-06	7.35E-06	6.90E-06	6.51E-06	6.17E-06	5.88E-06
1.01E-05	9.52E-06	8.68E-06	7.98E-06	7.42E-06	6.96E-06	6.57E-06	6.24E-06	5.94E-06	5.68E-06
9.61E-06	8.76E-06	8.06E-06	7.49E-06	7.03E-06	6.64E-06	6.30E-06	6.00E-06	5.73E-06	5.49E-06
8.84E-06	8.13E-06	7.56E-06	7.10E-06	6.70E-06	6.36E-06	6.06E-06	5.79E-06	5.55E-06	5.33E-06
8.21E-06	7.63E-06	7.16E-06	6.77E-06	6.42E-06	6.12E-06	5.85E-06	5.61E-06	5.38E-06	5.18E-06
7.70E-06	7.23E-06	6.83E-06	6.48E-06	6.18E-06	5.91E-06	5.66E-06	5.44E-06	5.23E-06	5.04E-06
7.30E-06	6.89E-06	6.55E-06	6.24E-06	5.97E-06	5.72E-06	5.49E-06	5.29E-06	5.09E-06	4.91E-06
6.96E-06	6.61E-06	6.30E-06	6.02E-06	5.78E-06	5.55E-06	5.34E-06	5.15E-06	4.97E-06	4.80E-06
6.67E-06	6.36E-06	6.08E-06	5.83E-06	5.60E-06	5.39E-06	5.20E-06	5.02E-06	4.85E-06	4.69E-06
6.42E-06	6.14E-06	5.89E-06	5.66E-06	5.45E-06	5.25E-06	5.07E-06	4.90E-06	4.74E-06	4.59E-06
6.20E-06	5.95E-06	5.71E-06	5.50E-06	5.30E-06	5.12E-06	4.95E-06	4.79E-06	4.64E-06	4.49E-06
6.00E-06	5.77E-06	5.56E-06	5.36E-06	5.17E-06	5.00E-06	4.84E-06	4.69E-06	4.54E-06	4.40E-06

Inductance Matrix for a Double Pancake (Columns 20-30)

21	22	23	24	25	26	27	28	29	30
4.40E-06	4.49E-06	4.59E-06	4.69E-06	4.80E-06	4.91E-06	5.04E-06	5.18E-06	5.33E-06	5.49E-06
4.54E-06	4.64E-06	4.74E-06	4.85E-06	4.97E-06	5.09E-06	5.23E-06	5.38E-06	5.55E-06	5.73E-06
4.69E-06	4.79E-06	4.90E-06	5.02E-06	5.15E-06	5.29E-06	5.44E-06	5.61E-06	5.79E-06	6.00E-06
4.84E-06	4.95E-06	5.07E-06	5.20E-06	5.34E-06	5.49E-06	5.66E-06	5.85E-06	6.06E-06	6.30E-06
5.00E-06	5.12E-06	5.25E-06	5.39E-06	5.55E-06	5.72E-06	5.91E-06	6.12E-06	6.36E-06	6.64E-06
5.17E-06	5.30E-06	5.45E-06	5.60E-06	5.78E-06	5.97E-06	6.18E-06	6.42E-06	6.70E-06	7.03E-06
5.36E-06	5.50E-06	5.66E-06	5.83E-06	6.02E-06	6.24E-06	6.48E-06	6.77E-06	7.10E-06	7.49E-06
5.56E-06	5.71E-06	5.89E-06	6.08E-06	6.30E-06	6.55E-06	6.83E-06	7.16E-06	7.56E-06	8.06E-06
5.77E-06	5.95E-06	6.14E-06	6.36E-06	6.61E-06	6.89E-06	7.23E-06	7.63E-06	8.13E-06	8.76E-06
6.00E-06	6.20E-06	6.42E-06	6.67E-06	6.96E-06	7.30E-06	7.70E-06	8.21E-06	8.84E-06	9.61E-06
6.26E-06	6.48E-06	6.73E-06	7.02E-06	7.37E-06	7.77E-06	8.28E-06	8.92E-06	9.69E-06	1.02E-05
6.54E-06	6.80E-06	7.09E-06	7.43E-06	7.85E-06	8.35E-06	9.00E-06	9.78E-06	1.03E-05	9.69E-06
6.86E-06	7.15E-06	7.50E-06	7.92E-06	8.43E-06	9.07E-06	9.86E-06	1.04E-05	9.78E-06	8.92E-06
7.22E-06	7.57E-06	7.99E-06	8.50E-06	9.15E-06	9.95E-06	1.05E-05	9.86E-06	9.00E-06	8.28E-06
7.64E-06	8.06E-06	8.58E-06	9.23E-06	1.00E-05	1.06E-05	9.95E-06	9.07E-06	8.35E-06	7.77E-06
8.13E-06	8.65E-06	9.31E-06	1.01E-05	1.06E-05	1.00E-05	9.15E-06	8.43E-06	7.85E-06	7.37E-06
8.73E-06	9.39E-06	1.02E-05	1.07E-05	1.01E-05	9.23E-06	8.50E-06	7.92E-06	7.43E-06	7.02E-06
9.47E-06	1.03E-05	1.08E-05	1.02E-05	9.31E-06	8.58E-06	7.99E-06	7.50E-06	7.09E-06	6.73E-06
1.04E-05	1.09E-05	1.03E-05	9.39E-06	8.65E-06	8.06E-06	7.57E-06	7.15E-06	6.80E-06	6.48E-06
1.10E-05	1.04E-05	9.47E-06	8.73E-06	8.13E-06	7.64E-06	7.22E-06	6.86E-06	6.54E-06	6.26E-06
1.33E-05	1.14E-05	9.85E-06	8.92E-06	8.24E-06	7.71E-06	7.27E-06	6.90E-06	6.57E-06	6.28E-06
1.14E-05	1.32E-05	1.13E-05	9.77E-06	8.84E-06	8.17E-06	7.64E-06	7.21E-06	6.83E-06	6.51E-06
9.85E-06	1.13E-05	1.31E-05	1.12E-05	9.69E-06	8.77E-06	8.10E-06	7.57E-06	7.14E-06	6.77E-06
8.92E-06	9.77E-06	1.12E-05	1.30E-05	1.11E-05	9.61E-06	8.69E-06	8.03E-06	7.50E-06	7.07E-06
8.24E-06	8.84E-06	9.69E-06	1.11E-05	1.28E-05	1.10E-05	9.53E-06	8.61E-06	7.95E-06	7.44E-06
7.71E-06	8.17E-06	8.77E-06	9.61E-06	1.10E-05	1.27E-05	1.09E-05	9.44E-06	8.54E-06	7.88E-06
7.27E-06	7.64E-06	8.10E-06	8.69E-06	9.53E-06	1.09E-05	1.26E-05	1.08E-05	9.36E-06	8.46E-06
6.90E-06	7.21E-06	7.57E-06	8.03E-06	8.61E-06	9.44E-06	1.08E-05	1.25E-05	1.07E-05	9.28E-06
6.57E-06	6.83E-06	7.14E-06	7.50E-06	7.95E-06	8.54E-06	9.36E-06	1.07E-05	1.24E-05	1.06E-05
6.28E-06	6.51E-06	6.77E-06	7.07E-06	7.44E-06	7.88E-06	8.46E-06	9.28E-06	1.06E-05	1.23E-05
6.02E-06	6.22E-06	6.45E-06	6.71E-06	7.01E-06	7.37E-06	7.81E-06	8.39E-06	9.20E-06	1.06E-05
5.79E-06	5.96E-06	6.16E-06	6.39E-06	6.65E-06	6.94E-06	7.30E-06	7.74E-06	8.31E-06	9.12E-06
5.57E-06	5.73E-06	5.91E-06	6.11E-06	6.33E-06	6.58E-06	6.88E-06	7.23E-06	7.67E-06	8.24E-06
5.37E-06	5.51E-06	5.67E-06	5.85E-06	6.05E-06	6.27E-06	6.52E-06	6.81E-06	7.17E-06	7.60E-06
5.18E-06	5.32E-06	5.46E-06	5.62E-06	5.79E-06	5.99E-06	6.21E-06	6.46E-06	6.75E-06	7.10E-06
5.01E-06	5.13E-06	5.26E-06	5.41E-06	5.56E-06	5.74E-06	5.93E-06	6.15E-06	6.40E-06	6.69E-06
4.85E-06	4.96E-06	5.08E-06	5.21E-06	5.35E-06	5.51E-06	5.68E-06	5.87E-06	6.09E-06	6.33E-06
4.69E-06	4.80E-06	4.91E-06	5.03E-06	5.16E-06	5.30E-06	5.45E-06	5.62E-06	5.81E-06	6.03E-06
4.55E-06	4.64E-06	4.75E-06	4.86E-06	4.98E-06	5.10E-06	5.24E-06	5.40E-06	5.57E-06	5.75E-06
4.41E-06	4.50E-06	4.59E-06	4.70E-06	4.81E-06	4.92E-06	5.05E-06	5.19E-06	5.34E-06	5.51E-06

Inductance Matrix for a Double Pancake (Columns 30-40)

31	32	33	34	35	36	37	38	39	40
5.68E-06	5.88E-06	6.11E-06	6.38E-06	6.70E-06	7.08E-06	7.54E-06	8.13E-06	8.85E-06	9.32E-06
5.94E-06	6.17E-06	6.45E-06	6.76E-06	7.14E-06	7.62E-06	8.21E-06	8.93E-06	9.41E-06	8.85E-06
6.24E-06	6.51E-06	6.83E-06	7.21E-06	7.69E-06	8.29E-06	9.02E-06	9.50E-06	8.93E-06	8.13E-06
6.57E-06	6.90E-06	7.28E-06	7.76E-06	8.37E-06	9.10E-06	9.58E-06	9.02E-06	8.21E-06	7.54E-06
6.96E-06	7.35E-06	7.84E-06	8.44E-06	9.19E-06	9.67E-06	9.10E-06	8.29E-06	7.62E-06	7.08E-06
7.42E-06	7.91E-06	8.52E-06	9.27E-06	9.76E-06	9.19E-06	8.37E-06	7.69E-06	7.14E-06	6.70E-06
7.98E-06	8.60E-06	9.35E-06	9.85E-06	9.27E-06	8.44E-06	7.76E-06	7.21E-06	6.76E-06	6.38E-06
8.68E-06	9.44E-06	9.94E-06	9.35E-06	8.52E-06	7.84E-06	7.28E-06	6.83E-06	6.45E-06	6.11E-06
9.52E-06	1.00E-05	9.44E-06	8.60E-06	7.91E-06	7.35E-06	6.90E-06	6.51E-06	6.17E-06	5.88E-06
1.01E-05	9.52E-06	8.68E-06	7.98E-06	7.42E-06	6.96E-06	6.57E-06	6.24E-06	5.94E-06	5.68E-06
9.61E-06	8.76E-06	8.06E-06	7.49E-06	7.03E-06	6.64E-06	6.30E-06	6.00E-06	5.73E-06	5.49E-06
8.84E-06	8.13E-06	7.56E-06	7.10E-06	6.70E-06	6.36E-06	6.06E-06	5.79E-06	5.55E-06	5.33E-06
8.21E-06	7.63E-06	7.16E-06	6.77E-06	6.42E-06	6.12E-06	5.85E-06	5.61E-06	5.38E-06	5.18E-06
7.70E-06	7.23E-06	6.83E-06	6.48E-06	6.18E-06	5.91E-06	5.66E-06	5.44E-06	5.23E-06	5.04E-06
7.30E-06	6.89E-06	6.55E-06	6.24E-06	5.97E-06	5.72E-06	5.49E-06	5.29E-06	5.09E-06	4.91E-06
6.96E-06	6.61E-06	6.30E-06	6.02E-06	5.78E-06	5.55E-06	5.34E-06	5.15E-06	4.97E-06	4.80E-06
6.67E-06	6.36E-06	6.08E-06	5.83E-06	5.60E-06	5.39E-06	5.20E-06	5.02E-06	4.85E-06	4.69E-06
6.42E-06	6.14E-06	5.89E-06	5.66E-06	5.45E-06	5.25E-06	5.07E-06	4.90E-06	4.74E-06	4.59E-06
6.20E-06	5.95E-06	5.71E-06	5.50E-06	5.30E-06	5.12E-06	4.95E-06	4.79E-06	4.64E-06	4.49E-06
6.00E-06	5.77E-06	5.56E-06	5.36E-06	5.17E-06	5.00E-06	4.84E-06	4.69E-06	4.54E-06	4.40E-06
6.02E-06	5.79E-06	5.57E-06	5.37E-06	5.18E-06	5.01E-06	4.85E-06	4.69E-06	4.55E-06	4.41E-06
6.22E-06	5.96E-06	5.73E-06	5.51E-06	5.32E-06	5.13E-06	4.96E-06	4.80E-06	4.64E-06	4.50E-06
6.45E-06	6.16E-06	5.91E-06	5.67E-06	5.46E-06	5.26E-06	5.08E-06	4.91E-06	4.75E-06	4.59E-06
6.71E-06	6.39E-06	6.11E-06	5.85E-06	5.62E-06	5.41E-06	5.21E-06	5.03E-06	4.86E-06	4.70E-06
7.01E-06	6.65E-06	6.33E-06	6.05E-06	5.79E-06	5.56E-06	5.35E-06	5.16E-06	4.98E-06	4.81E-06
7.37E-06	6.94E-06	6.58E-06	6.27E-06	5.99E-06	5.74E-06	5.51E-06	5.30E-06	5.10E-06	4.92E-06
7.81E-06	7.30E-06	6.88E-06	6.52E-06	6.21E-06	5.93E-06	5.68E-06	5.45E-06	5.24E-06	5.05E-06
8.39E-06	7.74E-06	7.23E-06	6.81E-06	6.46E-06	6.15E-06	5.87E-06	5.62E-06	5.40E-06	5.19E-06
9.20E-06	8.31E-06	7.67E-06	7.17E-06	6.75E-06	6.40E-06	6.09E-06	5.81E-06	5.57E-06	5.34E-06
1.06E-05	9.12E-06	8.24E-06	7.60E-06	7.10E-06	6.69E-06	6.33E-06	6.03E-06	5.75E-06	5.51E-06
1.22E-05	1.05E-05	9.04E-06	8.16E-06	7.53E-06	7.03E-06	6.62E-06	6.27E-06	5.97E-06	5.70E-06
1.05E-05	1.21E-05	1.04E-05	8.96E-06	8.09E-06	7.46E-06	6.96E-06	6.56E-06	6.21E-06	5.91E-06
9.04E-06	1.04E-05	1.20E-05	1.03E-05	8.87E-06	8.01E-06	7.39E-06	6.90E-06	6.49E-06	6.15E-06
8.16E-06	8.96E-06	1.03E-05	1.19E-05	1.02E-05	8.79E-06	7.94E-06	7.32E-06	6.83E-06	6.43E-06
7.53E-06	8.09E-06	8.87E-06	1.02E-05	1.18E-05	1.01E-05	8.71E-06	7.86E-06	7.25E-06	6.76E-06
7.03E-06	7.46E-06	8.01E-06	8.79E-06	1.01E-05	1.17E-05	1.00E-05	8.63E-06	7.79E-06	7.18E-06
6.62E-06	6.96E-06	7.39E-06	7.94E-06	8.71E-06	1.00E-05	1.16E-05	9.92E-06	8.55E-06	7.71E-06
6.27E-06	6.56E-06	6.90E-06	7.32E-06	7.86E-06	8.63E-06	9.92E-06	1.15E-05	9.83E-06	8.47E-06
5.97E-06	6.21E-06	6.49E-06	6.83E-06	7.25E-06	7.79E-06	8.55E-06	9.83E-06	1.14E-05	9.74E-06
5.70E-06	5.91E-06	6.15E-06	6.43E-06	6.76E-06	7.18E-06	7.71E-06	8.47E-06	9.74E-06	1.13E-05

REFERENCES

[Abet53] P.A. Abetti, F.J. Maginniss, "Natural Frequencies of Coils and Windings Determined by Equivalent Circuit," *AIEE Transactions*, Vol.72, Part III, p.495-504, June 1953.

[Arsoy00a] A. Arsoy, Y. Liu, P.F. Ribeiro, W.Xu, "Power Converter and SMES in Controlling Power System Dynamics", accepted to be presented in the 2000 Annual Meeting and World Conference on Industrial Applications of Electrical Energy, Italy, October 2000.

[Arsoy00b] A. Arsoy, Y. Liu, P.F. Ribeiro, F. Wang, "The Impact of Energy Storage on the Dynamic Performance of Static Synchronous Compensator", accepted to be presented in the Third International Power Electronics and Motion Control Conference, China, August 2000.

[Arsoy99a] A. B. Arsoy, Z. Wang, Y. Liu, P.F. Ribeiro, "Transient Modeling and Simulation of A SMES Coil and the Power Electronics Interface," *IEEE Transactions on Applied Superconductivity*, vol.9, no.4, p.4715-4724, December, 1999.

[Arsoy99b] A. B. Arsoy, Y. Liu, P.F. Ribeiro, "An Investigation of the Dynamic Performance of a Static Synchronous Compensator with Superconducting Magnetic Energy Storage," *Proceedings of the 1999 Annual Power Electronics Seminar at Virginia Tech*, vol. 17, p. 401-405, September 19-21, 1999.

[Arsoy98] A. B. Arsoy, Z. Wang, Y. Liu, P.F. Ribeiro, "Electromagnetic Transient Interaction of A SMES Coil and the Power Electronics Interface," *Proceedings of the 16th Annual VPEC Seminar*, vol.16, pp. 361-367, September 13-15, 1998.

[Balci98] Osman Balci, "Verification, Validation, and Testing", In The Handbook of Simulation, J. Banks, Editor, John Wiley & Sons, New York, NY, Chapter 10, p. 335-393, August 1998.

[Baner90] S. Banerjee, J.K. Chatterjee, S.C. Tripathy, "Application of Magnetic Energy Storage Unit as Load-Frequency Stabilizer," *IEEE Transactions on Energy Conversion*, vol. 5, no. 1, p. , March, 1990.

[Bauma92] P.D. Baumann, "Energy Conservation and Environmental Benefits That May Be Realized From Superconducting Magnetic Energy Storage," *IEEE Transactions on Energy Conversion*, vol. 7, no. 2, June 1992.

[Bauti97] A. Bautista, P. Esteban, L. Garcia-Tabares, P. Peon, E. Martinez, J. Sese, A. Camon, C. Rillo, R. Iturbe, "Design, Manufacturing and Cold Test of a Superconducting Coil and Its Cryostat for SMES Applications," *IEEE Transactions on Applied Superconductivity*, vol. 7, no. 2, p. 853-856, June 1997.

[Berne98] S. Bernet, R. Teichmann, A. Zuckerburger, P. Steimer, "Comparison of High Power IGBTs and Hard Driven GTOs for High Power Inverters," *The Proceedings of Applied Power Electronics Conference*, February 1998.

[Borga99] L. Borgard, "Grid Voltage Support at Your Fingertips," *Transmission and Distribution World*, October 1999.

[Boom72] R.W. Boom and H.A. Peterson, "Superconductive Energy storage for Power Systems," *IEEE Transactions on Magnetics*, vol. MAG-8, p.701-703, September 1972.

[Carro98] E.J. Carroll, "Power Electronics for Very High Power Applications," *IEEPEVD*, September 1998

[Chowd87] P. Chowdhury, "Calculation of Series Capacitance for Transient Analysis of Windings," *IEEE Transactions on Power Delivery*, vol. PWRD-2, no. 1, p. 133-139, Janury 1987.

[Degen95] R.C. Degeneff, Calculating Voltage Versus Time and Impedance Versus Frequency for the SMES Coil, A report submitted to Babcock & Wilcox by Utility Systems Technologies, Inc, May 1995.

[Degen77] R.C. Degeneff, "A General Method for Determining Resonances in Transformer Windings," *IEEE Transactions on Power Apparatus and Systems*, vol. 96, no. 2, p. 423-430, March/Apr. 1977.

[Domme97] H. W. Dommel, "Techniques for Analyzing Electromagnetic Transients," *IEEE Computer Applications in Power*, vol.10 no.3, p. 18-23, July 1997.

[Dugan96] R.C. Dugan, M.F. McGranaghan, H.W. Beaty, *Electrical Power Systems Quality*, McGraw-Hill, 1996.

[Ekstro89] Ekstrom and G. Anderson, " Guidelines for Application of Metal Oxide Arresters without Gaps for Converter Stations," *Electra*, No.127, pp. 111-135, 1989.

[Feak97] S. D. Feak, "Superconducting Magnetic Energy Storage (SMES) Utility Application Studies," *IEEE Transactions on Power Systems*, vol. 12, no. 3, p. 1094-1102, August, 1997.

[Giese98] R.F. Giese, *Progress Toward High Temperature Superconducting Magnetic Energy Storage (SMES) – A Second Look*, Argonne National Laboratory, December 1998

[Green91] A Greenwood, *Electrical Transients in Power Systems*, John Wiley, New York, 1991.

[Grov73] F.W. Grover, Inductance Calculations: Working Formulas and Tables, Instrument Society of America, New York 1973.

[Gyugy94] L. Gyugyi, "Dynamic Compensation of AC Transmission Lines by Sloid State Synchronous Voltage Sources," *IEEE Transactions on Power Delivery*, vol.9, no.2, p. 904-911, April 1994 .

[Han93] B.M. Han and G.G. Karady, " A new Power Conditioning System for Superconducting Magnetic Energy Storage," *IEEE Transactions on Energy Conversion*, vol.8, no.2, p.214-220, June 1993.

[Harri95] Harris Semiconductor CA Series, Industrial High Energy Metal Oxide Disc Varistors, March 1995.

[Hassa93] I.D. Hassan, R. M. Bucci, K.T. Swe, "400MW SMES Power Conditioning System Development and Simulation", *IEEE Transactions on Power Electronics*, vol.8, no.3, p.237-249, July 1993.

[Hasse83] W.V. Hassenzahl, "Superconducting Magnetic Energy Storage," *Proceedings of the IEEE,* vol.71, no.9, p.1089-1098, September 1983.

[Hasse89] W.V. Hassenzahl, "Superconducting Magnetic Energy Storage," *IEEE Transactions on Magnetics,* vol.25, no.2, p.750-758, March 1989.

[Hayas99] H. Hayashi, K. Tsutsumi, F. Irie, T. Teranishi, S. Hanai, L. Kushida, "Analysis and Countermeasure for the Problem Due to Abnormal Voltage in a SMES Magnet," CEC/ICM Canada, July 1999.

[Hingo00] N.G. Hingorani, L. Gyugyi, Understanding FACTS Concepts and Technology of Flexible AC Transmission Systems, IEEE Press, New York, 2000.

[Huang95] X. Huang, S.F. Kral, G.A. Lehmann, Y.M. Lvosky, M. Xu, "30 MW Babcock and Wilcox SMES Program for Utility Applications," *IEEE Transactions on Applied Superconductivity,* vol. 5, no. 2, p. 428-432, June 1995.

[Ieeew99] IEEE Working Group, Modeling and Analysis of System Transients using Digital Programs, IEEE, 1999.

[Ise99] T. Ise, J. Ishii, S. Kumagai, "Compensation of Harmonics and Negative Sequence Components in Line Current and Voltage by a SuperSMES" *IEEE Transactions on Applied Superconductivity,* vol. 9, no.2 pp. 334-337, June 1999.

[Ise86] T. Ise, Y. Murakami, K. Tsuji, "Simultaneous Active and Reactive Power Control of Superconducting magnetic Energy Storage", *IEEE Transactions on Power Delivery,* vol. PWRD-1, no.1, p.143-149, January 1986.

[Jiang96] Q. Jiang, M.F. Conlon, "The Power Regulation of a PWM Type Superconducting Magnetic energy Storage Unit," *IEEE Transactions on Energy Conversion,* vol. 11, no. 4, p. 168-174, March, 1996.

[Kamol99] D. Kamolyabutra, Y. Mitani, T. Ise, K. Tsuji, "Experimental Study on Power System Stabilizing Control Scheme for the SMES with Solid State Phase Shifter (SuperSMES)," *IEEE Transactions on Applied Superconductivity,* vol. 9, no.2 pp. 326-329, June 1999.

[Karas99] V. Karasik, K. Dixon, C. Weber, B. Batchelder, P. Ribeiro, "SMES for Power Utility Applications: A Review of Technical and Cost Considerations," IEEE Transactions on Applied Superconductivity, vol.9, no.2 p.541-546, June 1999.

[Kral97] S.F. Kral, et al., "Alaska SMES: Form and Function for the World's Largest Magnet," Presented at the Cryogenic Engineering Conference, July 1997.

[Kral95] S.F. Kral, M. Aslam, P.F. Ribeiro, X. Huang, M. Xu, "Superconducting Power Delivery Systems for Transmission & Distribution Applications," *presented at the 57th American Power Conference,* April 1995.

[Kumar89] P. Kumar, "Applications of Superconducting Magnetic Energy Storage Systems in Power Systems", A Master Thesis, Virginia Tech, August 1989.

[Kundu94] P. Kundur, *Power System Stability and Control,* McGraw-Hill Inc., 1994.

[Kusto91] R.L. Kustom, J.J. Skiles, J. Wang, K. Klontz, T. Ise, K. Ko, F. Vong, "Research on Power Conditioning Systems for Superconductive Magnetic Energy Storage (SMES)", *IEEE Transactions on Magnetics*, vol.27, no.2, p.2320-2322, March 1991.

[Larse92] E. Larsen, N. Miller, S. Nilsson, S. Lindgren, "Benefits of GTO-Based Compensation Systems for Electric Utility Applications," *IEEE Transactions on Power Delivery*, vol. 7, no. 4, p. 2056-2062, October 1992.

[Lasse91a] R.H. Lasseter and S.G. Jalali, "Power Conditioning Systems for Superconductive Magnetic Energy Storage", *IEEE Transactions on Energy Conversion*, Vol.6 No.3 p.381-387, September 1991.

[Lasse91b] R. H. Lasseter, S.J. Jalali, "Dynamic Response of Power Conditioning Systems for Superconductive Magnetic Energy Storage," *IEEE Transactions on Energy Conversion*, vol. 6, no. 3, p. 388-393, September, 1991

[Lee99] Y-S. Lee, "Superconducting Magnetic Energy Storage Controller Design and Stability Analysis for a Power System with Various Load Characteristics," *Electric Power Systems Research*, vol. 51, p.33-41, 1999.

[Lieur95] D. Lieurance, F. Kimball, C. Rix, C. Luongo, "Design and Cost Studies for Small Scale Superconducting Magnetic Energy Storage Systems," *IEEE Transactions on Applied Superconductivity*, vol. 5, no. 2, p. 350-353, June 1995.

[Luong95] C.A. Luongo, the Bechtel SMES Team, "Review of the Bechtel Team's SMES Design and Future Plans for a Technology Demonstration Unit," *IEEE Transactions on Applied Superconductivity*, vol. 5, no. 2, p. 422-427, June 1995.

[Luong96] C.A. Luongo, "Superconducting Storage Systems," *IEEE Transactions on Magnetics*, vol.32, no.4, p.2214-2223, July 1996.

[Manit88] Manitoba HVDC Research Center, "PSCAD™/EMTDC™ User's Manual", 1988.

[Mao96] H. Mao, D. Boroyevich, F.C. Lee, "Multi-Level 2-Quadrant Boost Choppers For Superconducting Magnetic Energy Storage," *The Proceedings of the Eleventh Annual Applied Power Electronics Conference and Exposition*, vol. 2, pp. 876-882, p.876-882, 1996.

[Masud87] M. Masuda, T. Shintomi, "The conceptual Design of Utility Scale SMES," *IEEE Transactions on Magnetics*, vol. MAG-23, no.2, March 1987.

[McNut74] W.J. McNutt, T.J. Blalock, R. A. Hinton, "Response of Transformer Windings to System Transient Voltage," *IEEE Transactions on Power Apparatus and Systems*, Vol. PAS-93, pp.457-467, March/April 1974.

[Melio88] A.P. Sakis Meliopoulos, Power System Grounding and Transients, Marcel Dekker Inc. 1988.

[Miri95] A. M. Miri, C. Sihler, M. Droll, A. Ulbricht, "Modelling the Transient Behaviour of a Large Superconducting Coil Subjected to High Voltage Pulses," *The Proceedings of International Conference on Power System Transients*, no. 563, p. 57-62, September, 1995.

[Miri98] A.M. Miri, C. Sihler, H. Salbert, K.-U Vollmer, "Investigation of the Transient Behaviour of a Superconducting Magnetic Energy Storage (SMES) Generating High Power

Pulses," *European Transactions on Electrical Power Engineering,* vol. 8, no. 1, p. 13-19, Jan./Feb. 1998.

[Mitan88] Y. Mitani, K. Tsuji, Y. Murakami, "Application of Superconducting Magnet Energy Storage to Improve Power System Dynamic Performance," *IEEE Transactions on Power Systems,* vol. 3, no. 4, p. 1418-1425.

[Mitsu94] H. Mitsui, "Electrical Insulation Technology for Superconducting Magnets in Japan," *IEEE Electrical Insulation Magazine,* vol. 10, no. 4, p.23-32, July/August 1994.

[Mohan95] N. Mohan, T.M. Undeland, W.P. Robbins, Power Electronics Converters, Applications and Design, John Wiley, New York, 1995.

[Nayak95] O. Nayak, G. Irwin, A. Neufeld, "GUI Enhances Electromagnetic Transients Simulation Tools," *IEEE Computer Applications in Power,* vol. 8, no. 1, p. 17-22, January 1995.

[Ngamr99] I. Ngamroo, Y. Mitani, K. Tsuji, "Application of SMES Coordinated with Solid State Phase Shifter to Load Frequency Control" *IEEE Transactions on Applied Superconductivity,* vol. 9, no.2 pp. 322-325, June 1999.

[Pariz97] M. Parizh, A.K. Kalafala, R. Wilcox, "Superconducting Magnetic Energy Storage for Substation Applications," *IEEE Transactions on Applied Superconductivity*, vol. 7, no. 2, p. 849-852, June 1997.

[Passe97] J-C. Passelergue, N. Hadsjaid, Y. Besanger, R. Feuillet, "On Using FACTS and Power System Stabilizers to Damp Low Frequency Oscillations," *EPE97,* p. 3.959- 3.964. 1997.

[Patil98] K.V. Patil, J. Senthil, J. Jiang, R.M. Mathur, 'Application of StatCom for Damping Torsional Oscillations in Series Compensated AC Systems," *IEEE Transactions on Energy Conversion,* vol. 13, no. 3, p. 237-243, September 1998.

[Peter75] H.A. Peterson, N. Mohan, R. W. Boom, "Superconductive Energy Storage Inductor Converter Units for Power Systems," *IEEE Transactions on Power Apparatus and Systems,* vol. PAS-94, no.4, p.1337-1347, July/August 1975.

[Rahim96] A.H.M.A. Rahim, A.M. Mohammad, M.R. Khan, "Control of Sub-synchronous Resonant Modes in a Series Compensated System Through Superconducting Magnetic Energy Storage Units," *IEEE Transactions on Energy Conversion,* vol. 11, no. 1, p. 175-180, March, 1996.

[Rehan99] C. Rehtanz, "Systematic Use of Multifunctional SMES in Electric Power Systems," *IEEE Transactions on Power Systems,* vol. 14, no.4, p.1422-1427, November 1999.

[Ribei99], P. F. Ribeiro, "SMES for Enhanced Flexibility and Performance of FACTS Devices," *IEEE Summer Meeting,* July 1999.

[Roger79] J.D. Rogers, H.J. Boening, J.C. Bronson, D.B. Colyer, W.V. Hassenzahl, R.D. Turner, R.I. Schermer, "30-MJ Superconducting Magnetic Energy Storage (SMES) Unit for Stabilizing an Electric Transmission System," *IEEE Transactions on Magnetics,* vol. MAG-15, no.1, pp. 820-823, January 1979.

[Roger83] J.D. Rogers, R.I. Schermer, B.L.Miller, J.F. Hauer, "30 MJ Superconducting Magnetic Energy Storage System for Electric Utility Transmission Stabilization," *Proceedings of the IEEE*, vol.71, no.9, p.1099-1109, Sep. 1983.

[Sauer98] P. W. Sauer, M.A. Pai, *Power System Dynamics and Stability*, Prentice Hall, New Jersey, 1998.

[Schau98] C. Schauder, et. al., "AEP UPFC project: Installation, Commissioning and Operation of the ± 160MVA StatCom (phase I)," *IEEE Transactions on Power Delivery*, vol. 13, no. 4, p. October 1998.

[Schau95] C.Schauder, M.Gernhardth, E. Stacy, T.W. Cease, A. Edris, "Development of a 100 MVAR Static Condenser for Voltage Control of Transmission Systems," *IEEE Transactions on Power Delivery*, vol. 10, no. 3, p. 1486-1496, July 1995.

[Schau93] C. Schauder, H. Mehta, "Vector Analysis and Control of Advanced Static VAR Compensators," *IEE Proceedings-C*, vol.140, no.4, p.299-306, July 1993.

[Schoe93] S.M. Schoenung, W.R. Meier, R. L. Fagaly, M. Heiberger, R.B. Stephens, J.A. Leuer, R.A. Guzman, "Design, Performance, and Cost Characteristics of High Temperature Superconducting Magnetic Energy Storage," *IEEE Transactions on Energy Conversion*, vol. 8, no. 1, p. 33-38, March 1993.

[Schoe96] A.M. Schoenung, C. Burns, "Utility Energy Storage Technologies," *IEEE Transactions on Energy Conversion*, vol. 11, no.3, p.658-665, September 1996.

[Schwe87] S.W. Schwenterly, "Design and Testing of Electrical Insulation for Superconducting Coils," *Advances in Cryogenic Engineering*, vol. 33, p271-281, 1987.

[Sen98] K.K. Sen, E.J. Stacey "UPFC – Unified Power Flow Controller: Theory, Modeling and Applications," *IEEE Transactions on Power Delivery*, vol. 13, no. 4, p. 1453-1460, October 1998.

[Sen99] K.K. Sen, "STATCOM – STATic synchronous COMpensator: Theory, Modeling and Applications," *IEEE Transactions on Power Delivery*, vol. 2, p.1177-1183, February 1999.

[Shira94] H. Shirahama, Y. Sakurai, Y. Matsuda, Y. Ishigaki, K. Murai, "Instantaneous Control Method with a GTO Converter for Active and Reactive Powers in Superconducting Magnetic Energy Storage," *IEEE Transactions on Power Electronics*, vol.9, no.1, p.1-6, January 1994.

[Skile96] J.J. Skiles, R.L. Custom, K-P Ko, V. Wong, K-S Ko, F. Vong, K. Klontz, "Performance of a Power Conversion System for Superconducting Magnetic Energy Storage," *IEEE Transactions on Power Systems*, vol.11, no.4, p.1718-1723, November 1996

[Stees92] J.G. De Steese, J.E. Dagle, K.L. Gaustad, D.J. Trudnowski, *Electric Utilities of Superconducting Magnetic Energy Storage*, Pacific Northwest Laboratory, prepared for Bonneville Power Administration, October 1992.

[Tam90] K-S Tam, P. Kumar, "Impact of Superconducting Magnetic Energy Stoarage on Electric Power Transmission," *IEEE Transactions on Energy Conversion"*, vol. 5, no.3, pp. 501-511, September 1990

[Thero93] P.G. Therond, I Joly, M. Volker, "Superconducting Magnetic Energy Storage (SMES) for Industrial Applications – Comparison with Battery Systems," *IEEE Transactions on Applied Superconductivity,* vol.3, no.1 pp. 250-253, March 1993.

[Tomin] T. Tominaga, O. Takashiba, H. Fujita, "Design and Tests of the Superconducting Magnet for Energy Storage," *IEEE Transactions on Applied Superconductivity,* p. 408-412.

[Wirga76] K.A. Wirgau, "Inductance Calculation of an Air-Core Disk Winding," *IEEE Transactions on Power Apparatus and Systems,* vol. PAS-95, no. 1, p. 394-400, Jan/Feb, 1976.

[Wohlw95] J.W. Wohlwend, S. Singh, D.B. Montgomery, "Design of a Central Solenoid Coil for the ITER Magnet System," *IEEE Transactions on Applied Superconductivity*, vol. 5, no. 2, p. 433-436, June 1995.

VITA

Aysen (Basa) Arsoy was born in Pazar/Rize-TURKEY on July 28 1972. After graduating from a high school in her hometown, she attended Istanbul Technical University (ITU) where she received a Bachelor of Science Degree in Electrical Engineering, June 1992. She attended the University of Missouri-Rolla (UMR) from 1994 to 1996, and received a Master of Science Degree in Electrical Engineering.

In the Fall 1996, Aysen began her doctoral studies in power systems engineering at Virginia Tech. During her study, she has held the positions of graduate teaching and research assistant.

Aysen is a fellowship receiver from Higher Education Council in Turkey. She has been a member of ITU alumni association since 1992. She is also a member of the IEEE Power Engineering Society.